Reservoir Characterization Integrating Well Observations, Seismic Data and Production History

Bjørn Kåre Hegstad and Henning Omre
Department of Mathematical Sciences
Norwegian University of Science and Technology
Trondheim, Norway

September 1998

Preface

This is the final report from the project "Reservoir characterization integrating well, seismic and production data".

The goal for this project is to establish a stochastic model integrating all kinds of information in reservoir characterization and to specify a corresponding sampling procedure. A synthetic test case is used to explore the model and how much different sources of information increase accuracy and reduce uncertainty.

We would like to thank Alfhild Eide for allowing us to use here work on integration of seismic data as a base for the current work. Without her results we would not have a flying start. We are also grateful to Håkon Tjelmeland and Alfhild Eide for allowing us to use their software for fast generation of large Gaussian fields. Also our contacts in Norsk Hydro, Charlotte Tjølsen and Eivind Damsleth, have been giving us valuable feedback and help on how reservoir characteristics are related.

The project is financed by Norsk Hydro A.S.

September 1998

Bjørn Kåre Hegstad and Henning Omre.

Summary

A stochastic model for a 3D reservoir integrating well observations, seismic data and production history is presented.

A true reservoir, not constructed by generating a realization from the prior model, is defined. Data are observed from this reservoir and various simulation studies including different amount of data is performed.

The stochastic model is illustrated by a directed graph. This graph is used to illustrate the relations between the variables involved. These relations could be physical relations, empirical relations between reservoir characteristics, the relation between observations and reality, and conditional independence. Simplifying assumptions are discussed and utilized to define a sampling algorithm. The algorithm is defined by sequential sampling of Gaussian and log-Gaussian fields, and a accept-reject step where Markov chain Monte Carlo or rejection sampling can be used. The time consuming part in the algorithm, is the evaluation of a fluid flow simulator.

The simulation study demonstrates that seismic data adds valuable global information on the reservoir characteristics and reduce the number of fluid flow simulation runs for each accepted realization. In some cases the ratio of accepted realizations is doubled when conditioning on seismic data.

It also demonstrates that the global structure of the true reservoir is well reproduced when conditioning on data, even if it has nearly zero probability density in the prior model. The prior model is flexible and adapt to data.

The simulation study demonstrates that even when well observations carry little information in areas not being close to the wells, production characteristics are well reproduced when also seismic data are included. The global nature of information contents from seismic data does compensate for the local nature of well observations to some extent.

1 Introduction

The goal in reservoir characterization is to forecast production characteristics under various recovery strategies. The production characteristics should be forecasted with as much accuracy and as little uncertainty as possible. Hence all information about the reservoir under study should be included. The available information is general geological knowledge and reservoir specific observations. General geological knowledge could be knowledge about evolution of the geological formations and experience from analogs and comparable reservoirs. Reservoir specific observations may be local observations in wells as core plugs and well logs, global observations as seismics, or so-called dynamic data as transient pressure and production history.

The production forecast is linked to the reservoir characteristics through a fluid flow simulator. Hence both future production characteristics and reservoir characteristics with corresponding uncertainties are of interest.

Much work is done to include different sources of information into reservoir characterization. For references to seismic data see Bortoli et al. (1993), Haas and Dubrule (1994), Abrahamsen et al. (1996) and Eide (1999), for production history see Gómez-Hernández et al. (1997), RamaRao et al. (1995), Certes and de Marsily (1991), de Marsily et al. (1984), Bissell et al. (1992), Oliver (1994), Wen et al. (1997) and Xue and Datta-Gupta (1997), and Landa (1997) for both kinds of information sources. Many of these references present ad hoc procedures are suggested, and the results are often hard to interpret.

Stochastic modeling provides a framework for integrating different information sources with corresponding uncertainty in a consistent way, see Omre and Tjelmeland (1997), Hegstad and Omre (1997), Hegstad (1997) and Eide et al. (1997). The framework discussed in these references is utilized in the current report.

1.1 Prior stochastic model

Consider the evaluation of a petroleum reservoir. Let the production characteristics $p(q,t)$ be some response from the reservoir as e.g. oil production rates, pressure drops and gas oil ratios. Assume that the production characteristics are observed, possibly with an error, up to time t_o. The recovery strategy q could be the number and position of infill wells, how to inject gas, water or chemicals, and opening and closing criteria for injection and production wells.

The objective of the reservoir evaluation is to forecast the production characteristics $p(q,t)$ for a given strategy q for time $t > t_o$. Let the reservoir characteristics $r = r(x)$ represent properties as porosity, permeability, initial saturation, fluid properties, etc.. The spatial reference variable x indicates in general a spatial variability of these properties.

Define $v(r,q,t)$ to be a fluid flow simulator. If the reservoir characteristics r are known exhaustively and a perfect fluid flow simulator $v_o(\cdot,\cdot,\cdot)$ is available, the production characteristics p can be found by

$$p(q,t) = v_o(r,q,t), \qquad t > 0 \; .$$

Let hereafter the variable q be implicitly assumed and not visible in the notation. The reservoir characteristics r will be largely unknown at the stage of evaluation. Based on general geological knowledge a prior stochastic model R for the reservoir characteristics can be defined. The model is represented by the probability density function (pdf) $f(r)$, and the variable R is a stochastic field representing the reservoir characteristics. The prior model must be consistent with the prior knowledge of the geological reality of the formation which the reservoir is a part of, and give a realistic description of the prior uncertainty about the reservoir characteristics r.

This entails that also the production characteristics can be considered as stochastic by

$$P(t) = v_o(R, t), \qquad t > 0$$

with the associated pdf $f(p)$ expressing the prior uncertainty of the production characteristics.

Using a non-perfect fluid flow simulator $v(\cdot, \cdot)$ the relation is

$$P(t) = v(R, t) + U_P, \qquad t > 0 \tag{1}$$

where U_P is an error term representing modeling error using $v(\cdot, \cdot)$.

1.2 Observations

The reservoir specific observations, denoted D, may be grouped into three types: production history denoted D_p, in general all kind of dynamical data for $t \leq t_o$, seismic data denoted D_s and well observations denoted D_w being core plugs and well logs. Hence $D = (D_p, D_s, D_w)$. Let $d = (d_p, d_s, d_w)$ denote the actual observations from the reservoir under study. The first kind of observations is in time-domain, while the rest are in space domain. The seismic data are assumed to be depth-converted and given in space coordinates. The depth-conversion problem is not discussed here. The acoustic waves are supposed to have constant velocity in the entire reservoir.

The link between reservoir characteristics and seismic data can be modeled as

$$[D_s | R = r] = g_s(r) + U_s$$

where $[D_s|R = r]$ is a stochastic variable representing the seismic observations given that the reservoir characteristics are r. This variable is often termed "D_s conditioned on R" or "D_s given R". The term $g_s(r)$ is in general a forward transfer function, in this case a seismic forward model, and U_s is a stochastic variable representing modeling error and measurement error.

Similarly for the link between reservoir characteristics and well observations

$$[D_w | R = r] = g_w(r) + U_w$$

where $g_w(r)$ is modeling the the observations process and U_w is the error term.

Finally the link between the production characteristics and time domain observations can be modeled as

$$[D_p | P = p] = g_p(p) + U_{p^o}$$

where $g_p(p)$ is modeling the observations process and U_{p^o} represents modeling and measure error in the observation process. The error term U_{p^o} must not be confused with U_p in expression (1) which represents error introduced by using a fluid flow simulator.

The link between the observations and the reservoir characteristics and production characteristics, is represented by the likelihood function $f(d|p,r)$ expressing how likely it is to observe d given that the true reservoir characteristics are r and the true production characteristics are p. The three types of observations D_p, D_s and D_w are obtained by different tools and procedures, and hence can be regarded as conditionally independent given the reservoir characteristics r and the production characteristics p. Moreover, the production observations depend only on p and the space domain observations depend only on r. Hence the likelihood may be factorized as

$$f(d|p,r) = f(d_p|p)\ f(d_s|r)\ f(d_w|r).$$

The likelihood for the well observations $f(d_w|r)$ is usually relative simple to define since d_w relates directly to the reservoir characteristics. Also the likelihood for the production history $f(d_p|p)$ is simple. The likelihood for the seismic data, $f(d_s|r)$, is analytically tractable under suitable assumptions on the seismic forward model. This is discussed below, see also Eide et al. (1997).

1.3 Posterior model

The variables of interest are now $[P|D=d]$ and $[R|D=d]$ with associated pdfs $f(p|d)$ and $f(r|d)$ respectively. These pdfs express the uncertainty about P and R after all reservoir specific observations are taken into account, the so-called posterior pdfs. The challenge is to include these observations in a consistent and effective way. These pdfs can be found if the joint pdf $f(p,r|d)$ associated with the joint variable $[P,R|D=d]$ is available. The posterior distribution $f(p,r|d)$ is expressed through Bayes rule as

$$f(p,r|d) = \text{const} \cdot f(d_p|p) f(d_s|r) f(d_w|r) f(p|r) f(r).$$

Note that the pdf $f(p|r)$ may be extremely time consuming to evaluate since it involves evaluation of the fluid flow simulator $v(r,t)$. In this study the prior model and likelihoods are defined such that sampling the posterior is tractable. All assumptions and simplifications are carefully explained.

1.4 Outline of report

This work is mainly based on Eide et al. (1997), Eide (1997), Hegstad and Omre (1997) and Hegstad (1997) and is an extension of Omre and Tjelmeland (1997). These references should be read for a more thorough treatment of some of the details. In Section 2 a stochastic model for integrating well data, seismic data and production history is illustrated and explained. The prior model is described in Section 2.1, the links between data and the production characteristics and reservoir characteristics, are defined in Section 2.2. In Section 2.3 the simplifications in the posterior model derived from assumptions in the prior model and likelihood model are explained. In Section 2.4 these simplifications are utilized to define a simple sequential scheme for sampling the posterior pdf, that is the production characteristics and reservoir characteristics conditioned on all available data. In Section 3 a base case geological and fluid flow model is defined and parameter values in the stochastic model are given. In Section 4 the true reservoir is defined. It is not constructed by generating a sample from the prior stochastic model. As a result the true reservoir turns out to be in an extremely low probable area of the prior stochastic model. The differences from more typical and probable realizations from the prior model are discussed. In Section 5 and Section 6 the properties of the stochastic model are explored. In these sections the change in properties of reservoir characteristics and production characteristics when the amount of data included is varied, is studied. In Section 7 the information contents of the well observations are made more local, and the resulting influence of the different information sources on simulated production characteristics are explored. Finally in Section 8 some final comments and conclusions are made, and subjects for further research are proposed.

1.5 A note on notation

Consider a finite dimensional Gaussian field Y with expectation vector μ_Y and covariance matrix Σ_Y, i.e.

$$Y \sim N(\mu_Y, \Sigma_Y)$$

Let Y be defined on a three-dimensional grid. Element (i, j) in the covariance matrix is defined by

$$(\Sigma_Y)_{ij} = Cov(Y(x_i), Y(x_j)) = \sigma_Y^2 \rho_Y(x_i, x_j)$$

where $x = (x^{(1)}, x^{(2)}, x^{(3)})$ is the spatial reference running over the grid indexes in the two horizontal and the vertical direction respectively, σ_Y^2 is the variance of Y and $\rho_Y(\cdot, \cdot)$ is the spatial correlation function. All Gaussian fields in this report is on this form and this notation is used hereafter.

2 Stochastic model

The stochastic model is illustrated by a directed graph in Figure 1. The details are explained in the following sections. In this study all specified distributions in the stochastic model are Gaussian or transformation of Gaussian distributions. This is not necessary for the validity of the stochastic model. Also other assumptions as e.g. zero expectation on error terms and exact observations of acoustic impedance in wells, can be relaxed with the model still being valid. These model choices and simplifications are done to make sampling from the stochastic model conditioned to data as simple as possible. Many of the choices of functional relations are inspired by the Troll field, but completely different relations can be used when other reservoirs are modeled. The Troll field is in the North Sea and consists of two facies C-sand and M-sand with the former being high-permeable and the latter low-permeable. The high-permeable facies is though, Tjølsen and Damsleth (1998), to have high porosity and low acoustic impedance, while the low-permeable facies is though to have low porosity and high acoustic impedance. The Troll field in known to have a layered structure, but this knowledge is not utilized in the prior model except for introducing long correlation lengths.

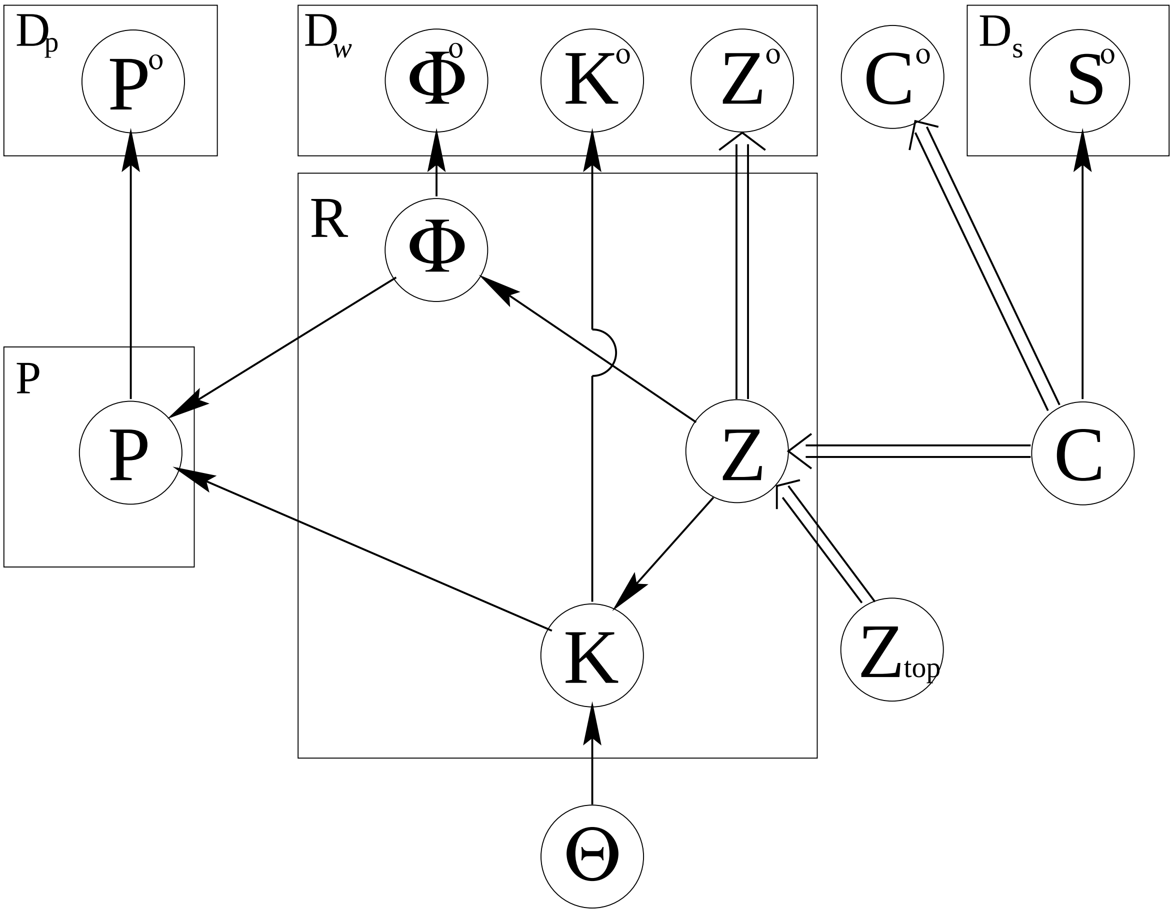

Figure 1: A directed graph representing the stochastic model. A double arrow from A to B implies that B is deterministic, given A. A double arrow from A_1 to B and from A_2 to B implies that B is deterministic, given both A_1 and A_2. An arrow from A to B implies that the conditional distribution of B given A is defined a priori in the model. An arrow from A_1 to B and from A_2 to B implies that the conditional distribution for B given both A_1 and A_2, is defined a priori in the model. S^o denotes seismic observations, C reflection coefficients and C^o denotes well observations of reflection coefficients. Z denotes acoustic impedance, Z^o well observations of acoustic impedance and Z_{top} denotes acoustic impedance on top of the reservoir under study. Φ denotes porosity, Φ^o well observations of porosity, K permeability and K^o well observations of permeability. Θ_K denotes parameters in the conditional distribution for K, P production characteristics and P^o observed production characteristics i.e. production history. A circle indicates a stochastic variable.

2.1 Prior model

2.1.1 Prior model; reservoir characteristics R

Let the reservoir characteristics be $R = (K, \Phi, Z)$ where K is permeability, Φ porosity and Z acoustic impedance.

Acoustic impedance; Z
The prior distribution of acoustic impedance Z, is discussed in relation with reflection coefficients C, under. The crucial point is that the prior model of both permeability and porosity, are defined conditioned on Z. This is illustrated by the arrows from Z to K and Φ in Figure 1.

Porosity; Φ
Given acoustic impedance $Z = z$, the porosity is modeled as

$$[\Phi | Z = z] = \mu_\Phi(z) + U_\Phi \tag{2}$$

where $\mu_\Phi(z)$ is a known function of z, but else arbitrary, and U_Φ is a Gaussian field with expectation zero and covariance matrix Σ_Φ. Hence, conditioned on $Z = z$ the stochastic variable Φ is Gaussian:

$$[\Phi | Z = z] \sim N(\mu_\Phi(z), \Sigma_\Phi)$$

This is illustrated by the arrow from Z to Φ on Figure 1. The corresponding pdf is in general denoted $f(\phi|z)$. Empirical studies, see Eide (1997), have shown a linear dependency between porosity and impedance within a facies, i.e.

$$\mu_\Phi(z) = a + bz \tag{3}$$

which is the form of $\mu_\Phi(z)$ used here.

Permeability; K
Given the impedance $Z = z$ and model parameters $\Theta = \theta$, the log-permeability is modeled as

$$[\ln K | Z = z, \Theta = \theta] = \mu_K(z; \theta) + U_K(z) \tag{4}$$

where $\mu_K(z; \theta)$ is a known function of z with model parameters θ, but else arbitrary, and $U_K(z)$ is a Gaussian field with expectation zero and covariance matrix Σ_K where the variance may vary with acoustic impedance. The model parameters Θ could be properties as mean permeability. Hence, conditioned on $Z = z$ and $\Theta = \theta$ the stochastic variable $\ln K$ is Gaussian

$$[\ln K | Z = z, \Theta = \theta] \sim N(\mu_K(z; \theta), \Sigma_K)$$

This is illustrated by the arrow from Z to K and the arrow from Θ to K in Figure 1. The corresponding pdf is in general denoted $f(k|z, \theta)$. Data from the Troll field, Tjølsen and Damsleth (1998), suggest no correlation between permeability and acoustic impedance within a facies. As a function of facies, however, there is a correlation. Facies with high impedance tend to have low permeability, and similar but opposite for facies with low impedance. Hence the function $\mu_K(z; \theta)$ may be written as

$$\mu_K(z; \theta) = \begin{cases} \theta_1 & \text{where } z \geq z_{\text{th}} \\ \theta_2 & \text{where } z < z_{\text{th}} \end{cases} \tag{5}$$

where $\theta_1 < \theta_2$ and z_{th} is some threshold value. Hence facies 1 tends to have an acoustic impedance above z_{th}. Similarly entry (i, i) in the covariance matrix is defined as

$$(\Sigma_K)_{ii} = \begin{cases} \sigma^2_{K,1} & \text{if } z \geq z_{\text{th}} \\ \sigma^2_{K,2} & \text{if } z < z_{\text{th}} \end{cases}$$

where z is evaluated at the grid block corresponding to entry (i, i) in the covariance matrix. The mean log-permeabilities are in general unknown. Hence the mean log-permeabilities $\theta = (\theta_1, \theta_2)$ are modeled as independent Gaussian variables with expectation $\mu_\Theta = (\mu_{\Theta_1}, \mu_{\Theta_2})$ and covariance matrix Σ_Θ with $(\Sigma_\Theta)_{ii} = \sigma^2_{\Theta_i}$.

Hence the stochastic variable $[\ln K, \Theta | Z = z]$ is a Gaussian field.

2.1.2 Prior model; production characteristics P

Production data are modeled with a fluid flow simulator taking permeability and porosity as input from the stochastic model. In addition initial saturation, initial pressure and other parameters necessary for the fluid flow simulator must be specified, but these are considered as known here. Moreover, the fine scale geological grid is upscaled to a coarser simulation grid. Given porosity $\Phi = \phi$ and permeability $K = k$ as input for a fluid flow simulator, the production characteristics are modeled as

$$P = v((\phi, k), t) + U_P, \quad t > 0$$

where $v(\cdot, \cdot)$ is the fluid flow simulator, t is the time reference and U_p is a Gaussian field with expectation zero and covariance matrix Σ_P representing modeling error. This is illustrated by the arrows from Φ to P and from K to P. Hence conditioned on $K = k$ and $\Phi = \phi$, the stochastic variable P is Gaussian

$$[P | (K = k, \Phi = \phi)] \sim N(v((k, \phi), t), \Sigma_P). \tag{6}$$

The corresponding pdf is in general denoted $f(p|r)$ or $f(p|(k, \phi))$.

2.1.3 Prior model; reflection coefficients C

The reflection coefficients are modeled as a Gaussian field with expectation zero and covariance structure Σ_C, i.e. $C \sim N(0, \Sigma_C)$. The pdf is in general denoted $f(c)$. The reflection coefficients are related to acoustic impedance in a vertical trace as

$$C_i = \frac{Z_{i+1} - Z_i}{Z_{i+1} + Z_i} \tag{7}$$

where increasing index indicates increasing depth. It can be interpreted as a relative change in acoustic impedance. The relation can be inverted and expressed as

$$Z_{i+1} = \frac{1 + C_i}{1 - C_i} Z_i \tag{8}$$

along a vertical trace. Given the field $Z_0 = Z_{\text{top}}$, this defines a non-linear, deterministic relation between C and Z. This is illustrated by a double arrow from Z_{top} to Z and from C

to Z in Figure 1. The corresponding prior model for Z is hence clearly non-Gaussian. This model is however uniquely determined by the prior model for reflection coefficients C and Z_{top} and relation (8). Note that by relation (7) also reflection coefficients C are uniquely determined given Z and Z_{top}.

2.1.4 Prior model; top layer of acoustic impedance Z_{top}.

Z_{top} is a field involved in the transformation from reflection coefficients to acoustic impedance in relation (8). In the prior model a choice could be a constant field with value equal the expected value of the facies in the layer on top of the reservoir. An other choice could be a Gaussian field, but note that impedance Z is clearly non-Gaussian as discussed in Section 2.1.3. For simplicity Z_{top} is in this study chosen to be a constant field when no well observations are present. In the presents of well observations it must be chosen such that the well observations Z^o are reproduced when relation (8) is used, i.e. the pdf $f(z_{\text{top}}|z^o, c)$ must be chosen in a consistent way. See Appendix B for how this problem is solved in this study. This problem is however a subject for further research.

2.2 Likelihood model

2.2.1 Likelihood model; well observations D_w

Recall that well observations are $D_w = (K^o, \Phi^o, Z^o)$ being permeability, porosity and acoustic impedance respectively, along the well trajectories.

Porosity well observations are on the form

$$[\Phi^o|\Phi = \phi] = g_\Phi(\phi) + U_{\Phi^o}$$

where $g_\Phi(\phi)$ is modeling the well-logging procedure and U_{Φ^o} is a Gaussian field representing model error and measurement error. This is illustrated by the arrow from Φ to Φ^o in Figure 1.

Similarly for permeability well observations K^o,

$$[K^o|K = k] = g_K(k) + U_{K^o} \ ,$$

where $g_K(k)$ is modeling the well-logging procedure and U_{K^o} is a Gaussian field representing model error and measurement error. This is illustrated by the arrow from K to K^o in Figure 1.

For acoustic impedance the well observations are modeled as

$$[Z^o|Z = z] = g_Z(z)$$

where $g_Z(z)$ is a subset of z. This deterministic relation is illustrated by the double arrow from Z to Z^o in Figure 1. The observations are assumed to be exact to simplify the posterior pdf.

In addition all well observations of different reservoir characteristics are supposed to be point observations from the same spatial locations. Also this assumption is introduced to simplify the posterior pdf, see discussion below.

2.2.2 Likelihood model; production observations D_p

Production history can be all kinds of production characteristics observed at observations times up to time t_o. In this study the observed production characteristics P^o are oil production rates from the two production wells, the corresponding gas-oil-ratios, and bottom hole pressure in the injection well, see also Figure 2 for an outline of the well pattern.

Production data are on the form

$$[P^o|P = p] = g_P(p) + U_{P^o}$$

where U_{P^o} is an error term with expectation zero and covariance matrix Σ_{P^o} representing observation errors and modeling errors introduced by using $g_P(p)$. This is illustrated by the arrow from P to P^o in Figure 1. The transfer function $g_P(p)$ could be production characteristics at observation times up to time t_o. The corresponding likelihood function is in general denoted $f(d_p|p)$.

2.2.3 Likelihood model; seismic data D_s

Note that in this study the seismic data D_s are also denoted S^o, see Figure 1. Seismic amplitude data are modeled as a convolution between a seismic wavelet and a vertical sequence of reflection coefficients, and corrupted with noise. The seismic data are covering the complete reservoir. The stochastic model for the seismic data conditioned on the reflection coefficients $C = c$, can be written as

$$[S^o|C = c] = g_S(c) + U_{S^o} = Ac + U_{S^o}$$

where S^o is seismic amplitude data, A is a matrix defined by the seismic wavelet and C is the field of reflection coefficients. This relation is illustrated by the arrow from C to S^o in Figure 1. The error term U_{S^o} is a Gaussian field with expectation zero and covariance matrix Σ_{S^o}, that is

$$[S^o|C = c] \sim N(Ac, \Sigma_{S^o}).$$

The corresponding likelihood function is in general denoted $f(d_s|r)$. Note that the corresponding variance $\sigma^2_{S^o}$ is scaled to the case where $\mathrm{Var}(C) = 1$. Since also C is a Gaussian field, (C, S^o) is Gaussian hence the conditional pdf $f(c|d_s)$ representing the variable $[C|D_s = d_s]$ is a Gaussian pdf as well.

2.2.4 Likelihood model; derived reflection coefficients well observations C^o.

For reflection coefficients the well observations are modeled as

$$[C^o|C = c] = g_C(c)$$

where $g_C(c)$ is a subset of c. This deterministic relation is illustrated by the double arrow from C to C^o in Figure 1. The well observations of reflection coefficients are in practice calculated from z^o given z_{top}. Hence c^o is uniquely determined when z^o and z_{top} are given. Hence in situations where both z^o and z_{top} are known, c^o is for simplicity not visible in the notation. Note that it is not obvious how to to calculate reflection coefficients in horizontal or deviating wells. Hence the function $g_C(c)$ gives only well observations of reflection coefficients in vertical wells.

2.3 Posterior model

Note that if c^o, ϕ^o and k^o are point observations or linear combinations of point observations, and U_{K^o} and U_{Φ^o} are Gaussian, the posterior pdfs $f(k|k^o, z)$, $f(\phi|\phi^o, z)$ and $f(c|c^o, d_s)$ are all Gaussian. This is the case in this study.

Recall that the reservoir characteristics R, consists of permeability K, porosity Φ and acoustic impedance Z, and that the reservoir specific observations D, are production data $D_p = P^o$, seismic data $D_s = S^o$ and well observations $D_w = (K^o, \Phi^o, Z^o)$.

2.3.1 Production characteristics and reservoir characteristics; P, R

The joint posterior pdf of $[P, R|D = d]$; the production characteristics P and the reservoir characteristics R given all reservoir specific observations, can be factorized by Bayes rule as

$$\begin{aligned} f(p, r|d) &= f(p, r|d_p, d_s, d_w) \\ &= \text{const} \cdot f(d_p|p, r, d_s, d_w) f(p|r, d_s, d_w) f(r|d_s, d_w) \\ &= \text{const} \cdot f(d_p|p) f(p|r) f(r|d_s, d_w) \ . \end{aligned} \tag{9}$$

The simplification in the last equality can be verified by inspecting Figure 1: Consider the first pdf after the last equality sign. Production data P^o is conditionally independent of all other variables given P, hence only p remains in the conditioning. Consider similarly the second pdf after the last equality sign. Production characteristics P are conditionally independent of both D_w and D_s given R, hence only r remains in the conditioning. The variables Θ, C and z_{top} not being in any of the boxes in Figure 1 are introduced under.

2.3.2 Reservoir characteristics; R

Consider the last pdf in expression (9). Note that the variables Θ, C and z_{top} are not variables of interest and hence not in the target pdf. To derive a workable factorization of the posterior pdf, these variables should, however, be included. Hence the pdf $f(r, z_{\text{top}}, c, \theta|d_s, d_w)$ is considered. This pdf is related to the the last pdf in expression (9) by

$$f(r|d_s, d_w) = \int_{\Omega_{Z_{\text{top}}}} \int_{\Omega_C} \int_{\Omega_\Theta} f(r, z_{\text{top}}, c, \theta|d_s, d_w) \ d\theta \ dc \ dz_{\text{top}}$$

where $\Omega_{Z_{\text{top}}}$, Ω_C and Ω_Θ are the set of all possible values of z_{top}, c and θ respectively. Note that the pdf $f(r|d_s, d_w)$ is obtained by just ignoring the $(z_{\text{top}}, c, \theta)$-entries when e.g. sampling from this pdf. The latter pdf can be factorized as

$$\begin{aligned} f(r, z_{\text{top}}, c, \theta|d_s, d_w) &= f(k, \phi, z, z_{\text{top}}, c, \theta|d_s, d_w) \\ &= f(k|\phi, z, z_{\text{top}}, c, \theta, d_s, d_w) \\ &\quad \cdot f(\phi|z, z_{\text{top}}, c, \theta, d_s, d_w) \\ &\quad \cdot f(\theta|z, z_{\text{top}}, c, d_s, d_w) \\ &\quad \cdot f(z|z_{\text{top}}, c, d_s, d_w) \\ &\quad \cdot f(z_{\text{top}}|c, d_s, d_w) \\ &\quad \cdot f(c|d_s, d_w, c^o) \\ &= f(k|z, \theta, d_w) f(\phi|z, d_w) f(\theta|z, d_w) f(z|z_{\text{top}}, c) f(z_{\text{top}}|c, d_w) f(c|d_s, d_w, c^o) \end{aligned} \tag{10}$$

The simplifications in the last equality can easily be verified by inspecting Figure 1: Consider the first and second pdf after the last equality sign. Permeability and porosity are conditionally independent given $Z = z$, hence ϕ is omitted in the first pdf. Moreover Θ and Φ are conditionally independent given $Z = z$, hence θ is omitted in the second pdf. Finally, both permeability and porosity are conditionally independent of reflection coefficients C, acoustic impedance on top of the reservoir Z_{top} and seismic data D_S given $Z = z$. Hence c, z_{top} and d_s are omitted in both pdfs.

Consider the third pdf after the last equality sign. The stochastic parameter Θ is clearly conditionally independent of C, Z_{top} and D_s given $Z = z$, hence c, z_{top} and d_s are omitted in this pdf.

Consider the fourth pdf after the last equality sign. Since acoustic impedance Z is deterministically determined given $Z_{\text{top}} = z_{\text{top}}$ and $C = c$, only these remain in the conditioning. Note furthermore, that this is not a traditional pdf but a Dirac delta function putting all probability mass on the value z calculated from z_{top} and c by relation (8).

Consider the fifth pdf after the last equality sign. Z_{top} is clearly conditionally independent of D_s given both $C = c$ and $D_w = d_w$. Hence d_s is omitted in this pdf.

Consider the last pdf on the right hand side of equation (10). Recall that the derived observations C^o are uniquely determined by Z^o and Z_{top}, and have so far been suppressed in the notation for simplicity, see also the discussion in Section 2.2.4. Since z_{top} is absent in this pdf, c^o becomes visible here.

Recall that $d_w = (k^o, \phi^o, z^o)$. Hence further simplifications in (10) can be performed since well observations of permeability, porosity and acoustic impedance are point observations from the same spatial locations. The posterior pdf $f(r, z_{\text{top}}, c, \theta | d_s, d_w)$ can be written as

$$\begin{aligned} f(r, z_{\text{top}}, c, \theta | d_s, d_w) &= f(k, \phi, z, z_{\text{top}}, c, \theta | d_w, d_s) \\ &= f(k|z, \theta, k^o) f(\phi|z, \phi^o) f(\theta|z, k^o) f(z|z_{\text{top}}, c) f(z_{\text{top}}|c, z^o) f(c|d_s, c^o) \end{aligned} \tag{11}$$

Consider the first three pdfs on the right hand side of equation (11) corresponding to the first three pdfs on the right hand side of equation (10). Since K and Φ are conditionally independent given $Z = z$, ϕ^o is omitted in the first pdf while k^o is omitted in the second pdf. Since Θ is conditionally independent of Φ given $Z = z$, ϕ^o is omitted in the third pdf. Since Z^o is a subset of Z, conditioning on both is redundant in the first, second and third pdfs. Hence z^o is omitted in all these pdfs.

Consider the fifth pdf on the right hand side of equation (11) corresponding to the fifth pdf on the right hand side of equation (10). Since Z^o are exact point observations, i.e. Z^o being a subset of Z, neither $K^o = k^o$ nor $\Phi^o = \phi^o$ give extra information on the acoustic impedance and can be omitted in the fifth pdf.

Consider the last pdf in the right hand side of equation (11) corresponding to the last pdf on the right hand side of equation (10). It is assumed that the properties of C in the stochastic model do not change with facies or values of reservoir characteristics. Hence neither $K^o = k^o$, $\Phi^o = \phi^o$ nor $Z^o = z^o$ give extra information on the reflection coefficients and d_w can be omitted in this pdf.

This demonstrates that samples from $f(r, z_{\text{top}}, c, \theta | d_w, d_s) = f(k, \phi, z, z_{\text{top}}, c, \theta | d_w, d_s)$ and hence $f(r|d_w, d_s)$ can be obtained through sequential sampling from $f(c|c^o, d_s)$, $f(z_{\text{top}}|c, z^o)$, $f(\theta|z, k^o)$, $f(\phi|z, \phi^o)$, and $f(k|z, \theta, k^o)$. The sequence of the fourth and fifth and the third and fourth pdfs being arbitrary. All the pdfs except $f(z_{\text{top}}|c,z^o)$ are Gaussian or log-Gaussian fields and are easy to sample. Sampling from $f(z_{\text{top}}|c,z^o)$ is discussed in Appendix B.

2.4 Sampling from the posterior model

The joint pdf $f(p,r|d)$ is available if $f(p,r,z_{\text{top}},c,\theta|d)$ is available by just ignoring the $(z_{\text{top}},c,\theta)$-entry. Hence consider $f(p,r,z_{\text{top}},c,\theta|d)$. Derivations above demonstrates that this pdf can be factorized as

$$f(p,r,z_{\text{top}},c,\theta|d) = \text{const}\cdot f(d_p|p,z_{\text{top}},c,\theta)f(p|r,z_{\text{top}},c,\theta)f(r,z_{\text{top}},c,\theta|d_s,d_w)$$

Since D_p is conditionally independent of Z_{top}, C and Θ given $P=p$, and P is conditionally independent of Z_{top}, C and Θ given $R=r$, then z_{top}, c and θ can be removed in the conditioning in the first two pdfs on the right hand side. Hence the posterior pdf $f(p,r,z_{\text{top}},c,\theta|d)$ can be represented as

$$\begin{aligned}
f(p,r,z_{\text{top}},c,\theta|d) &= \text{const}\cdot f(d_p|p)f(p|r)f(r,z_{\text{top}},c,\theta|d_s,d_w)\\
&= \text{const}\cdot f(d_p|p)f(p|r)f(k|k^o,z,\theta)f(\theta|k^o,z)f(\phi|\phi^o,z)f(z_{\text{top}}|c,z^o)f(c|c^o,d_s)
\end{aligned}$$

where $f(r,z_{\text{top}},c,\theta|d_s,d_w)$ is discussed above. This factorization calls for a sequential sampling scheme on the form

1. Generate $(r,z_{\text{top}},c,\theta)$ from $f(r,z_{\text{top}},c,\theta|d_s,d_w)$ by
   (a) Generate c from $f(c|c^o,d_s)$; a field of reflection coefficients conditioned on well observations of reflection coefficients and seismic data.
   (b) Generate z_{top} from $f(z_{\text{top}}|c,z^o)$; a field of acoustic impedance on the top of the reservoir conditioned on well observations of acoustic impedance and reflection coefficients.
   (c) Calculate z from c and z_{top} using expression (8); the field of acoustic impedance in the reservoir.
   (d) Generate ϕ from $f(\phi|\phi^o,z)$; a porosity field conditioned on well observations of porosity and the field of acoustic impedance.
   (e) Generate θ from $f(\theta|k^o,z)$; the expected log-permeability in the two facies conditioned on well observations of permeability and the field of acoustic impedance.
   (f) Generate k from $f(k|k^o,\theta,z)$; a permeability field conditioned on well observations of permeability, expected permeability in the two facies and the field of acoustic impedance.
2. Generate p from $f(p|r)$ defined by expression (6); the corresponding production performance.
3. Accept the five-tuple $(p,r,z_{\text{top}},c,\theta)$ by some rule including $f(d_p|p)$ as e.g. McMC or Rejection Sampling.
4. If accepted, the pair (p,r) is a realization from the target pdf $f(p,r|d)$.

Note that the sampling procedure is following the arrows in Figure 1 illustrating the stochastic model. A trained statistician can by only looking at this figure and knowing where Gaussian and/or linear relations are made, suggest this sampling scheme. More general McMC algorithms can be used giving more complex acceptance probabilities. The specific sampling scheme used in this study is Rejection sampling defined by

1. Generate $(r, z_{\text{top}}, c, \theta)$ from $f(r, z_{\text{top}}, c, \theta | d_s, d_w, c^o)$ as described above
2. Calculate $p = v(r, t), \quad t \leq t_o$, i.e. no modeling error is assumed. See Table 5 for production characteristics.
3. Accept the pair (p, r) with probability
   $f(d_p|p)/\max_p f(d_p|p) = \exp\{-0.5 \cdot (d_p - p)^T \Sigma_{P^o}^{-1} (d_p - p)\}$

2.5 Comments on the stochastic model

Notice that the prior model gives a mosaic of the two facies. This is not in accordance with what is known about the Troll field. This is a layered structure of two facies; M-sand and C-sand. Modeling these kinds of reservoirs seems inappropriate with the simple Gaussian model defined above. An object based model seems better suited. Object based models are however harder to condition consistently on several sources of reservoir specific observations, see Syversveen and Omre (1997a), Syversveen and Omre (1997b), Syversveen (1998) and Eide (1999). Gaussian fields are flexible, since all configurations have a positive probability. By conditioning to data through the likelihood functions, realizations from the stochastic model will reflect the information contained in the data. Having enough high-quality data realizations will be close to the truth, even if the truth is poorly represented by the prior model. For related ideas see literature on image analysis Ripley (1988), and references therein.

3 Base case

The geological model and production conditions are presented, and base case parameter values are defined.

3.1 Geological model

The geological model is defined on a uniform $50 \times 50 \times 15$ grid in the two horizontal and the vertical direction respectively. All correlation functions unless otherwise stated, are exponential on the form

$$\rho(x_i, x_j) = \exp(-3\|x_j - x_i\|_a^\nu)$$

where $a = (a^{(1)}, a^{(2)}, a^{(3)})$,

$$\|y\|_a = \sqrt{\left(\frac{y^{(1)}}{a^{(1)}}\right)^2 + \left(\frac{y^{(2)}}{a^{(2)}}\right)^2 + \left(\frac{y^{(3)}}{a^{(3)}}\right)^2}$$

and $a^{(1)}$ and $a^{(2)}$ can be interpreted as horizontal ranges and $a^{(3)}$ as the vertical range, all given in number of grid blocks. For all variables listed below, $a^{(1)} = a^{(2)} = 100$ and $a^{(3)} = 5$. The parameter ν will vary and be indexed e.g. ν_C for the parameter related to reflection coefficients C. The parameter values used unless anything else is stated, are listed in the tables below.

Reservoir characteristics; R					
Porosity; Φ		Permeability; K		Acoustic impedance; Z	
σ_Φ	0.015	$\sigma_{K,1}$	0.5	$(z_{\text{top}})_{ij}$	6473 for all (i,j)
ν_Φ	1.2	$\sigma_{K,2}$	0.62		
a	0.5430	ν_K	1.2		
b	$-4.5263 \cdot 10^{-5}$	z_{th}	5920		
		σ_{Θ_1}	0.6		
		σ_{Θ_2}	0.5		
		μ_{Θ_1}	8.5		
		μ_{Θ_1}	5.3		

Table 1: Base case parameter values for reservoir characteristics.

Well observations; D_w	
Well type	Position of observations
Injection well	$x^{(1)} = 23,\ x^{(2)} = 3, x^{(3)} = 1, \dots, 15$
Production well 1	$x^{(1)} = 8,\ \ x^{(2)} = 1, \dots, 50,\ x^{(3)} = 14$
Production well 2	$x^{(1)} = 43,\ x^{(2)} = 1, \dots, 50,\ x^{(3)} = 14$
$g_\Phi(\phi)$	ϕ
$g_K(k)$	k
$g_Z(z)$	z
σ_{Φ^0}	0
σ_{K^0}	0

Table 2: Grid position and base case parameter values for well observations. The latter entries represent exact point observations in the wells. The spatial position x is indexing the grid blocks with $x^{(1)}, x^{(2)}$ indicating horizontal directions and $x^{(3)}$ the vertical direction. Note that even if acoustic impedance is observed in all wells, the corresponding reflection coefficients can be calculated in the vertical injection well only.

Reflection coefficients; C	
σ_C	0.045
ν_C	1.4
$\rho_C(x_i, x_j)$	$\text{const} \cdot (2\rho(x_i, x_j) - \rho((x_i^{(1)}, x_i^{(2)}, x_i^{(3)} + 1), x_j) - \rho(x_i, (x_j^{(1)}, x_j^{(2)}, x_j^{(3)} + 1))$

Table 3: Base case parameter values for reflection coefficients. The spatial position x is indexing the grid blocks, and $x^{(3)} + 1$ indicates one grid block below $x^{(3)}$.

Seismic data, D_S	
σ_S	0.15
$\rho_S(x_i, x_j)$	0 if $x_i \neq x_j$, 1 otherwise.
Seismic pulse peak frequency	40 Hz
Grid cell thickness	1 ms

Table 4: Base case parameter values for seismic data.

Note that according to Table 2 the well observations are assumed to be without error. If there were no upscaling involved, this assumption would have given less uncertainty and better reproduction of production history than actually achieved in this study. By upscaling the geological grid prior to fluid flow, the numerical value of a grid cell in the fluid flow grid penetrated by a well, is an average of 25 grid cells in the geological grid, only one being the exact well observation, the rest being simulated values. Hence uncertainty in well observations should not only be introduced as an observations error, but also by which degree fine scale well observations represents coarse scale values. This is important to bear in mind if the geological grid is e.g. as coarse as the fluid flow grid. Then uncertainty in well observations are not only observation error, but also the non-representativity for a fine scale observation to a coarse scale grid.

3.2 Production

The fluid flow is modeled on a $10 \times 10 \times 15$ grid upscaled from the $50 \times 50 \times 15$ geological grid. The injection well is perforated in the top five grid layers only, while the production wells are perforated in the entire trace. Fluid flow is modeled by using ECLIPSE, see the model file in Appendix A. An outline of the reservoir with injection and production well is given in Figure 2.

Production characteristics; P	
Upscaling	
Reservoir characteristics	Procedure
Porosity	arithmetic
Permeability	harmonic
σ_P	0

Table 5: Upscaling and base case parameter value for production characteristics. The latter entry indicates no modeling error, i.e. the fluid flow simulator is perfect.

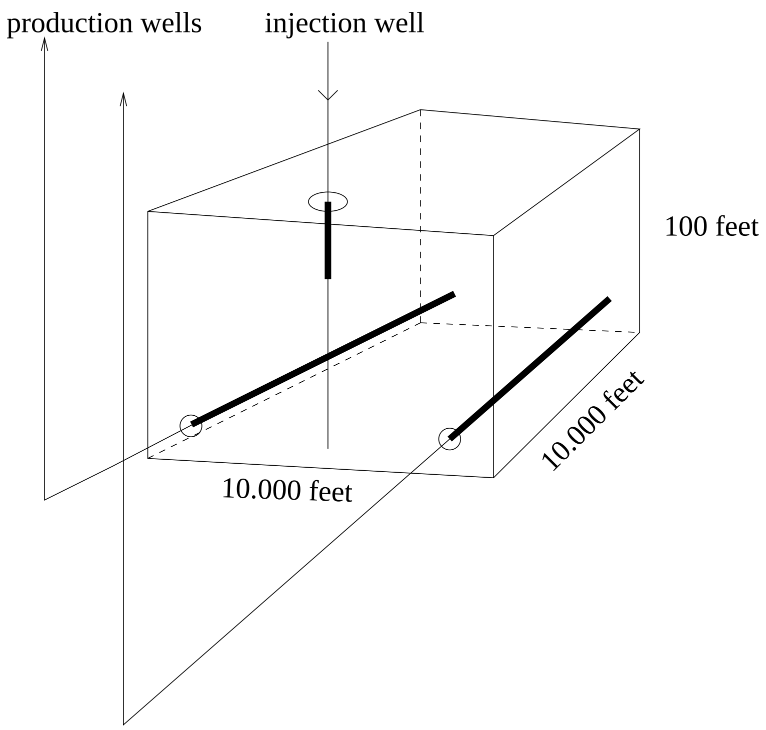

Figure 2: Outline of reservoir model. The thick lines indicates where the wells are perforated.

Production history; D_p	
Observed variables	Oil production rate in well 1 (opr1) Oil production rate in well 2 (opr2) Gas-oil ratio in well 1 (gor1) Gas-oil ratio in well 2 (gor2) Bottom hole pressure in injection well (bhp)
Observation period $\leq t_o$	911, 1216 or 1642 days
σ_{opr1}	2.5% of observed opr1
σ_{opr2}	2.5% of observed opr2
σ_{gor1}	50 days (from breakthrough time)
σ_{gor2}	50 days (from breakthrough time)
σ_{bhp}	2.5% of observed bhp

Table 6: Observed production characteristics and base case parameter values. Note that gor1 and gor2 are only used to give information on breakthrough time. Hence the absolute value of gas-oil ratio is not used.

4 The true reservoir

4.1 Background

The construction of the true reservoir is inspired by the Troll-field. It has a layered structure with alternating high-permeable and low-permeable facies called C-sands and M-sands. The true reservoir consists of three layers having the high-permeable layer in the middle. The geology is modeled on a $50 \times 50 \times 15$-grid, each layer being five grid cells high. The fluid flow is modeled on a $10 \times 10 \times 15$-grid. See Figure 2 and Table 2 for outline of reservoir and position of wells. The reservoir is mainly drained from top to bottom.

4.2 Construction

The true reservoir is constructed by generating three independent fields of reflection coefficients with standard deviation $\sigma_C = 0.035$. The first field represents the top layer on a $50 \times 50 \times 5$ grid and additional 10 grid layers giving a total of $50 \times 50 \times 15$-grid. The additional ten grid layers are used so seismic amplitude data can be generated in a meaningful way. The second field is generated on a $50 \times 50 \times 5$-grid representing the middle layer. The third field is generated on a $50 \times 50 \times 15$-grid representing the bottom layer. Figure 3 illustrates the extended grid used for seismic data generation. The central grid corresponds to the reservoir defined in the base case.

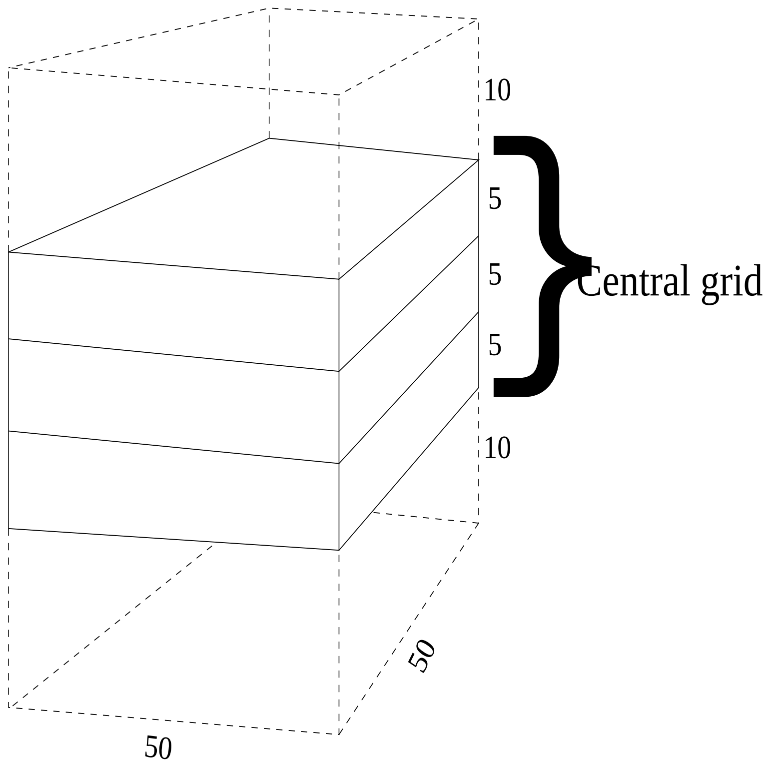

Figure 3: Outline of extended grid used for true reservoir. The numbers indicate the number of grid cells in each interval. The central grid corresponds to the base case reservoir in Figure 2

High negative and positive values are added at the interfaces of the top and middle layer and the middle and bottom layer respectively. Hence the resulting field is non-Gaussian. A histogram of the reflection coefficients on the central $50 \times 50 \times 15$-grid is displayed in Figure 4.

Acoustic impedance is calculated according to relation (8) on the $50 \times 50 \times (10+5+5+5+10)$-grid with z_{top} being a constant field of value 6473 on the top of this grid. A histogram of the resulting acoustic impedance on the central $50 \times 50 \times 15$-grid is displayed in Figure 5. Note that the histogram indicates a bi-modal distribution for acoustic impedance. Grouped by facies the histograms in Figure 5 displays uni-modal distributions within each facies. Note that the histograms are overlapping. The vertical line indicates z_{th} being the threshold value for classifying facies given acoustic impedance. See also Section 2.1.1.

Note that seismics are calculated on the central $50 \times 50 \times 15$-grid and all other conditional data as well observations are given on this central grid only.

The porosity field is generated according to relation (3) on the central grid. A histogram of the porosity values is displayed in Figure 6. Note that the histogram indicates a bi-modal distribution for porosity. Grouped by facies the histograms in Figure 6 displays uni-modal distributions within each facies. Note that the histograms are overlapping.

Log-permeability is generated by tree independent Gaussian fields with expectation $\theta_1 = 8.5$ in the high-permeable layer and $\theta_2 = 5.3$ in the low-permeable layers. Figure 7 displays two non-overlapping distributions of log-permeability clearly demonstrating different properties of permeability in different facies.

4.3 Facies-classification

Seismic data give indirectly information on acoustic impedance. Since histograms of acoustic impedance from different facies are overlapping, misclassification is expected, even if high-frequency low-noise seismic data are available. Figure 8 displays a cross plot of acoustic impedance values and log-permeability values. On the vertical axis for log-permeability the facies are clearly distinct, while on the horizontal axis for acoustic impedance there is a considerable overlap. The vertical line indicates the threshold value z_{th} used for classification based on estimated acoustic impedance. Better classification is hence obtained by using permeability instead of impedance, but permeability observations are only available in wells, while estimates of impedance are available over the entire reservoir after seismic amplitude data are observed.

4.4 A comment on standard deviation for reflection coefficients

Using derived well observations of reflection coefficients, estimates for σ_C will generally be higher than 0.035 which is used for the true reservoir. This is due to the large negative and positive values for reflection coefficients added at facies interfaces. As the tables in Section 3 indicate, the value 0.045 is used as the estimated value for σ_C in the prior model.

4.5 Displaying the true reservoir and observations

Figure 9 displays a cross section of the true reservoir for reflection coefficients, acoustic impedance, porosity and log-permeability. The impedance and porosity plots clearly illustrates the layered structure induced by adding extreme values for reflection coefficients at facies interfaces. Figure 10 displays corresponding trace plots of reflection coefficients and acoustic impedance in vertical traces corresponding to the cross section. Trace 1 displays values in the the first column from the left in the cross section, trace 10 displays the tenth column from the left in the cross section etc. In trace plots for acoustic impedance, the vertical line indicates the classification threshold z_{th}. In trace plots for reflection coefficients, the vertical line indicates the zero level. The horizontal lines corresponds to facies interfaces. Figure 11 displays the true but unobserved production characteristics for 16.0 years. This corresponds to the variable P in Figure 1.

Figure 12 displays observed acoustic impedance and log-permeability in the wells. Observed porosity is not displayed. Figure 13 displays a cross section of observed seismics and the corresponding field of reflection coefficients. Note the smearing of the high positive and negative values of reflection coefficients. Figure 14 displays 4.5 years of observed production history. Each dot indicates an observation. The vertical lines indicates 2.5 years and 3.33 years respectively. All these history periods are used under. Note that not all observation points are used in the history matching procedure because of the strong correlation in time between observation points.

4.6 Final comments

Note that the true reservoir is not constructed by generating a realization from the prior model defined in Section 2.1.1. First of all the reflection coefficients are not generated by taking realizations of a Gaussian field. It is constructed by three independent Gaussian fields added extreme values at the interfaces. Secondly the facies are not classified using acoustic impedance as in (4) and (5). The geometry and layering are given in advance. Hence there are high-permeable areas with high acoustic impedance and low-permeable areas with low acoustic impedance, and there will be misclassification even with extremely high quality seismics. See also Figure 8. Realizations from the prior model have extremely low probability of having facies with both high permeability and acoustic impedance values above z_{th}. Hence the true reservoir has nearly zero probability density in the prior stochastic model. However, when only considering porosity and permeability in the true reservoir, these fields do have a much larger probability density in the stochastic model since the conflict with acoustic impedance is not considered.

The most realistic prior stochastic model would hence be an object based model with one facies within each body, see also the discussion in Section 2.5. Gaussian fields are however flexible and even a poorly specified prior model can give realistic realizations conditioning on reservoir specific observations.

5 Exploring the stochastic model conditioned on the model parameters Θ.

In this section the model parameters $\Theta = (\Theta_1, \Theta_2)$ being the expected level of the log-permeability in the high-permeable and low-permeable areas respectively, are fixed at the true values. To explore the influence of different information sources, different combinations of well observations and seismic data are considered. Production history are not included in this section. Production history are included in Section 6 and Section 7. The behavior of production characteristics from models conditioned on $\Theta = \theta$ and different amounts of reservoir specific data are explored and discussed.

5.1 Exploring the prior stochastic model; $f(r|\theta)$, $f(p|\theta)$

In this section properties of realizations from the prior stochastic model are explored and compared with the true reservoir. In Figure 15 a realization displaying a cross section of reflection coefficients, acoustic impedance, porosity and log-permeability is presented. The realization is qualitatively different from the true reservoir displayed in Figure 9, by having a mosaic of high-permeable and low-permeable facies.

Figure 16 displays the vertical traces corresponding to the cross section in Figure 15. The layered structure clearly visible in true reservoir, see Figures 9 and 10, is absent.

Figure 17 displays the production characteristics from one hundred realizations from the prior model conditioned on the true θ-values. The black circles overlayed by a white line indicates the production characteristics of the true reservoir. Notice the generally early breakthrough times, and especially the behavior of bottom hole pressure (bhp) frequently starting at higher values and descending faster than for the true reservoir.

Realizations from the prior stochastic model conditioned on the true model parameters θ, display a considerable variability in production characteristics. The production response from the true reservoir seems to be within this uncertainty range, but the response is clearly not similar to a typical realization from the stochastic model.

5.2 Exploring the stochastic model conditioned on seismic amplitude data; $f(r|\theta, d_s)$, $f(p|\theta, d_s)$

In this section properties of realizations from the stochastic model conditioned on $\Theta = \theta$ and $S^o = d_s$ are explored and compared with the true reservoir and realizations from the prior model. Consider the Figures 18, 19 and 20. Note that the high permeable layer is getting more structured than for realizations from the prior model. By inspecting plots of acoustic impedance, it is clear that the layered structure is reproduced to some extent. The classification into facies is however clearly far from perfect. Consider the impedance traces in Figure 19. It got too large areas of low-impedance facies compared with the true reservoir, hence giving a considerable misclassification into high-permeable facies. Notice that the extreme values of reflection coefficients at interfaces can be recognize in Figure 19.

Due to the more layered structure, breakthrough times are delayed compared with realizations from the prior stochastic model. Notice especially the behavior of bottom hole pressure (bhp) getting closer to the true response.

The variability is reduced compared with realizations from the prior model. The production response from the true reservoir seems to be within this uncertainty range, but the response is clearly not similar to a typical realization from the stochastic model, at least not for oil production rates.

5.3 Exploring the stochastic model conditioned on high-frequency, low-noise seismic amplitude data; $f(r|\theta, d_s^*)$, $f(p|\theta, d_s^*)$

In this section properties of realizations from the stochastic model conditioned on θ and high-frequency, low-noise seismics are explored and compared with results above. The seismics in this section, are observed with seismic pulse peak frequency 800 Hz, compared with 40 Hz in all other cases, and observations noise with standard error $\sigma_S = 0.025$ compared with 0.15 in all other cases.

Consider Figures 21, 22, and 23. The layered structure can be recognized in the cross section, but it is far from perfect. Note especially that the structure of reflection coefficients in the trace plots, is extremely well reproduced, but with a higher variance. This is caused by using $\sigma_C = 0.045$ while it was only 0.035 in the true reservoir. Hence the impedance cannot be perfectly reproduced. Even if σ_C is set to 0.035 and the impedance field z_{top} is known, misclassification will be introduced since impedance values are overlapping between facies. Hence this procedure will interpret low-permeable facies as high-permeable facies where impedance is low.

Consider Figure 24. Note that the uncertainty in production characteristics is drastically reduced and better centered around the true value compared with the case with base case seismics in Figure 20. This is true for all production characteristics except bottom hole pressure, which seems to be systematically below the observed pressure, although with a smaller variance. This is probable due to no reproduction of well observations and systematic misclassifications in areas where the true reservoir got high-impedance values in the high-permeable facies and visa versa.

5.4 Exploring the stochastic model conditioned on well observations; $f(r|\theta, d_w)$, $f(p|\theta, d_w)$

In this section properties of realizations from the stochastic model conditioned on θ and well observations d_w are explored and compared with results above. Consider Figures 25, 26 and 27. Note that the structure of the middle layer can be recognized. The uncertainty in production characteristics is drastically reduced and there is a good fit in bottom hole pressure the first 1000 days. There seem to be a tendency of too early breakthrough. The well observations do, however, carry a substantial amount of information of both structure and production behavior since the true reservoir is layered and the correlation length is large compared with the size of the reservoir. Hence the well observations carry some global information on the structure of the true reservoir in this case.

The production response from the true reservoir seems to be similar to a typical realization from the stochastic model conditioned on well observations and the true model parameter θ.

5.5 Exploring the stochastic model conditioned on seismic amplitude data and well observations; $f(r|\theta, d_s, d_w)$, $f(p|\theta, d_s, d_w)$

In this section properties of realizations from the stochastic model conditioned on θ, well observations d_w and seismics d_s are explored and compared with results above. Consider Figures 28, 29 and 30. Note that the structure of the middle layer is well reproduced. The uncertainty in production characteristics is drastically reduced and there is a good fit in bottom hole pressure the first 1000 days. The production characteristics seems to be better centered around the true value and breakthrough times are delayed compared with conditioning on well observations only.

6 Exploring stochastic model conditioned on production history; d_p

In this section the model parameters $\Theta = (\Theta_1, \Theta_2)$ being the expected level of the log-permeability in the high-permeable and low-permeable areas respectively, are regarded as stochastic. Production history are always included, that is all realizations are "history matched". To explore the influence of different information sources different combinations of well observations and seismic data are considered. The behavior of production characteristics from models conditioned on different amounts of reservoir specific data are explored and discussed.

To include the production history in the conditioning, the accept-reject step is taken in the simulation algorithm outlined in Section 2.4. Recall that the proposed realizations are conditioned on well observations and seismic data directly due to Gaussian and linear assumptions. The fraction of accepted proposals is hence a measure of how well features important for fluid flow are reproduced when conditioning on these information sources only. High acceptance rate for a short production history indicates that important features near the wells are well reproduced. The acceptance rate when a long production history is included, indicates how well these features are reproduced in areas remote to the wells.

To obtain a background and better understanding of the acceptance rates, the corresponding discussion and plots of production characteristics in Section 5 should be studied. There the realizations are fixed at the true parameter values θ, and production history are not included, but the overall behavior is easily recognized and interpreted.

6.1 Exploring stochastic model conditioned on production history only; $f(r|d_p)$, $f(p|d_p)$

The acceptance rate is almost zero. Hence the true reservoir is in a low probability area in the prior model. Note that even for realizations giving a good match for oil production rates, other production characteristics for the same realization tend to be far away. This simultaneous behavior is not visible in Figure 17 discussed in Section 5.1, but becomes clear when production history is included in the conditioning.

6.2 Exploring stochastic model conditioned on production history and seismic data; $f(r|d_p, d_s)$, $f(p|d_p, d_s)$

The acceptance rate is still unacceptably low, even for short production histories. Some structure is captured, but production characteristics are still significantly different from the true case.

6.3 Exploring stochastic model conditioned on production data and well observations; $f(r|d_p, d_w)$, $f(p|d_p, d_w)$, $f(\theta|d_p, d_w)$

For production forecast consider Figure 31, 32 and 33 for 2.5, 3.33 and 4.5 years of observed production history respectively. This corresponds to 911, 1216 and 1642 days. Acceptance rate is 74% for 2.5 years of production history, 10% for 3.33 years and and 1.5% for 4.5 years.

The well observations are giving much information on features important for fluid flow areas near the wells.

For the model parameters consider Figures 34, 35 and 36 for 2.5, 3.33 and 4.5 years of production history respectively. In each plot the first display shows $f(\theta_1)$ being the smooth curve with the lowest mode, $f(\theta_1|d_w)$ being the other smooth curve and a density estimate of $f(\theta_1|d_p, d_w)$ being the irregular curve. The second display is similar, but for θ_2. The prior expectation for (θ_1, θ_2) is (8.3,5.5). The third display is a cross plot of the accepted samples θ_1 and θ_2 from $f(\theta_1|d_p, d_w)$. The parameter values in the true reservoir are 8.5 and 5.3 respectively. There does not seem to be any clear difference between $f(\theta|d_w)$ and $f(\theta|d_p, d_w)$. Hence production history do not seem to bring much information on the mean permeability values in this case.

6.4 Exploring stochastic model conditioned on all available data; $f(r|d)$, $f(p|d)$, $f(\theta|d)$

The corresponding joint pdf $f(p, r|d)$ is discussed in Section 2.3. For production forecast consider Figure 37, 38 and 39 for 2.5, 3.33 and 4.5 years of observed production history respectively. Acceptance rate is 88% for 2.5 years, 20% for 3.33 years and 3% for 4.5 years. The combination of seismic data and well observations seems to capture most of the important features of the real reservoir. Comparing this with results in Section 6.3 for both 3.33 and 4.5 years of production history the acceptance rate is doubled when seismic data are added to well observations. Note however, that even when well observations, seismic data and 4.5 years of production history are included, the long term behavior, i.e. after 5000 days, of the first production well is qualitatively different from the observed production history, see the first and fourth display (opr1 and gor1) in Figure 39. The gas-oil-ratio is increasing faster in the true reservoir than for the realizations from the posterior model. Similarly the oil production rate is decreasing faster. This discrepancy is probable due to the fact that the true reservoir is not constructed by generating a realization from the prior model and some features of the true reservoir are difficult to captured within this stochastic model. To investigate this further a randomization over true reservoir models should be performed.

For the model parameters consider Figures 40, 41 and 42 for 2.5, 3.33 and 4.5 years of production history respectively. The displays are as in Section 6.3 except that the irregular curves are density estimates of $f(\theta_1|d)$ and $f(\theta_2|d)$. For 2.5 and 3.33 years of production history, these data do not seem to bring much information on the mean permeability values. Note however that production history is well reproduced up to 3 years even before production history are included. For 4.5 years of production history there seem to be introduced a non-linear relation between θ_1 and θ_2 being u-shaped. This is not visible on the marginal pdf for θ_2, but the marginal pdf for θ_1 seems to have two modes. This could however, be a coincidence.

7 Making well observations more local

In this section the true reservoir is unchanged, but the information contents of the well observations are made more local in the stochastic model. This is achieved by halving the correlation lengths of the reservoir characteristics. This corresponds to use a bigger reservoir and not changing correlation lengths, but this can not be performed without changing the true reservoir making comparison difficult.

Hence the correlation lengths in the prior stochastic model is halved from 100 to 50 in the horizontal directions and from 5 to 3 in the vertical direction. It is intuitive that the more local the information contents of the well observations, the less the influence of the well observations on the reduction of uncertainty in the posterior model.

The model parameters $\Theta = (\Theta_1, \Theta_2)$ being the expected level of the log-permeability in the high-permeable and low-permeable areas respectively, are fixed at the true values (8.5,5.3) in Sections 7.1 and 7.2. In Section 7.3 the pdf $f(\theta|d_w)$ is used.

To explore the influence of different information sources, different combinations of well observations and seismic data are considered.

7.1 Exploring stochastic model conditioned on well observations; $f(r|\theta, d_w)$, $f(p|\theta, d_w)$

The parameter θ is fixed at the true value and only well observations are included. Consider Figure 43. The production history is well reproduced the first two years. There is however, a tendency for a too early breakthrough. Hence features important for fluid flow are well reproduced around wells giving a good match at early times. There is however not much information about areas remote to the wells.

7.2 Exploring stochastic model conditioned on well observations and seismic data; $f(r|\theta, d_s, d_w)$, $f(p|\theta, d_s, d_w)$

The parameter θ is fixed at the true value and both well observations and seismic data are included. Consider Figure 44. Compared with Figure 43 breakthrough is delayed, and production characteristics are centered around the true production history. Hence the seismic data are adding global information of structure important for fluid flow, also in areas remote to the wells. The bottom hole pressure seems however, to be systematically too high at early times.

7.3 Exploring stochastic model conditioned on all available data; $f(r|d)$, $f(p|d)$

Consider Figure 45, 46 and 47 for 2.5, 3.33 and 4.5 years of observed production history respectively. Acceptance rate is 60% for 2.5 years, 10% for 3.33 years and 1% for 4.5 years. The combination of seismic data and well observations seems to capture most of the important features of the real reservoir even if the correlation length is halved compared with the true reservoir.

Comparing this with results in Section 7.1 where nearly 0% would be accepted because of a too early breakthrough, demonstrates the importance of the seismic data.

The bottom hole pressure is still systematically too high, but less obvious for 4.5 years of production history. This could however be a result of few accepted samples.

Compared with the corresponding results with longer correlation lengths discussed in Section

6.4, the acceptance ratio is reduced, especially for longer production histories. By reducing the correlation lengths the predictive properties are in this case, not unexpectedly, reduced. The reduction in acceptance ratio is however, not as dramatic as for the case with no seismic data in Section 7.1.

Hence when well observations are mainly containing local information, only reservoir characteristics close to the wells and short term production history may be well reproduced, not unexpectedly. A longer production history is clearly more difficult to reproduce using local information only. Seismic data carry global information, and combined with well observations, this capture many of the features important for fluid flow in the reservoir.

8 Closing remarks

A stochastic model for a 3D reservoir integrating well observations, seismic data and production history is presented. The stochastic model is illustrated by a directed graph. Simplifying assumptions are discussed and utilized to define a sampling algorithm. The algorithm is defined by sequential sampling of Gaussian and log-Gaussian fields, and a accept-reject step where Markov chain Monte Carlo or rejection sampling can be used. The time consuming part in the algorithm, is the evaluation of a fluid flow simulator. Including seismic data adds valuable global information on the reservoir characteristics and reduce the number of fluid flow simulation runs for each accepted realization. In some cases the ratio of accepted realizations is doubled when seismic data are added.

A true reservoir, not constructed by generating a realization from the prior model, is defined. Data are observed from this reservoir and various simulation studies including different amount of data is performed.

The simulation study demonstrates that the global structure of the true reservoir is well reproduced, even if it has nearly zero probability density in the prior model. The prior model is flexible and adapt to data. A more realistic model as e.g. a marked point field can be used, but on the expense of complexity and slower algorithms in more general cases. Production characteristics for the first few years are well reproduced including well observations and production history. Even when all data sources are included, long term production performance deviates from production performance of the true reservoir. This is due to imperfection in the prior model formulation compared with the true reservoir. This kind of imperfection is however always present when modeling real petroleum reservoirs.

The simulation study demonstrates that the production history do not carry much information on the expected levels of permeability in the two facies within the range of uncertainty put on these parameters.

The simulation study demonstrates that even when well observations carry little information in areas not being close to the wells, production characteristics are well reproduced when also seismic data are included. The global nature of information contents from seismic data does compensate for the local nature of well observations to some extent. Well observations tends to have a local information contents due to uncertainty in measurements, lack of representativity of the measurements compared with the fluid flow simulation grid and a limited correlation length.

Not unexpectedly, production characteristics are significantly better reproduced when well observations are carrying more global information, even when only well observations are included.

To further investigate this methodology generally and this stochastic model specifically, the number of wells should also be varied. In addition the quality of and production characteristics from infill drilled wells determined from realizations from the posterior stochastic model, could say much about the quality of the posterior model. The quality of seismic data is also important for the results, and this issue should be investigated further, too. To draw more general conclusions several true reservoirs should be constructed and the exercise repeated. All these issues are, however, outside the scope of this project.

References

Abrahamsen, P., A. Buland, E. Bølviken, R. Hauge, A. L. Hektoen, and A. Skorstad (1996). Conditioning stochastic reservoir models on seismic amplitude traces-Stochastic inversion and simulation. Technical report, Norwegian Computing Centre, P.O. Box 114 Blindern,N-0314 Oslo, Norway. NR-note SAND/07/1996,.

Bissell, R., J. E. Killough, and Y. Sharma (1992). Reservoir History Matching Using the Methods of Gradients on a Workstation. *SPE European Petroleum Computer Conference*, pp. 61–65. Stavanger, Norway, May 25-27. SPE 24265.

Bortoli, L.-J., F. Alabert, A. Haas, and A. Journel (1993). Constraining stochastic images to seismic data: Stochastic simulation of synthetic seismograms. In A. Soares (Ed.), *Geostatistics Tróia '92*, pp. 325–337. Kluwer Academic Publishers.

Certes, C. and G. de Marsily (1991). Applications of the pilot point method to the identification of aquifer transmissivities. *Advances in Water Resources 14*(5), pp. 284–300.

Eide, A. L. (1997). Stochastic simulation of porosity and acoustic impedance conditioned to seismic data and well data from the Troll field. Technical Report Statistics 12/97, Norwegian University of Science and Technology.

Eide, A. L. (1999). Ph. D. thesis, Norwegian University of Science and Technology. To appear.

Eide, A. L., B. Ursin, and H. Omre (1997). Stochastic simulation of porosity and acoustic impedance conditioned to seismic data and well data. pp. 1614–1617. Proceedings from the 67th Annual Meeting of the Society of Exploration Geophysicists, Expanded Abstracts, SEG, Dallas, Texas.

Gómez-Hernández, J. J., J. E. Capilla, and A. Sahuquillo (1997). Inverse conditional simulation. In E. Y. Baafi and N. A. Schofield (Eds.), *Geostatistics Wollongong'96*, Volume I, pp. 282–291. Kluwer Academic Publishers. In proceedings from the Fifth International Geostatistical Congress, Wollongong, Australia, 22.-27. September 1996.

Haas, A. and O. Dubrule (1994). Geostatistical inversion - a sequential method of stochastic reservoir modeling constrained by seismic data. *First break 12*(11), pp. 561–569.

Hegstad, B. K. (1997). *Sampling from stochastic reservoir models constrained by production data.* Ph. D. thesis, Norwegian University of Science and Technology.

Hegstad, B. K. and H. Omre (1997). Uncertainty Assessment in History Matching and Forecasting. In E. Y. Baafi and N. A. Schofield (Eds.), *Geostatistics Wollongong'96*, Volume I, pp. 585–596. Kluwer Academic Publisher. Proceedings from the Fifth International Geostatistical Congress, Wollongong, Australia, 22.-27. September 1996.

Landa, J. L. (1997). *Reservoir parameter estimation constrained to pressure transients, performance history and distributed saturation data.* Ph. D. thesis, Stanford University.

de Marsily, G., C. Lavedan, M. Boucher, and G. Fasanino (1984). Interpretation of inference tests in a well field using geostatisical techniques to fit the permeability distribution in a reservoir model. In G. Verly, M. David, A. G. Journel, and A. Marechal (Eds.), *Geostatistics for Natural Resources Characterization*, NATO ASI series. Series C, Mathematical and physical sciences, pp. 831–849.

Oliver, D. S. (1994). Multiple Realizations of the Permeability Field From Well Test Data. *University of Tulsa Centennial Petroleum Engineering Symposium*, pp. 145–153. Tulsa, Oklahoma, USA, August 29-31, 1994. SPE 27970.

Omre, H. and H. Tjelmeland (1997). Petroleum geostatistics. In E. Y. Baafi and N. A. Schofield (Eds.), *Geostatistics Wollongong'96*, Volume I, pp. 41–52. Kluwer Academic Publishers. Proceedings from the Fifth International Geostatistical Congress, Wollongong, Australia, 22.-27. September 1996.

RamaRao, B. S., A. M. LaVenue, G. de Marsily, and M. G. Marietta (1995). Pilot point methodology for automated calibration of an ensemble of conditionally simulated transmissivity fields 1. Theory and computational experiments. *Water Resources Research 31*(3), pp. 475–493.

Ripley, B. D. (1988). *Statistical inference for spatial processes.* Cambridge University Press.

Syversveen, A. R. (1998). *Spatial stochastic points models for reservoir characterization.* Ph. D. thesis, Norwegian University of Science and Technology.

Syversveen, A. R. and H. Omre (1997a). Conditioning of marked point processes within a Bayesian framework. *Scandinavian Journal of Statistics 24*(3).

Syversveen, A. R. and H. Omre (1997b). Marked point models for facies units conditioned on well data. In E. Y. Baafi and N. A. Schofield (Eds.), *Geostatistics Wollongong'96.* Kluwer Academic Publishers. Proceedings from the Fifth International Geostatistical Congress, Wollongong, Australia, 22.-27. September 1996.

Tjølsen, C. and E. Damsleth (1998). Personal communication.

Wen, X., C. V. Deutsch, and A. S. Cullick (1997). High resolution reservoir models integrating multiple-well production data. *SPE Annual Technical Conference.* San Antonio, Texas, October 5-8. SPE 38728.

Xue, G. and A. Datta-Gupta (1997). Structure preserving inversion: An efficient approach to conditioning stochastic reservoir models to dynamic data. *SPE Annual Technical Conference.* San Antonio, Texas, October 5-8. SPE 38727.

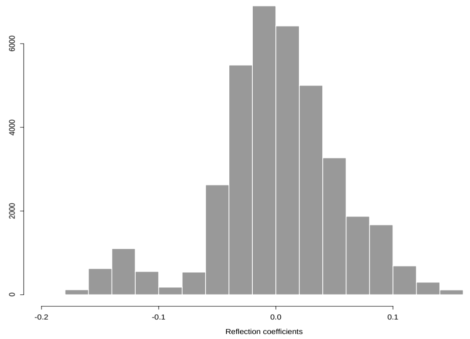

Figure 4: Histogram for reflection coefficients in true reservoir.

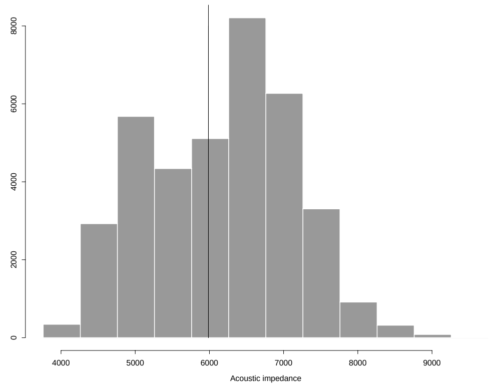

Total histogram

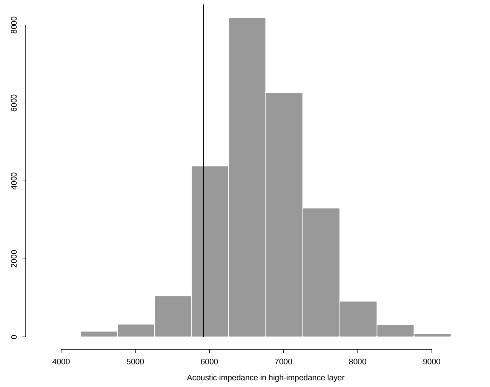

Histogram for high-impedance layers

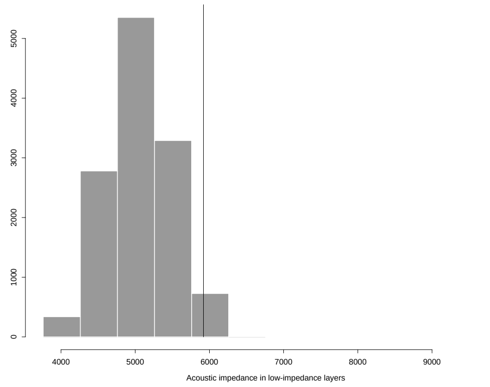

Histogram for low-impedance layers

Figure 5: Histograms for acoustic impedance. The first histogram is from the entire true reservoir. The second is from the high-impedance layers at top and bottom. The last histogram is from the middle layer with low impedance. The vertical line indicates the threshold value z_{th} in the stochastic model.

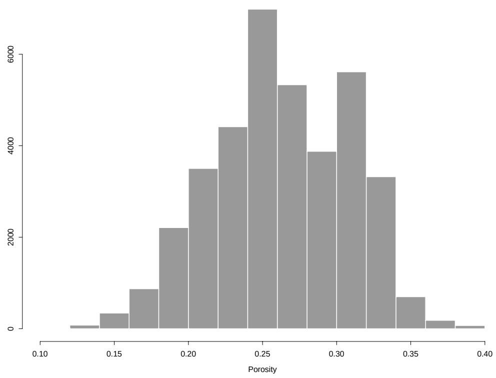

Total histogram

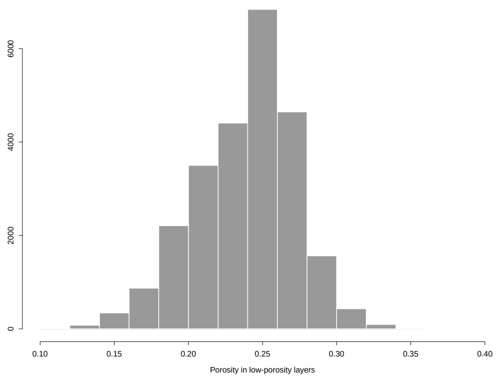

Histogram for low-porosity layers

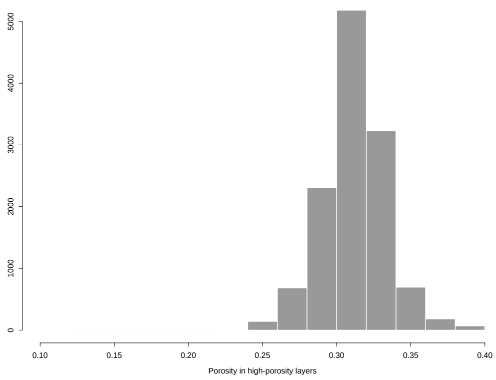

Histogram for high-porosity layers

Figure 6: Histograms for porosity. The first histogram is from the entire true reservoir. The second is from the low-porosity layers at top and bottom. The last histogram is from the middle layer with high-porosity.

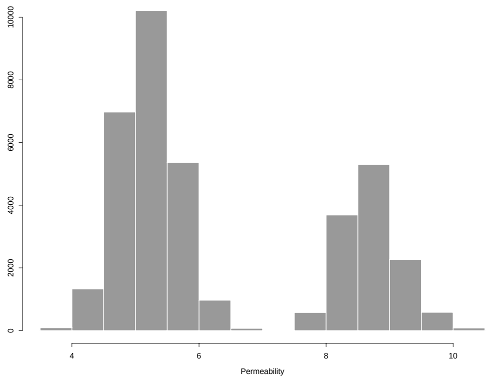

Total histogram

Figure 7: Histograms for permeability. The first mode displays values in the low-permeable top and bottom layers. The second mode displays values from the high-permeable layer in the middle.

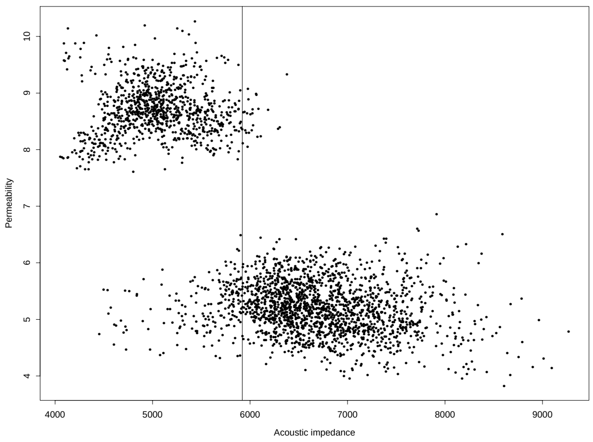

Figure 8: Cross plot of acoustic impedance and log-permeability in the true reservoir. The vertical line indicates the threshold value $z_{\rm th}$ in the stochastic model.

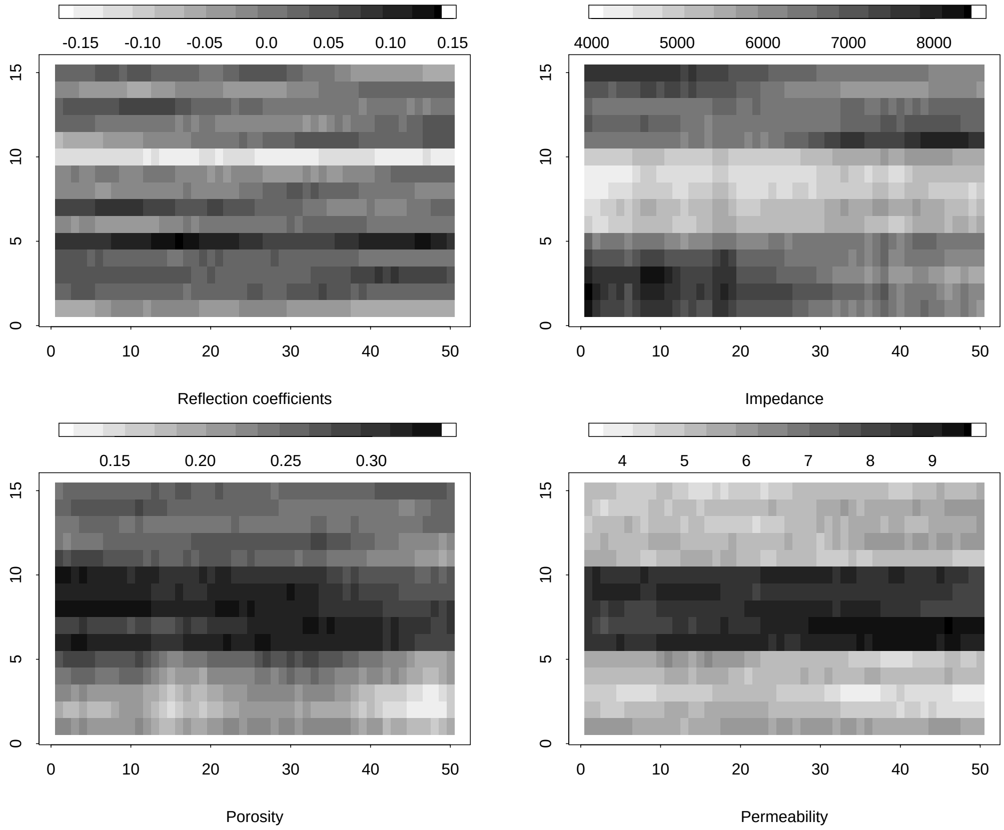

Figure 9: Cross section from the true reservoir displaying reflection coefficients, acoustic impedance, porosity and log-permeability respectively.

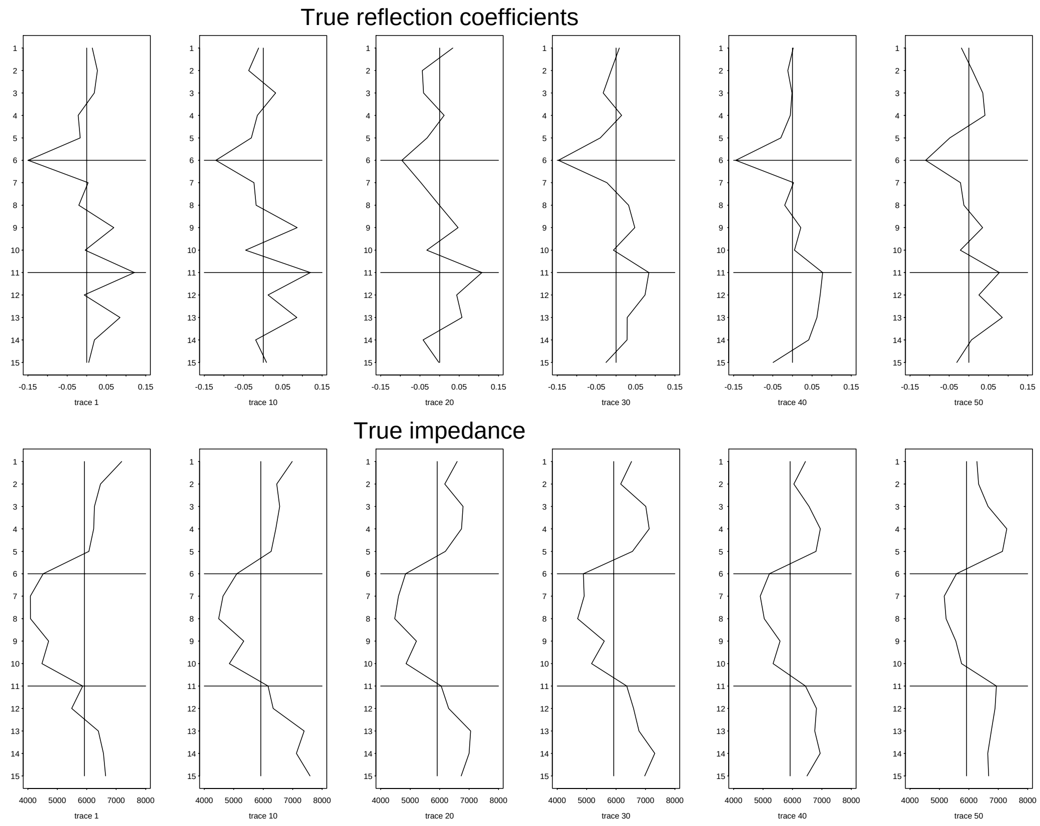

Figure 10: Trace plots of reflection coefficients and acoustic impedance corresponding to the cross plot in Figure 9. The vertical traces are the first, tenth, twentieth, thirtieth, fortieth and fiftieth trace respectively. The vertical lines indicate the threshold value $z_{\rm th}$. In realizations from the stochastic model acoustic impedance below $z_{\rm th}$ is interpreted as high-permeable facies according to expression (5).

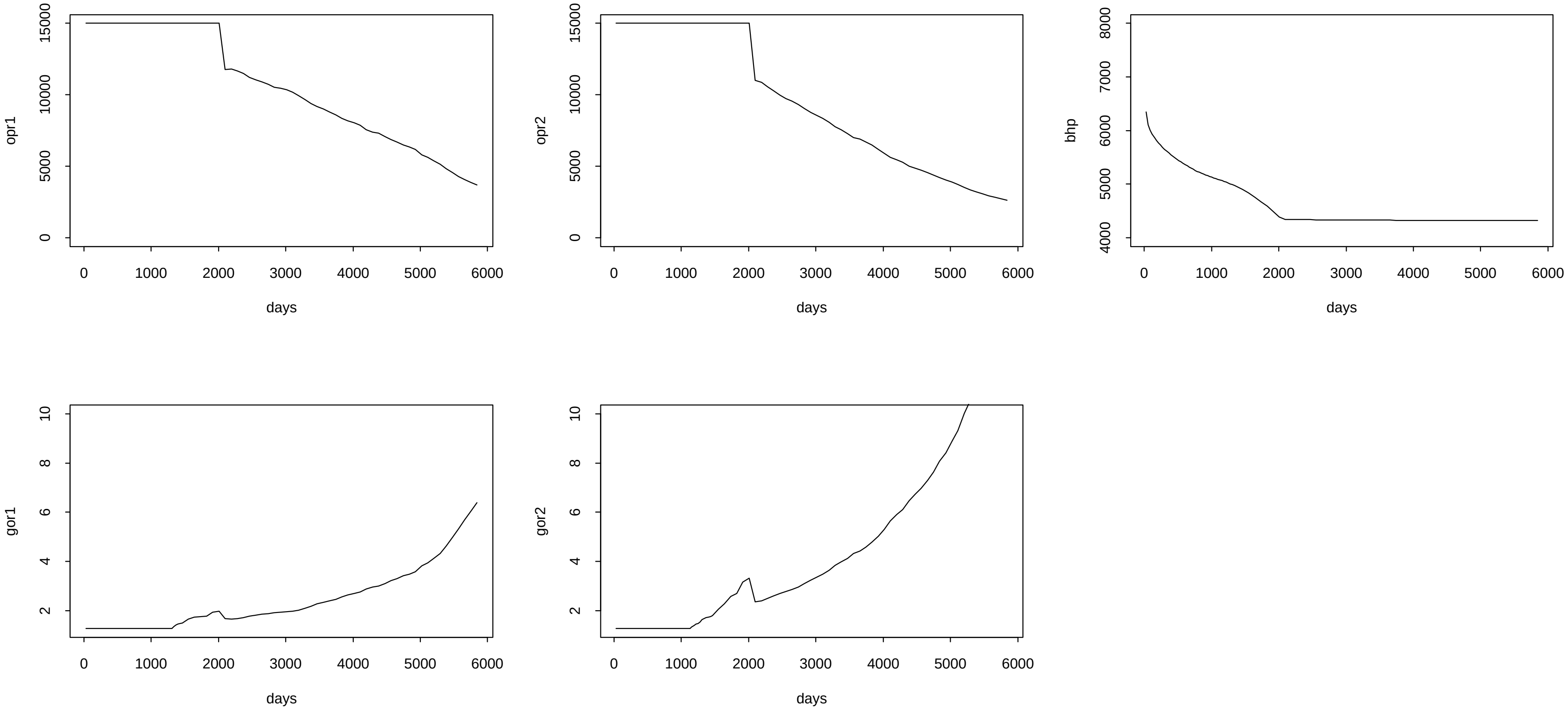

Figure 11: True but unobserved production characteristics from the true reservoir corresponding to the variable P in Figure 1.

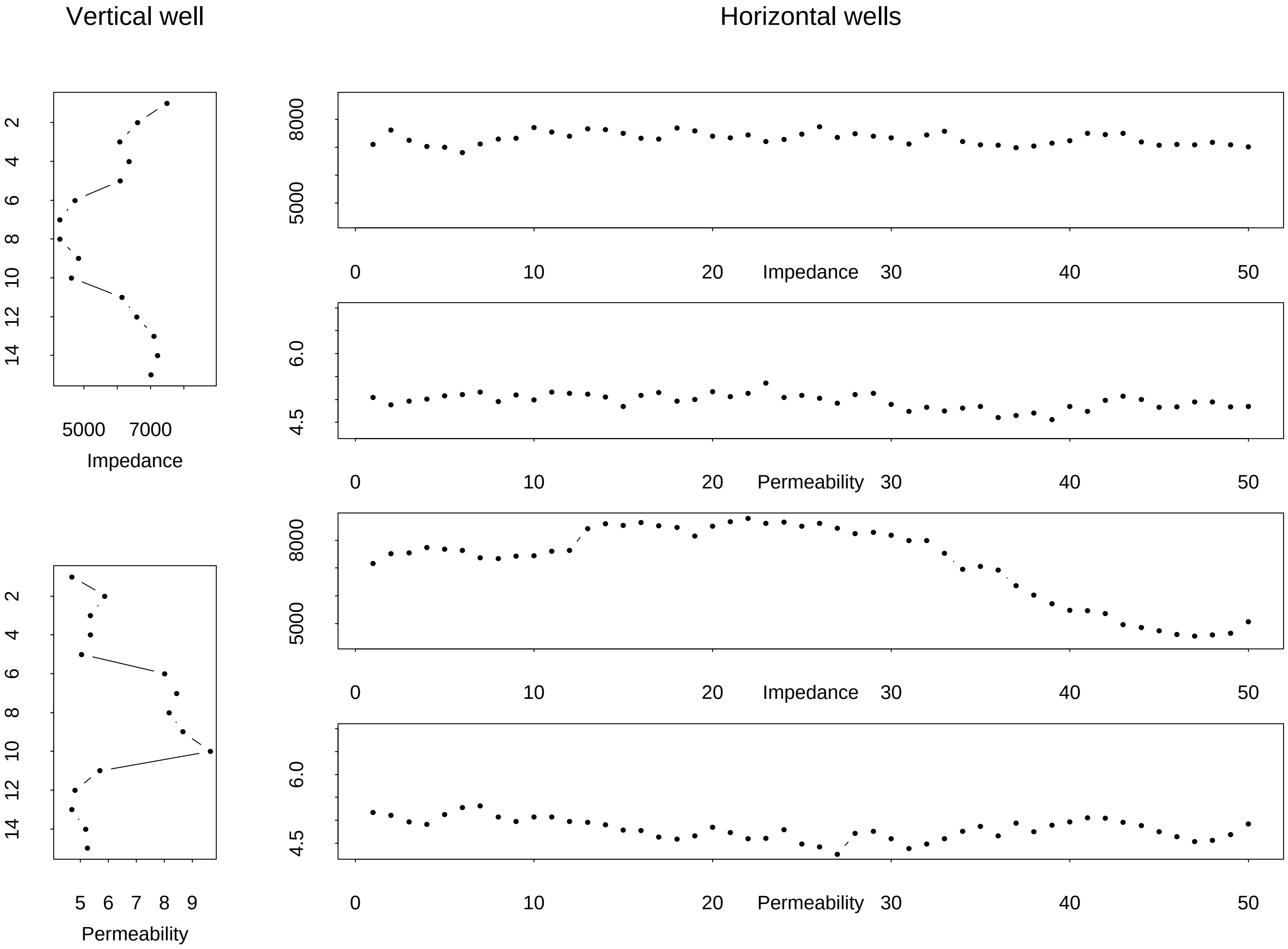

Figure 12: Observed acoustic impedance and log-permeability in the wells. The first two displays on the right hand side corresponds to observations from the same horizontal well.

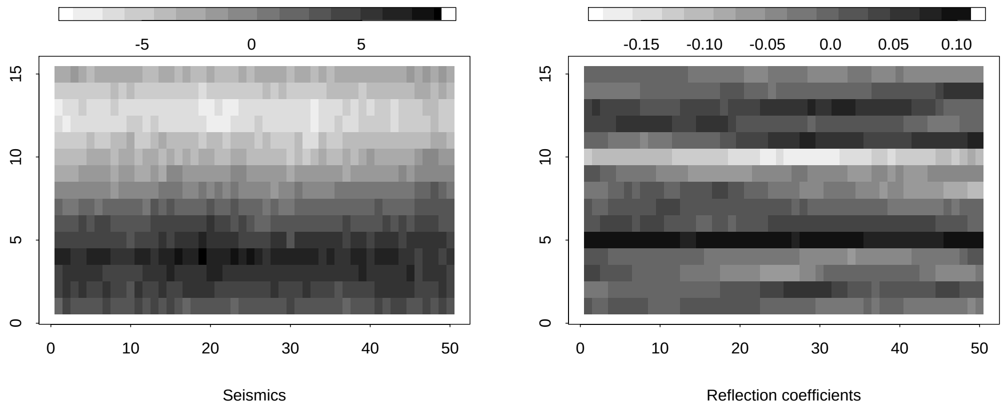

Figure 13: Cross section from the true reservoir displaying seismic data and reflection coefficients.

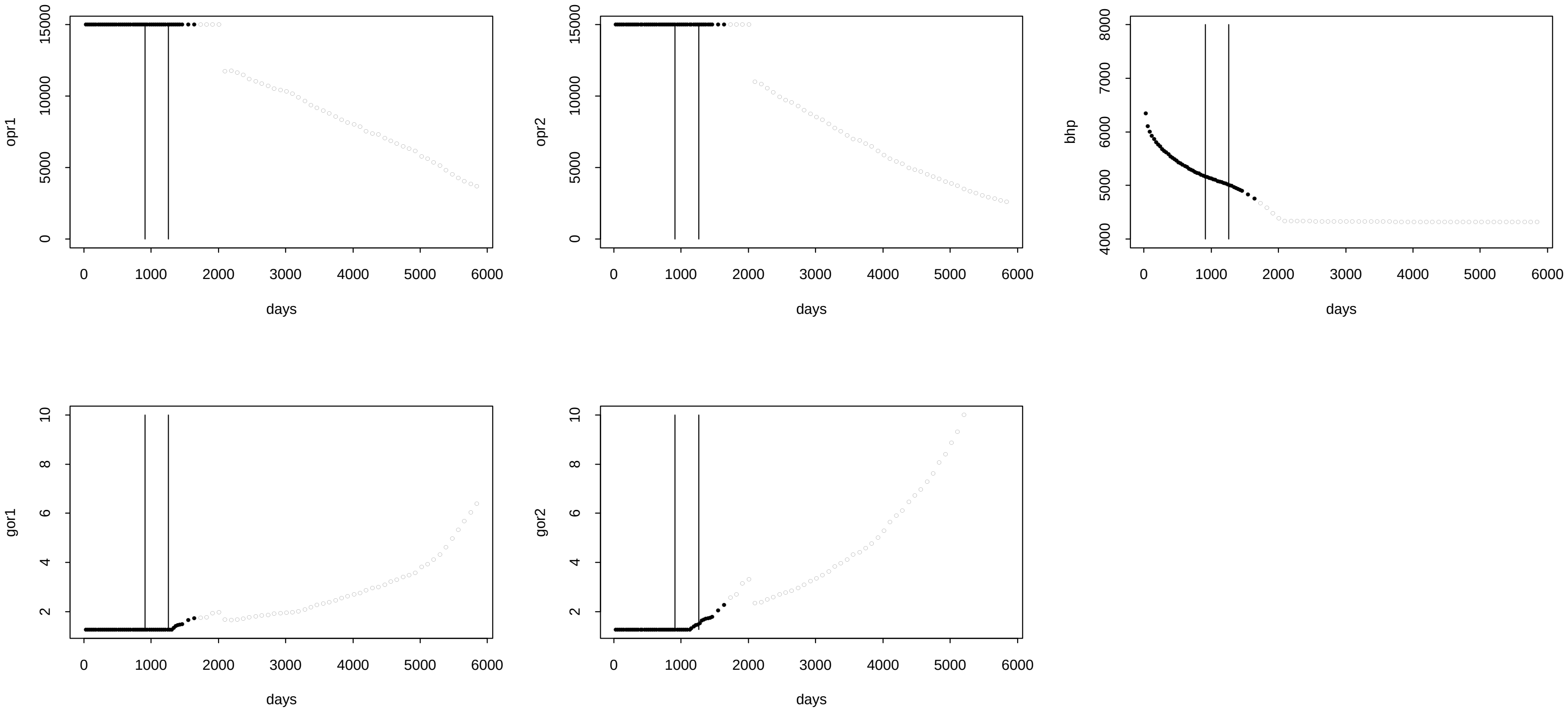

Figure 14: 4.5 years of observed production characteristics from the true reservoir. Each dot represents an observation. The vertical lines correspond to 2.5 years and 3.33 years respectively.

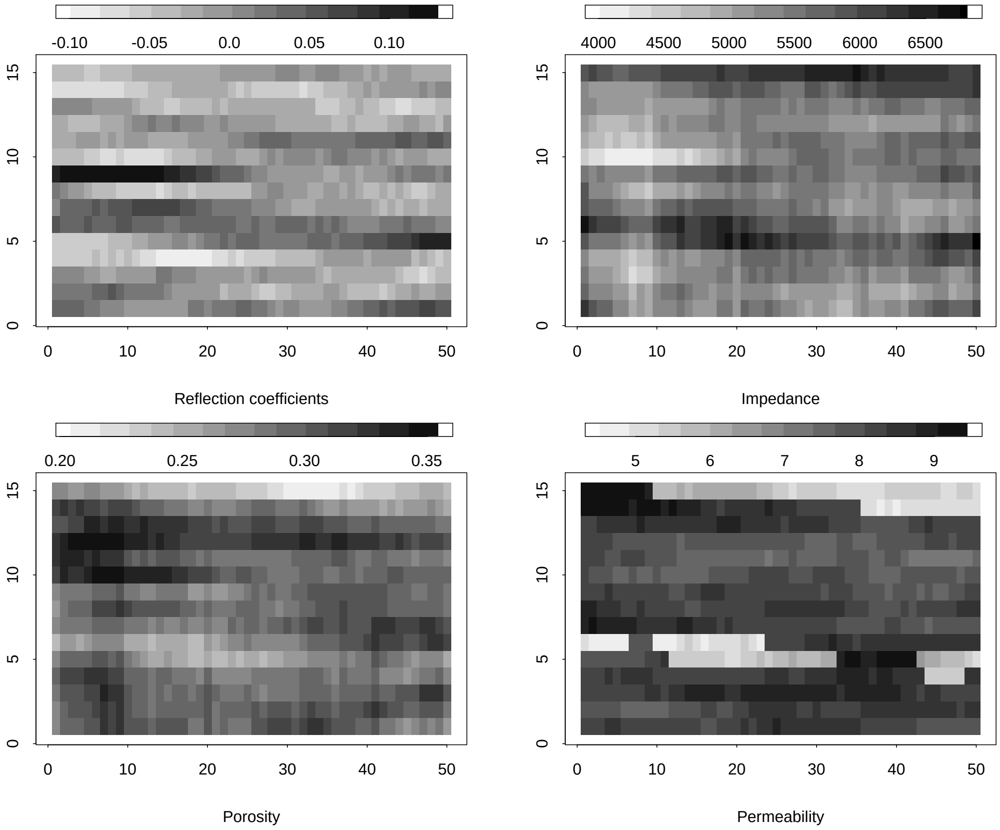

Figure 15: Cross section from a realization from the prior model displaying reflection coefficients, acoustic impedance, porosity and log-permeability respectively.

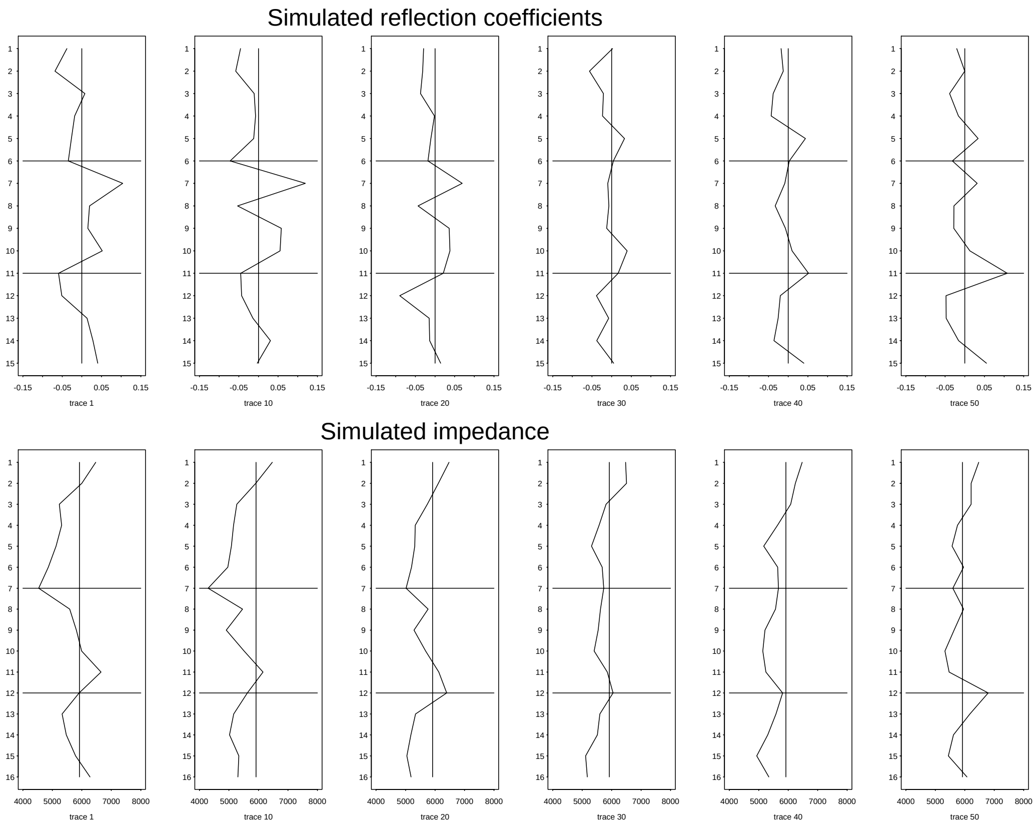

Figure 16: Trace plots of reflection coefficients and acoustic impedance corresponding to the cross plot in Figure 15. See also Figure 10 for detailed explanations.

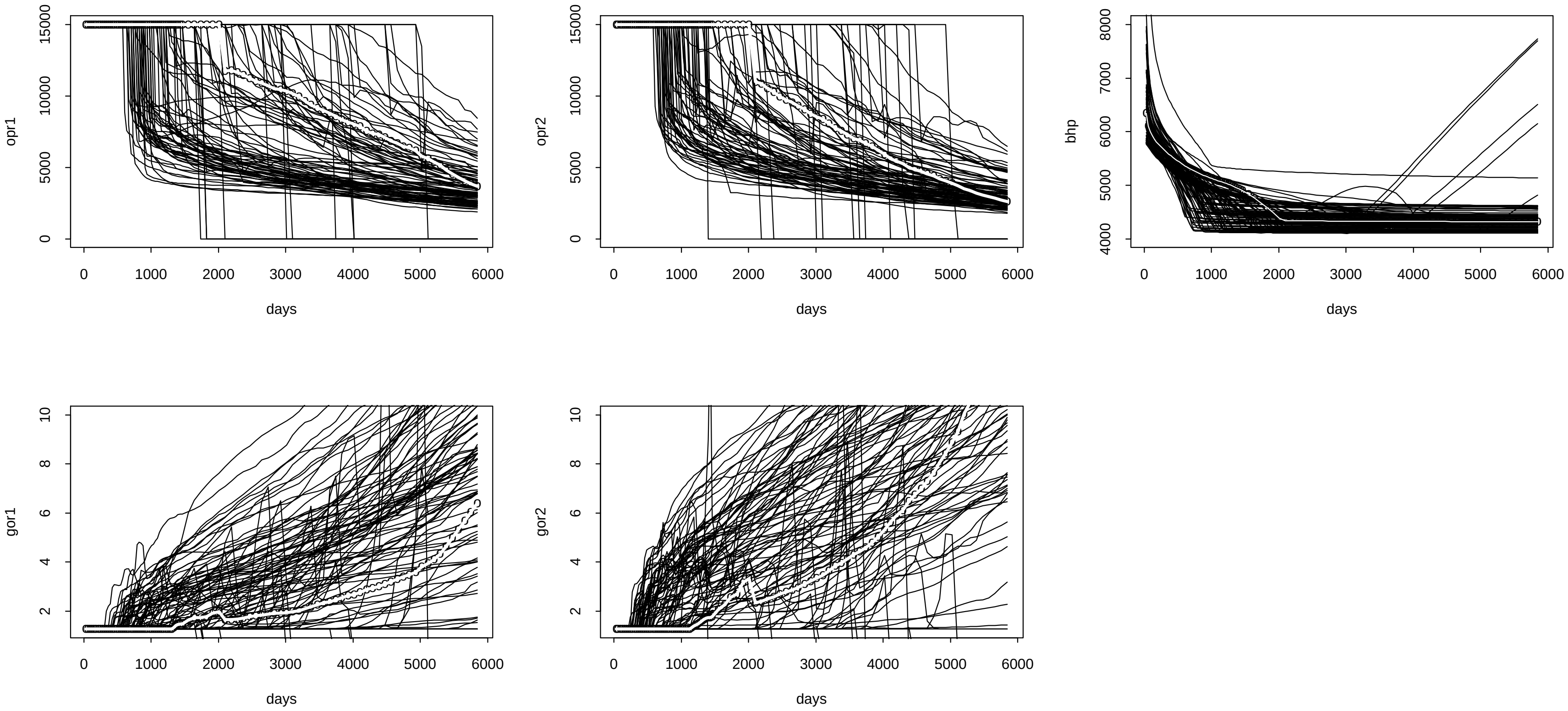

Figure 17: Production characteristics from one hundred realizations from the prior model conditioned on θ set to true values. The production characteristics from the true reservoir are indicated by black circles overlayed by a white line.

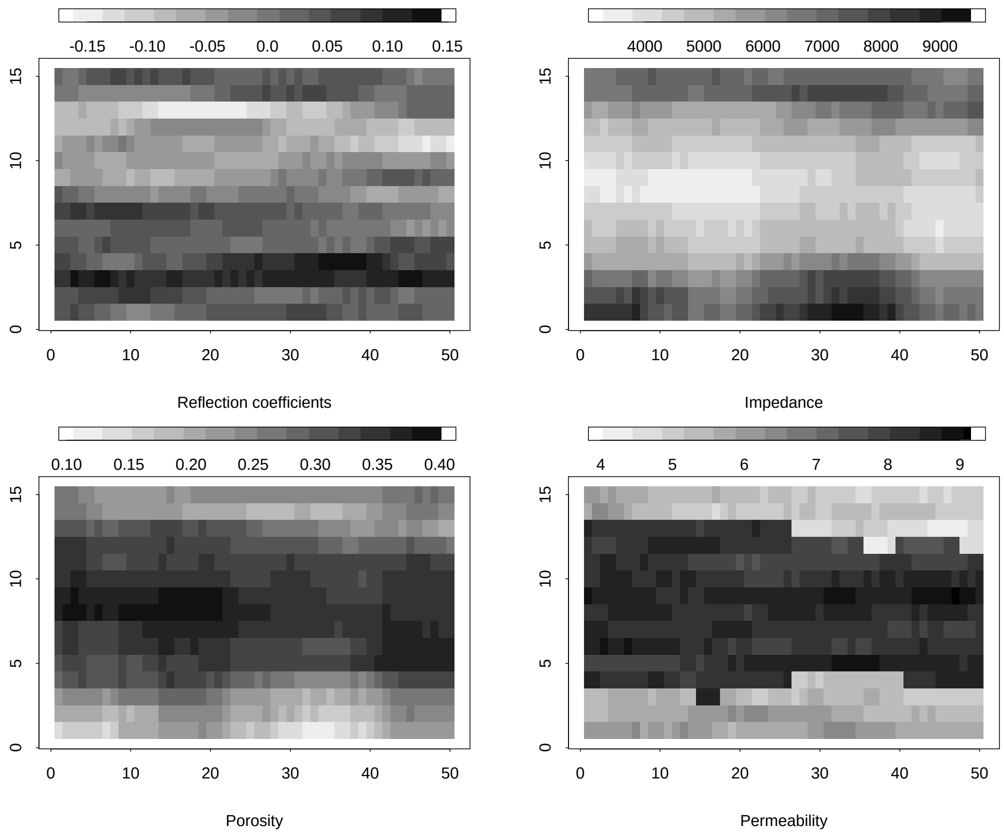

Figure 18: A cross section from a realization from the stochastic model conditioned on seismics and θ.

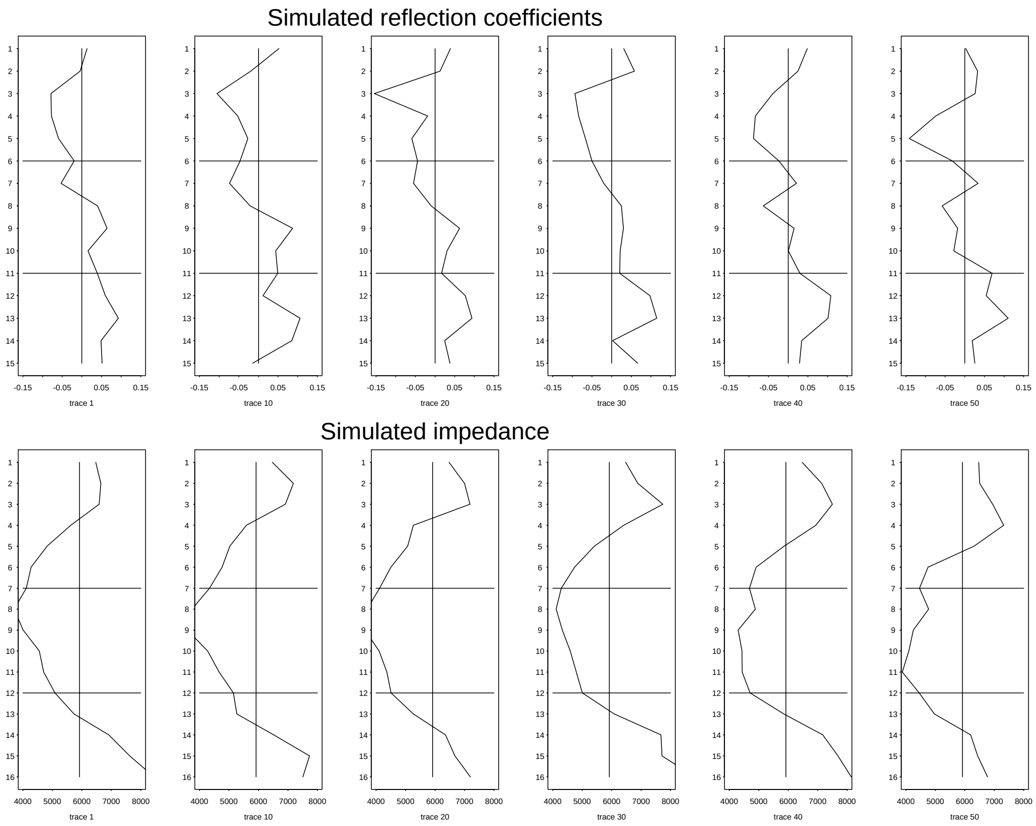

Figure 19: Trace plots of reflection coefficients and acoustic impedance corresponding to the cross plot in Figure 18. See also Figure 10 for detailed explanations.

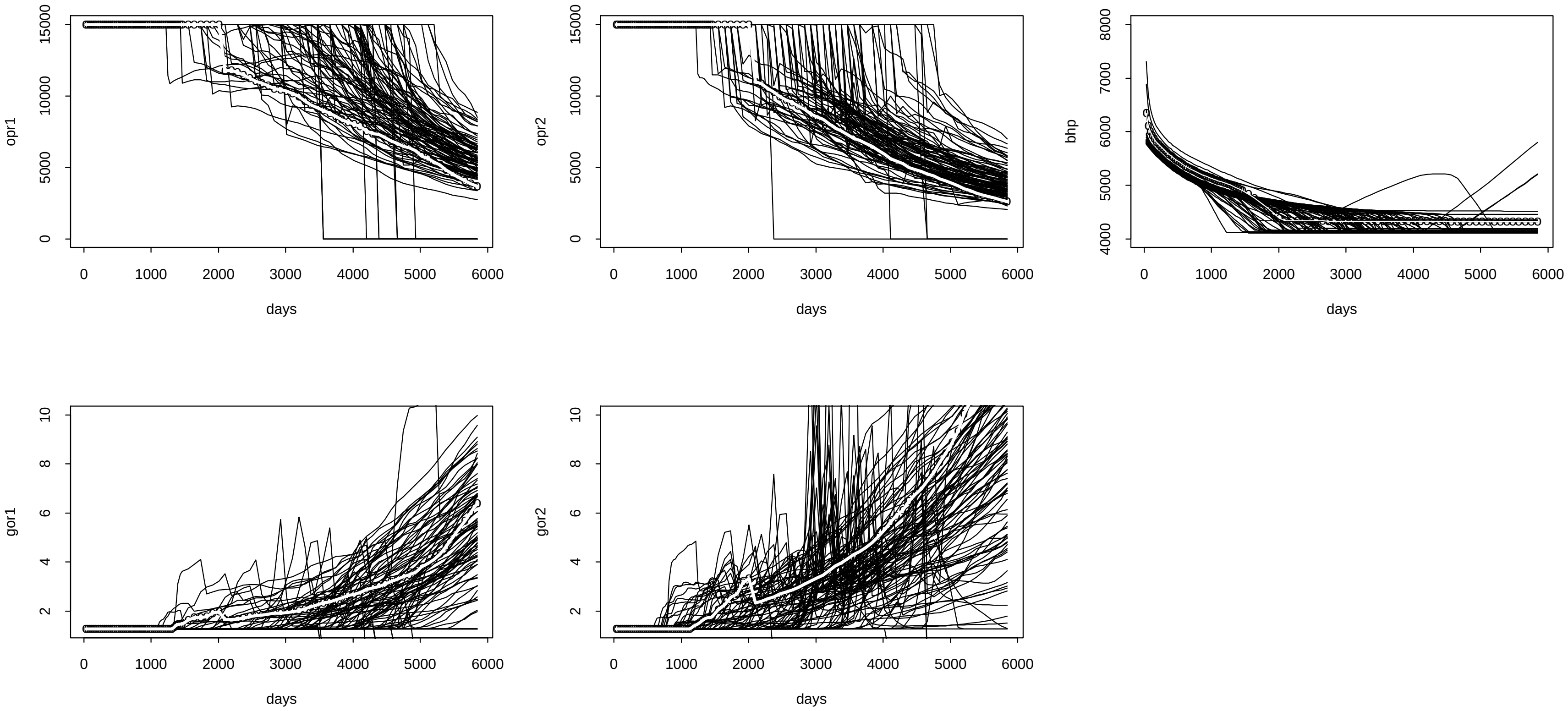

Figure 20: Production characteristics from one hundred realizations from the stochastic model conditioned on seismics and θ. The production characteristics from the true reservoir are indicated by black circles overlayed by a white line.

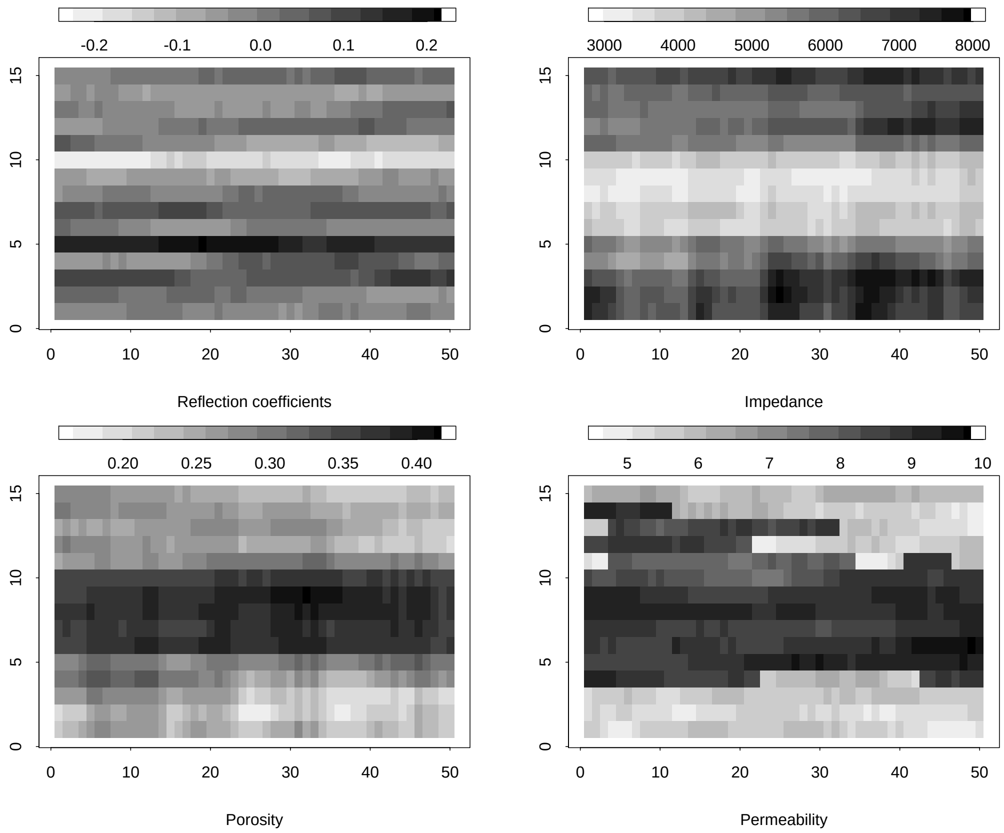

Figure 21: A cross section from a realization from the stochastic model conditioned on high quality seismics and θ.

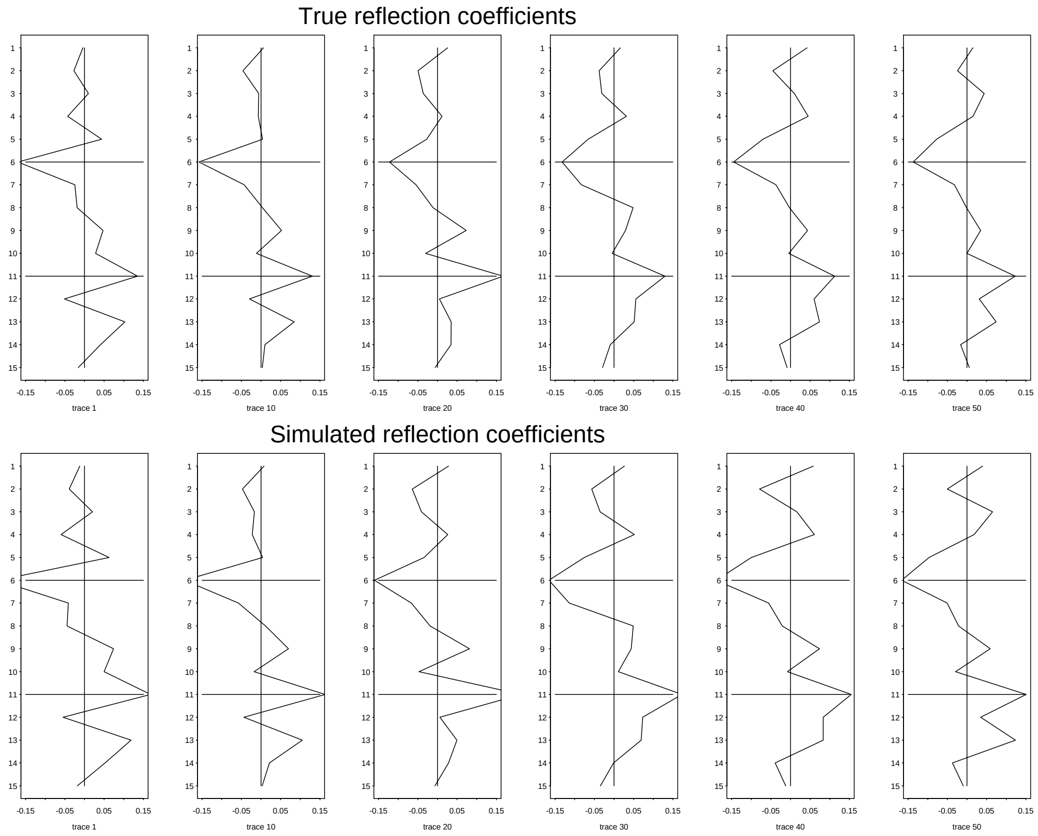

Figure 22: Trace plots of reflection coefficients corresponding to the cross plot in Figure 21. See also Figure 10 for detailed explanations.

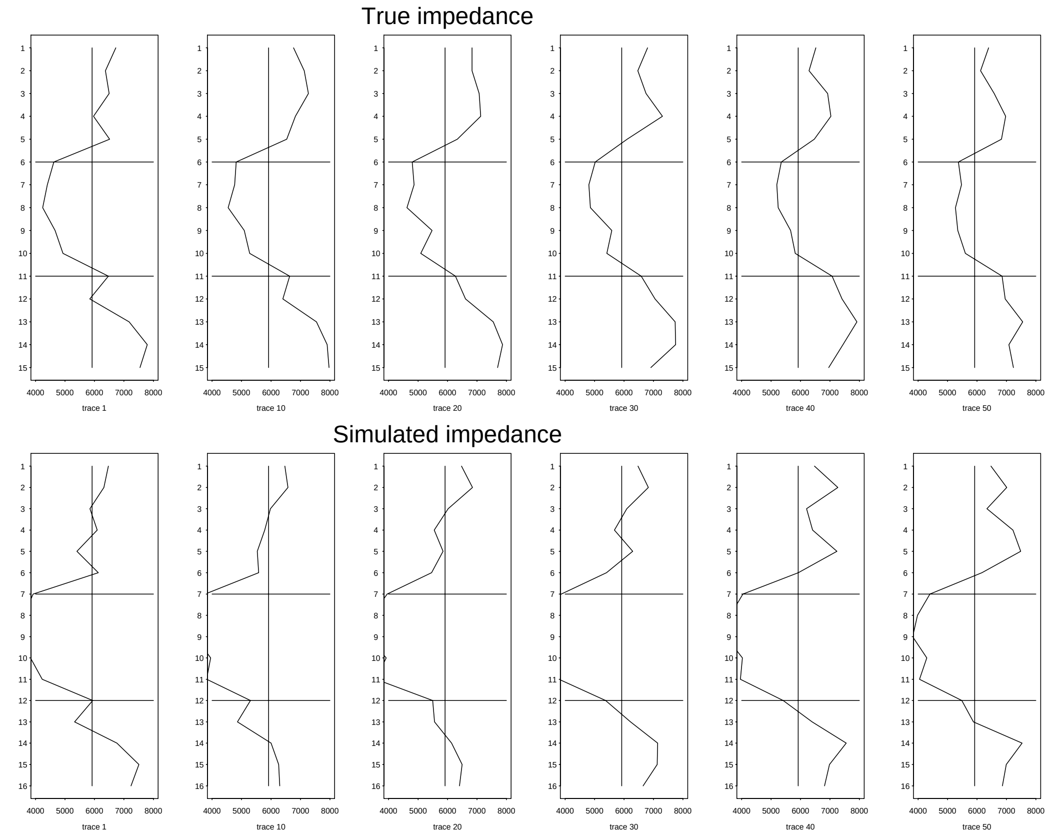

Figure 23: Trace plots of acoustic impedance corresponding to the cross plot in Figure 21. See also Figure 10 for detailed explanations.

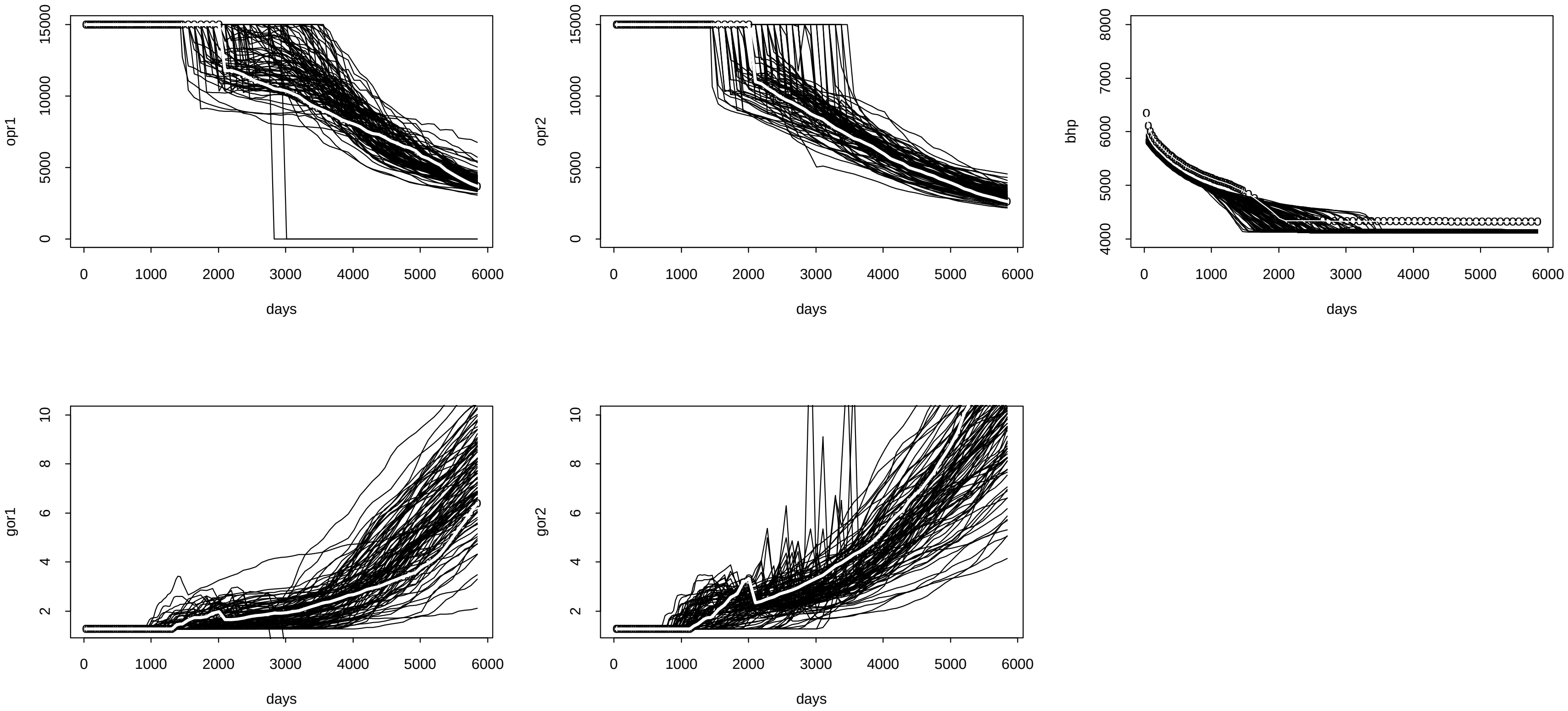

Figure 24: Production characteristics from one hundred realizations from the stochastic model conditioned on high quality seismics and θ. The production characteristics from the true reservoir are indicated by black circles overlayed by a white line.

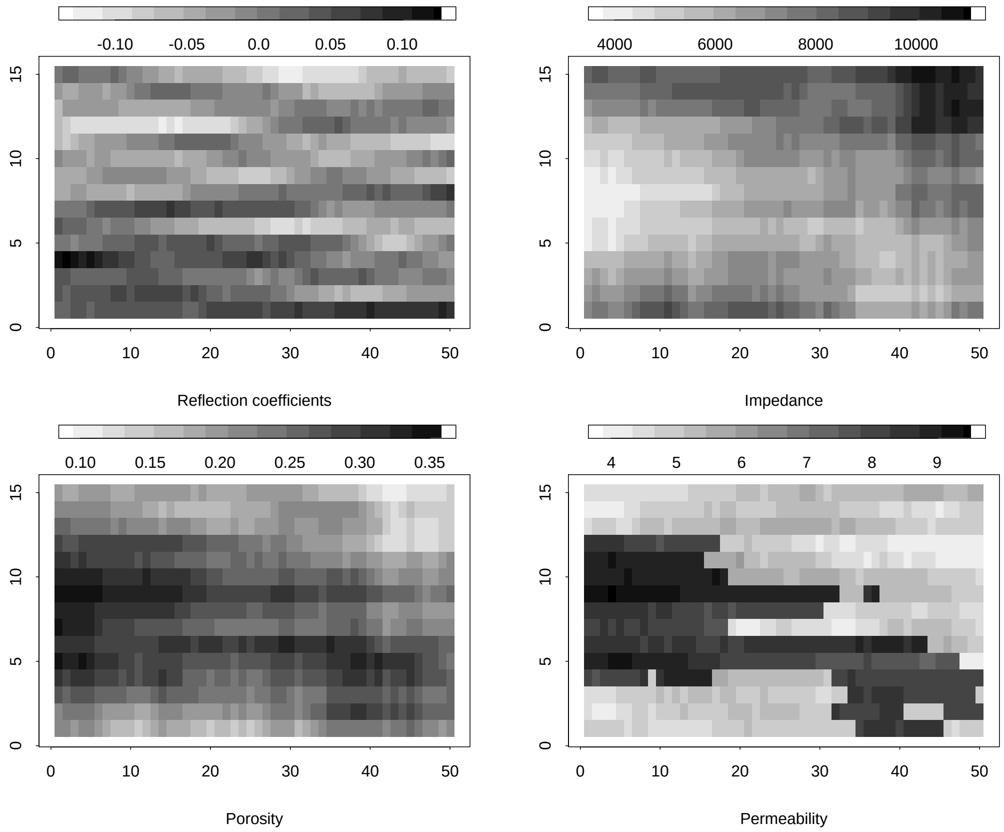

Figure 25: A cross section from a realization from the stochastic model conditioned on well observations and θ.

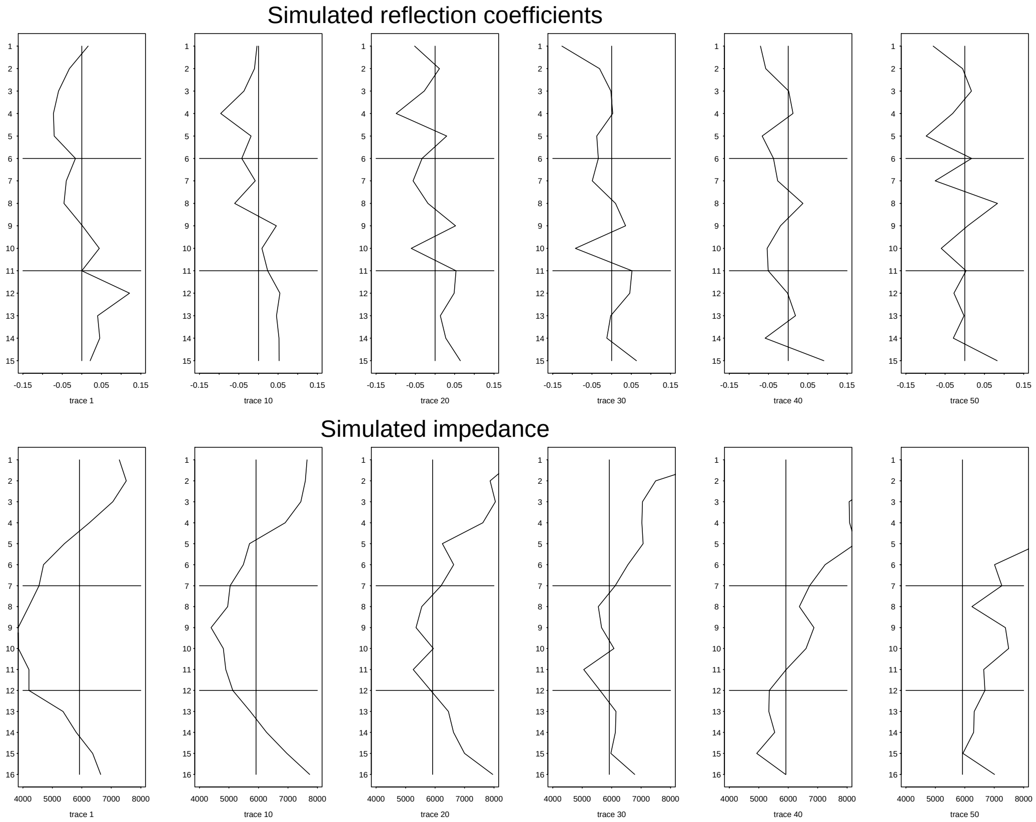

Figure 26: Trace plots of reflection coefficients and acoustic impedance corresponding to the cross plot in Figure 25. See also Figure 10 for detailed explanations.

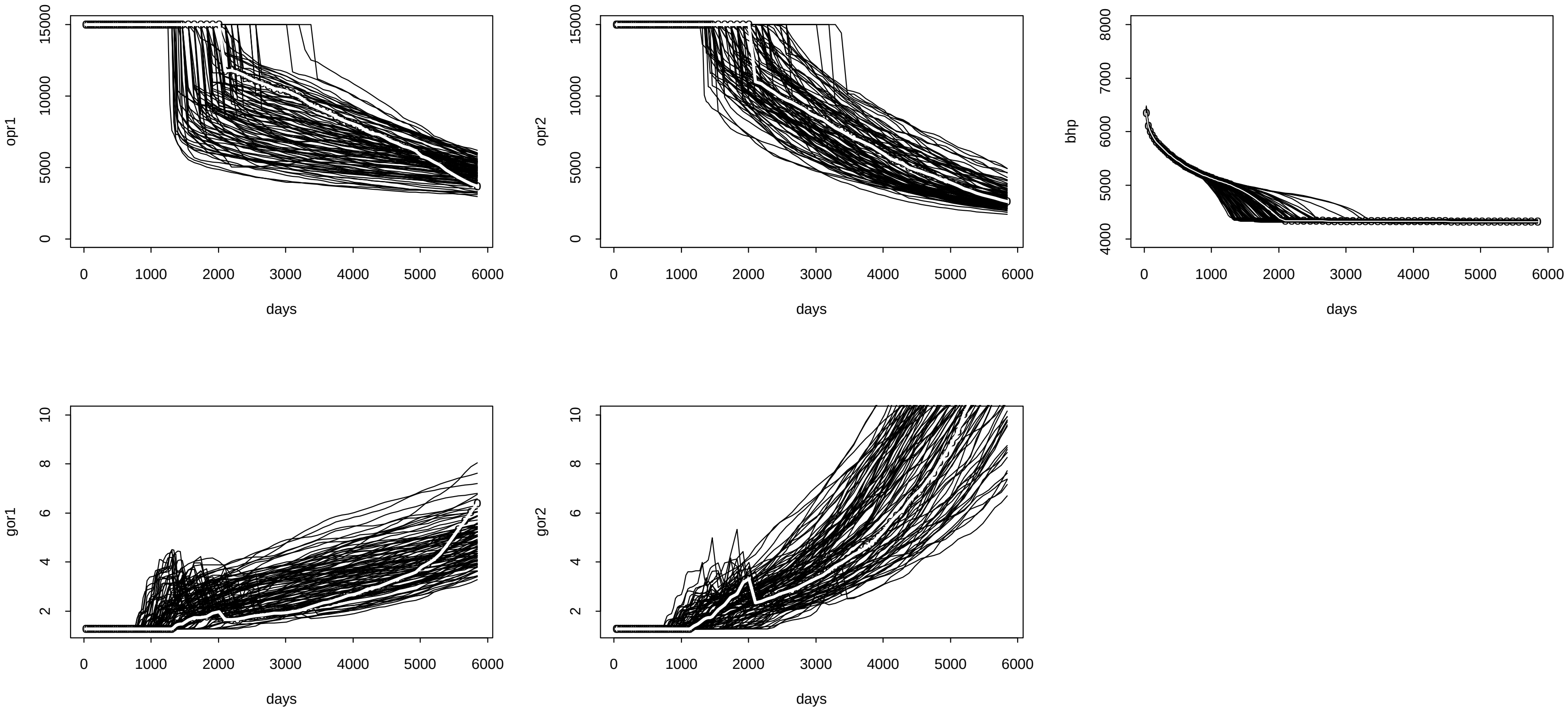

Figure 27: Production characteristics from one hundred realizations from the stochastic model conditioned on well observations and θ. The production characteristics from the true reservoir are indicated by black circles overlayed by a white line.

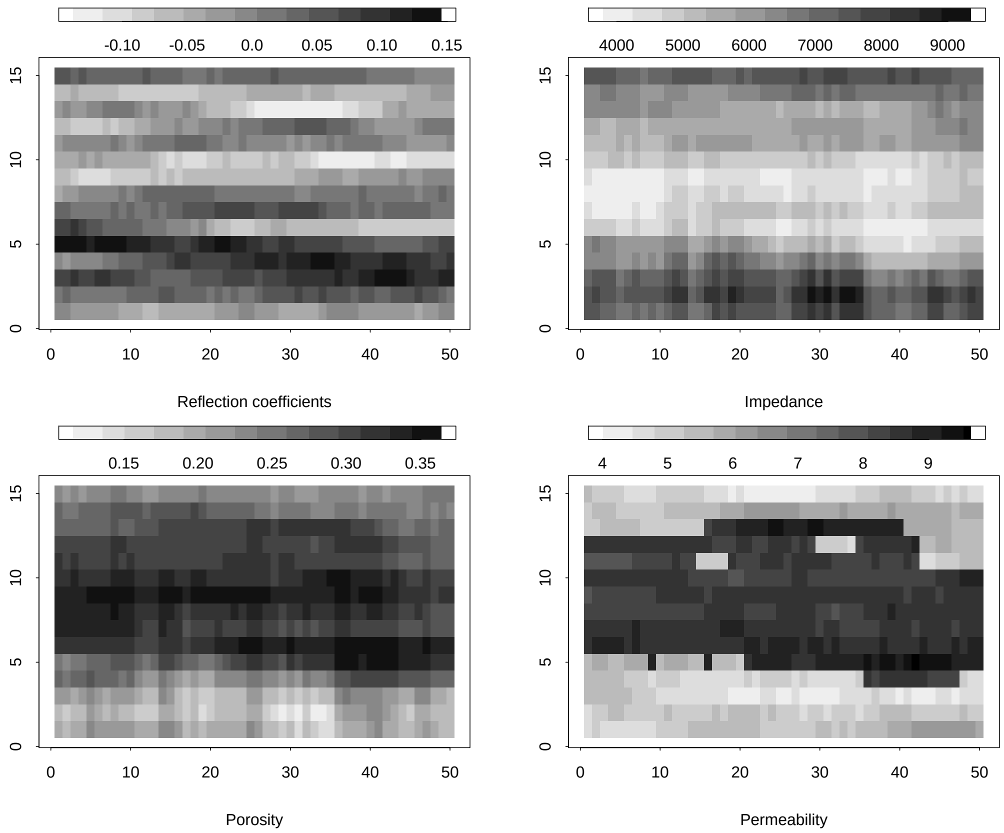

Figure 28: A cross section from a realization from the stochastic model conditioned on well observations, seismics and θ.

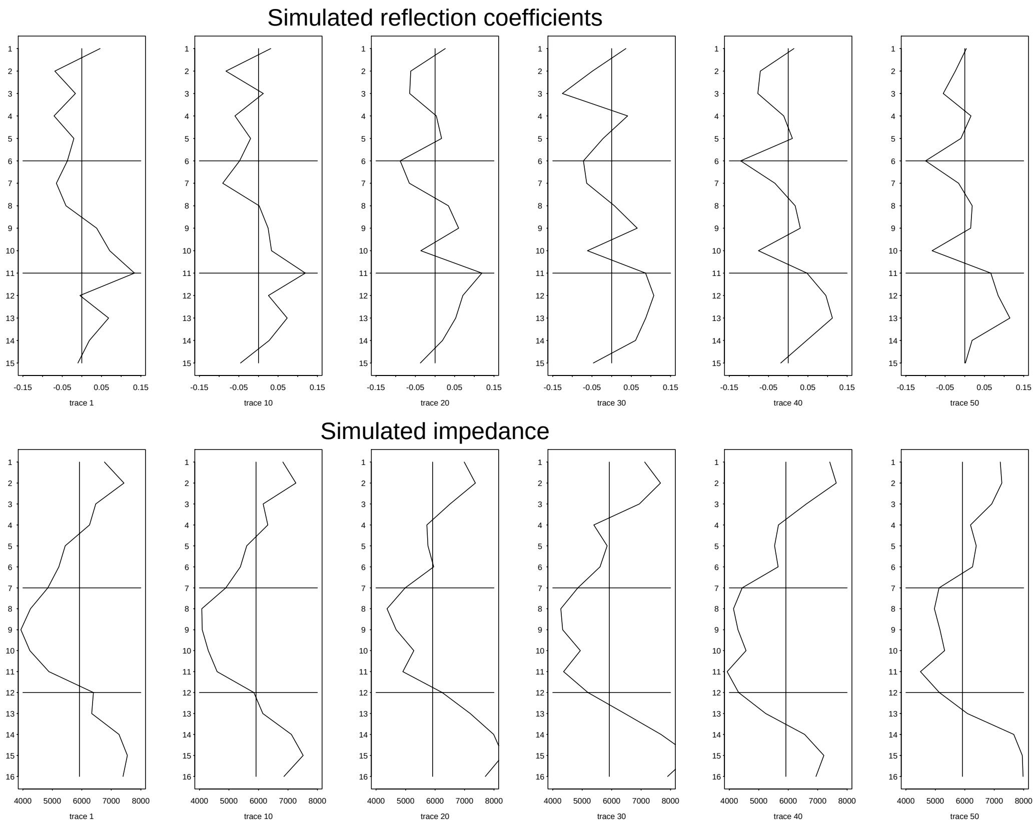

Figure 29: Trace plots of reflection coefficients and acoustic impedance corresponding to the cross plot in Figure 28. See also Figure 10 for detailed explanations.

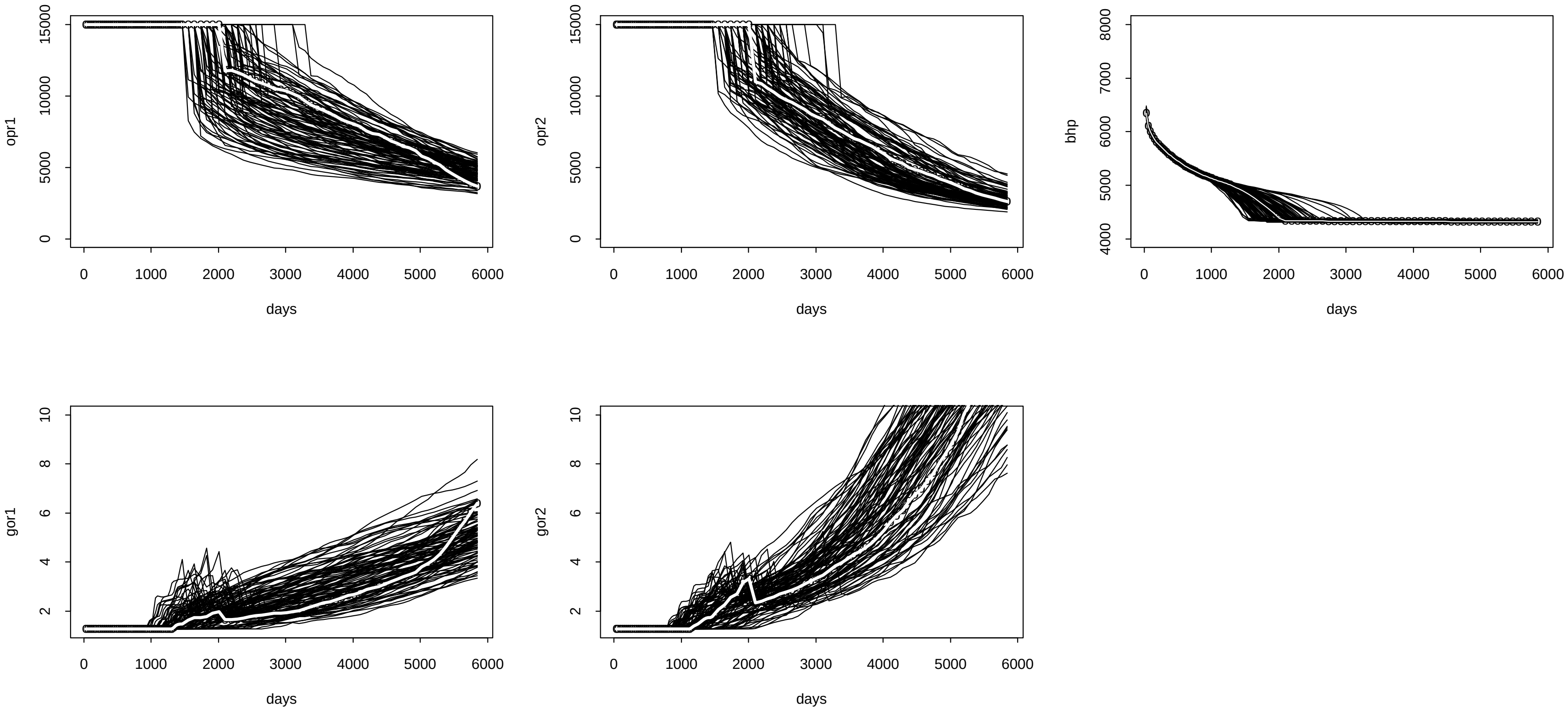

Figure 30: Production characteristics from one hundred realizations from the stochastic model conditioned on well observations, seismics and θ. The production characteristics from the true reservoir are indicated by black circles overlayed by a white line.

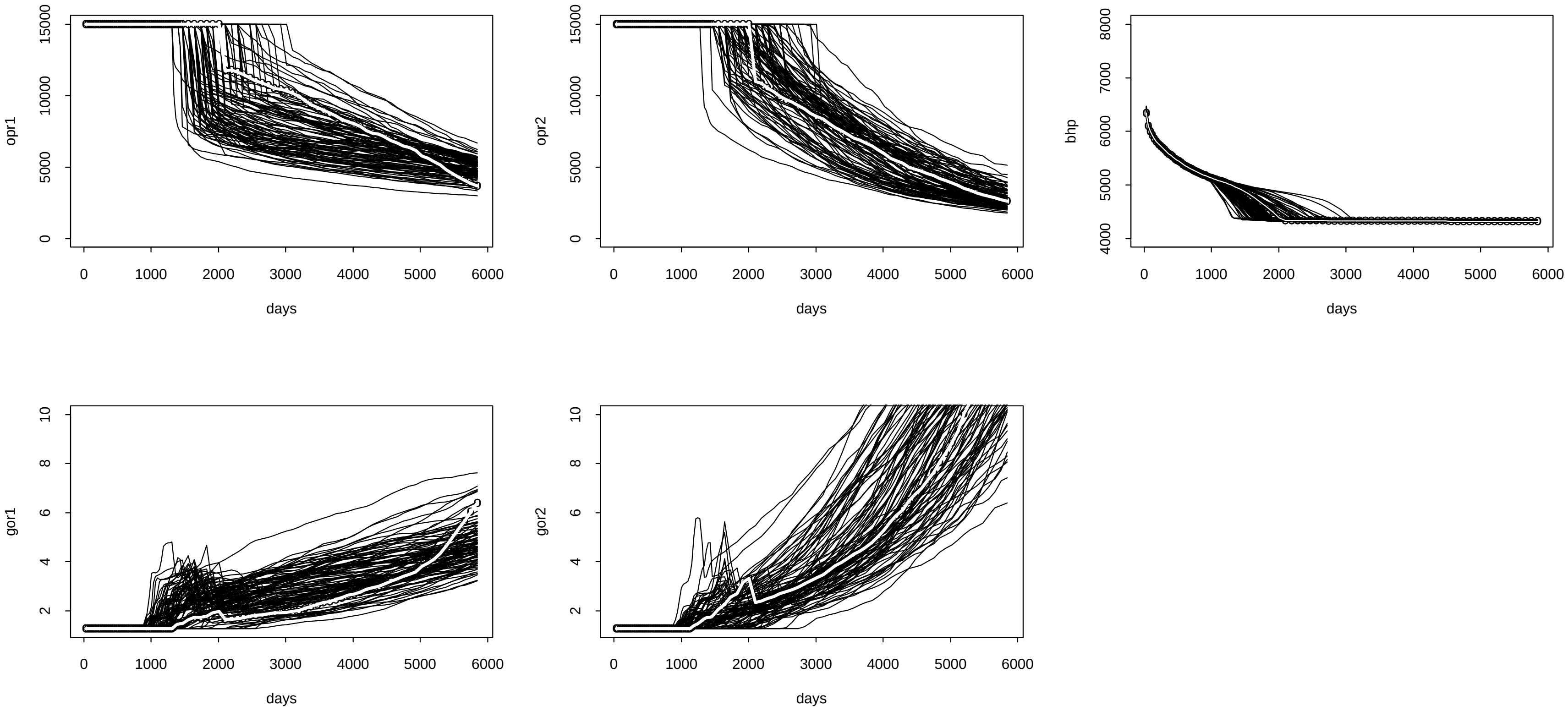

Figure 31: Production characteristics from 100 realizations from the stochastic model conditioned on well observations and 2.5 years (911 days) of production history. The production characteristics from the true reservoir are indicated by black circles overlayed by a white line.

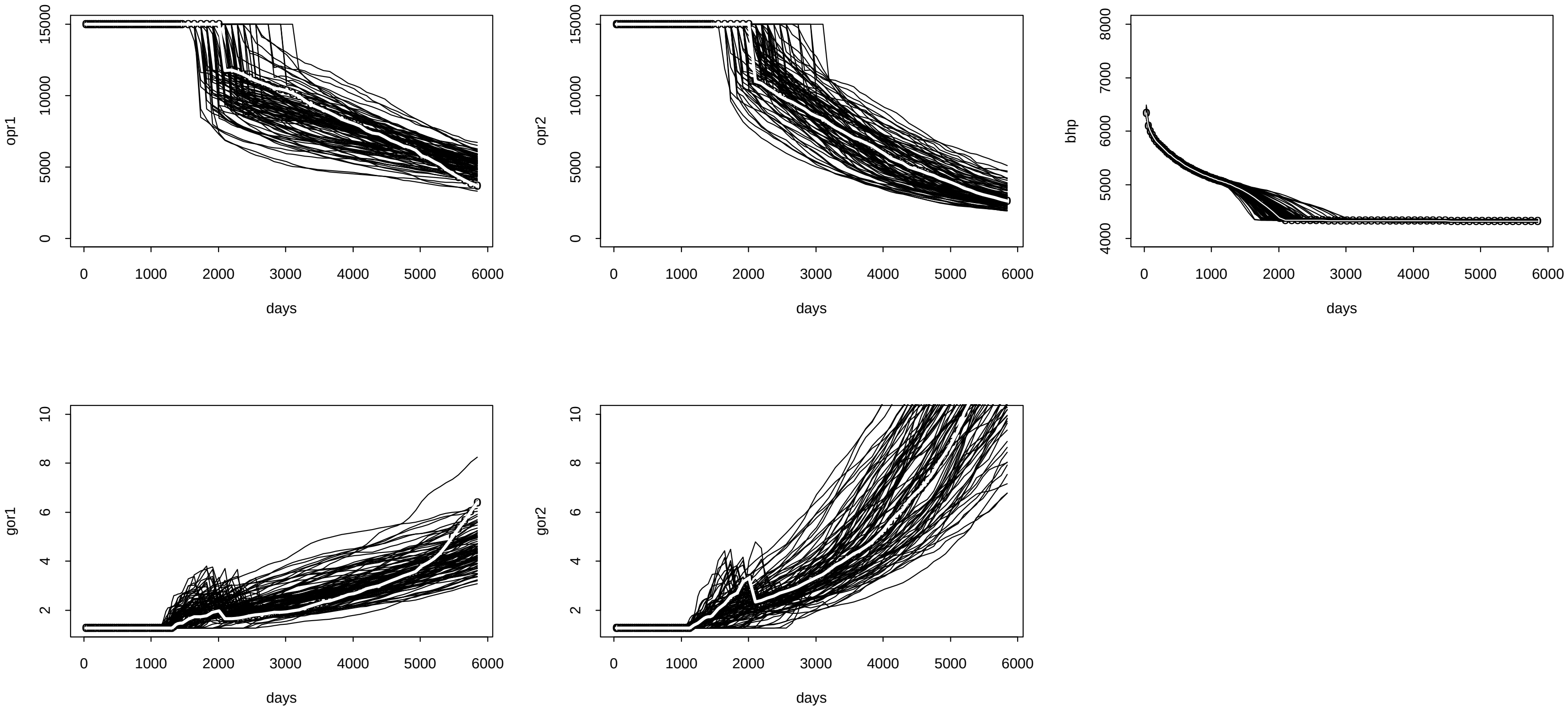

Figure 32: Production characteristics from 95 realizations from the stochastic model conditioned on well observations and 3.33 years (1216 days) of production history. The production characteristics from the true reservoir are indicated by black circles overlayed by a white line.

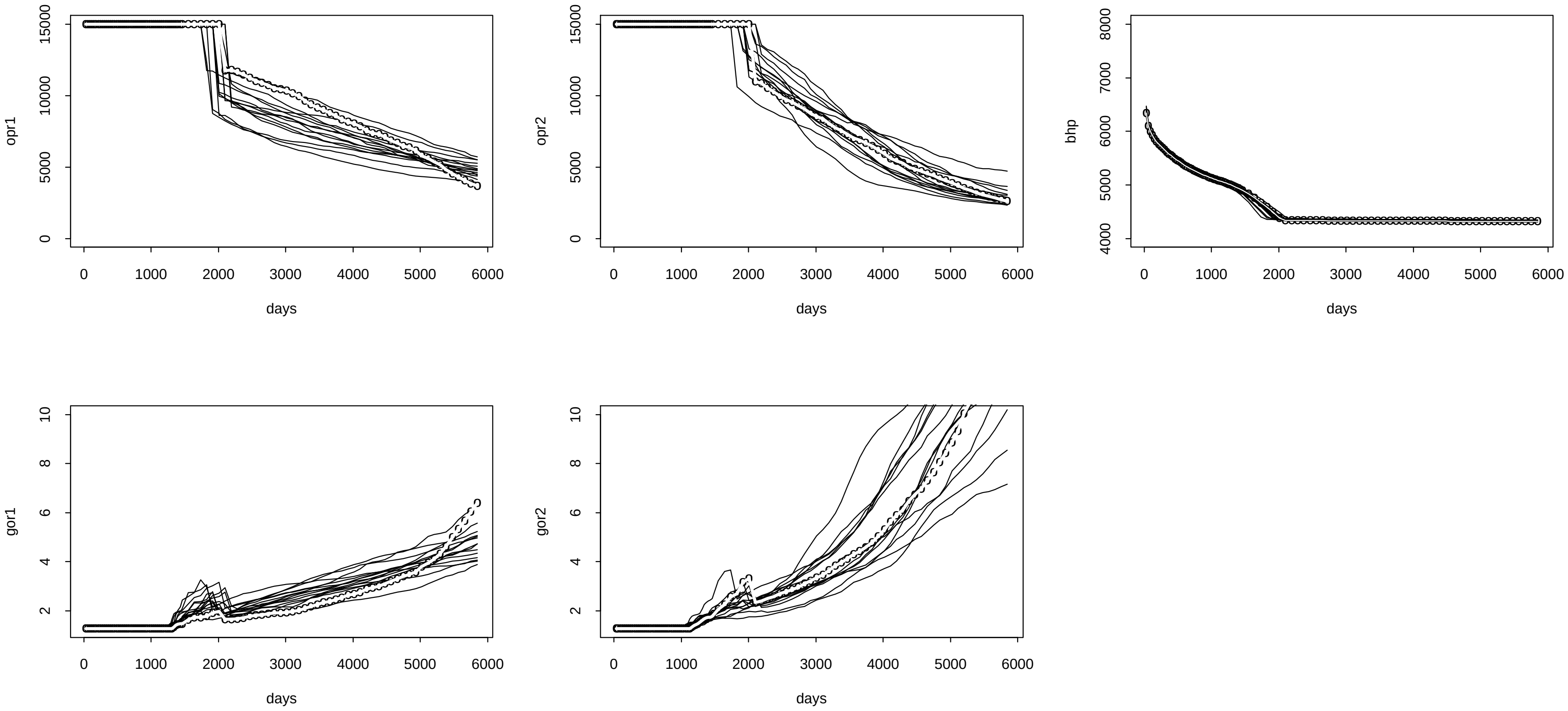

Figure 33: Production characteristics from 14 realizations from the stochastic model conditioned on well observations and 4.5 years (1642 days) of production history. The production characteristics from the true reservoir are indicated by black circles overlayed by a white line.

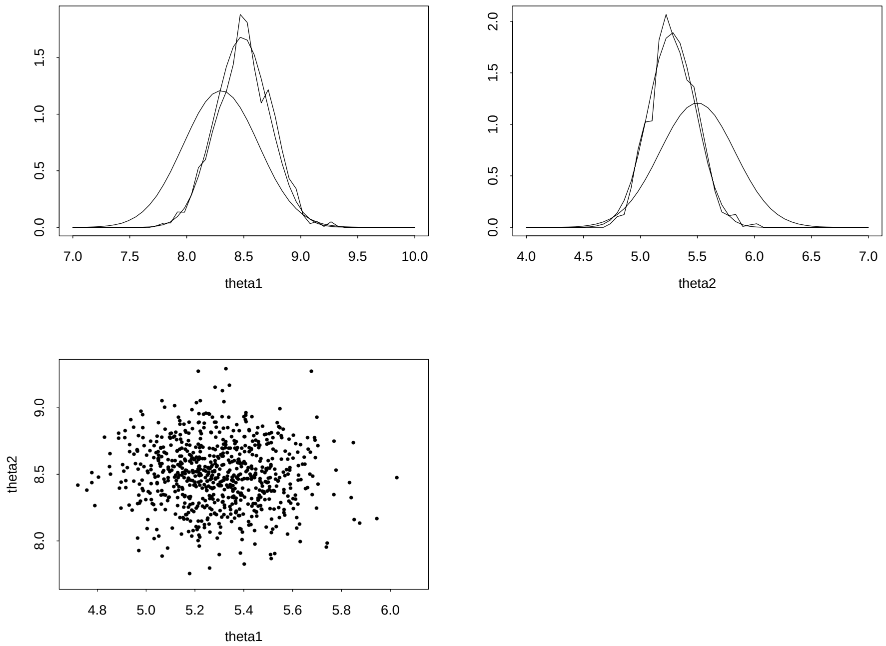

Figure 34: The first display shows plots of $f(\theta_1)$, $f(\theta_1|d_w)$, and $f(\theta_1|d_p, d_w)$ where d_p is 2.5 years of production history. The curve with the lowest mode is the prior pdf $f(\theta_1)$. The other smooth curve is the pdf for Θ_1 conditioned to well observations, $f(\theta_1|d_w)$. The irregular curve is a density estimate for $f(\theta_1|d_p, d_w)$, i.e when production history are included. The second display is similar to the first, but with θ_2. The last display is a cross plot of samples of $\theta = (\theta_1, \theta_2)$ from $f(\theta|d_p, d_w)$.

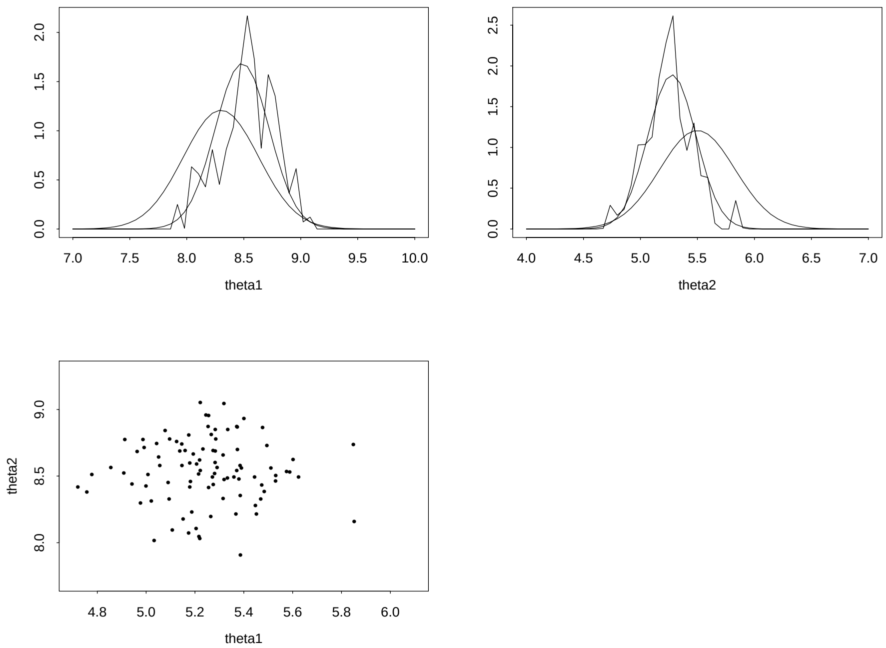

Figure 35: Plots of $f(\theta)$, $f(\theta|d_w)$, and $f(\theta|d_p, d_w)$ where d_p is 3.33 years of production history. See Figure 34 for details

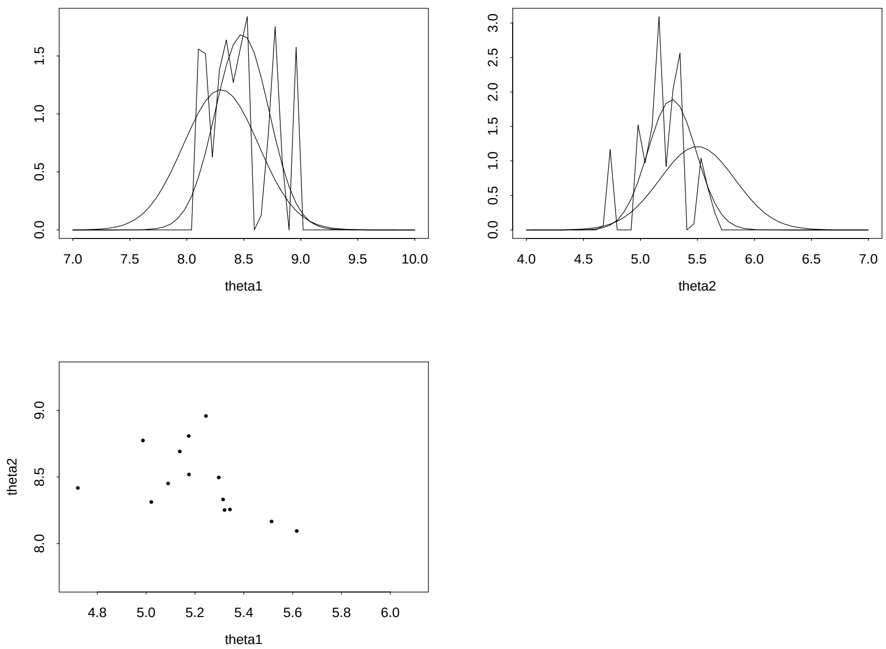

Figure 36: Plots of $f(\theta)$, $f(\theta|d_w)$, and $f(\theta|d_p, d_w)$ where d_p is 4.5 years of production history. See Figure 34 for details

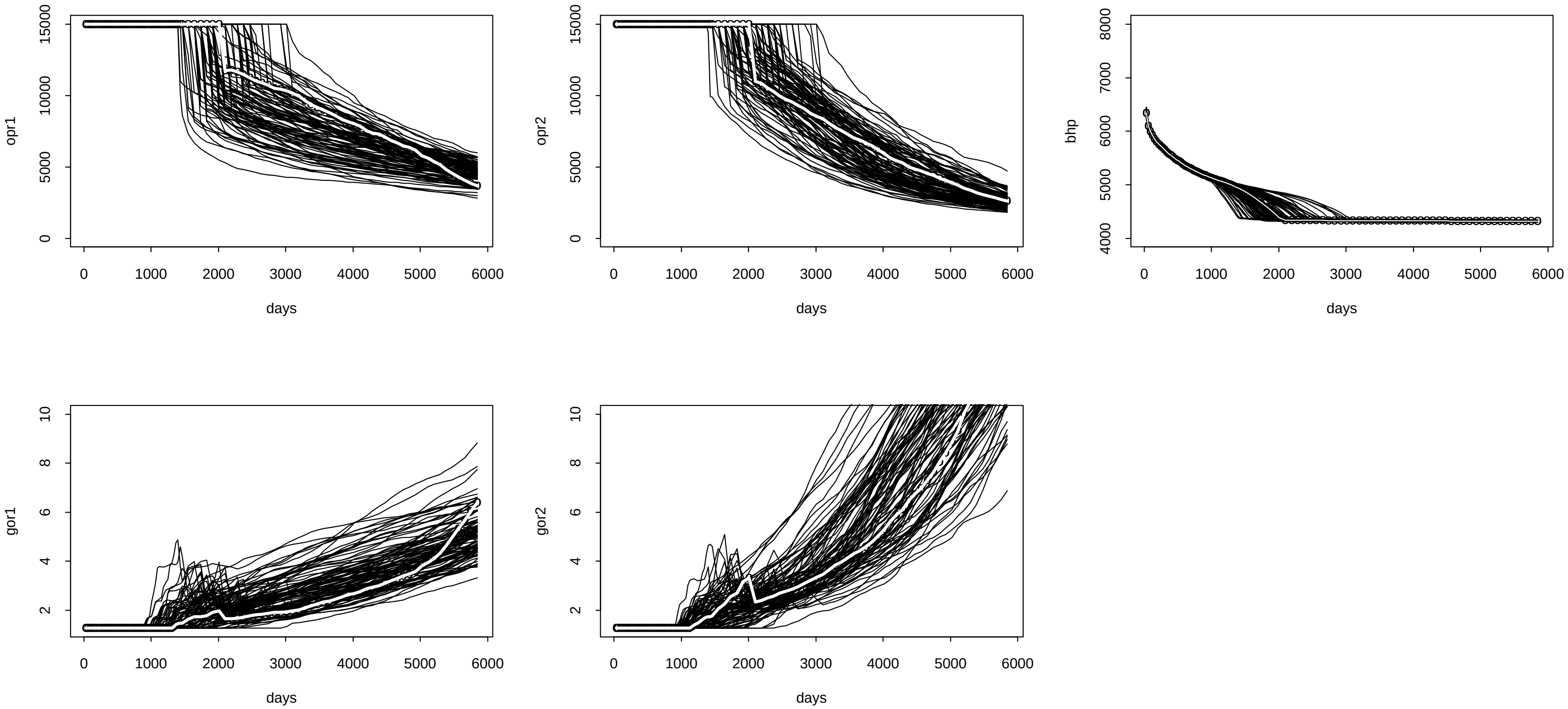

Figure 37: Production characteristics from 100 realizations from the posterior model conditioned on well observations, seismics and 2.5 years of production history. The production characteristics from the true reservoir are indicated by black circles overlayed by a white line.

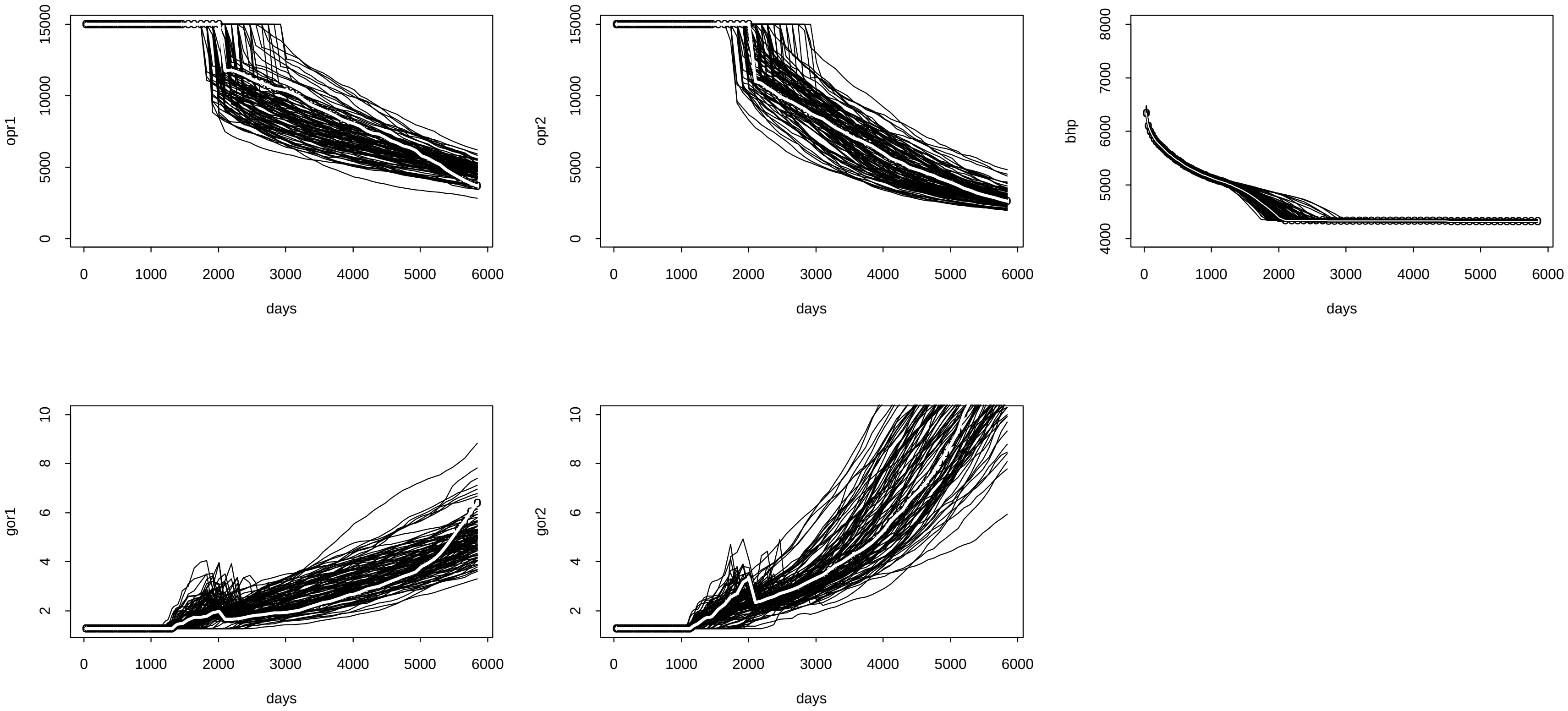

Figure 38: Production characteristics from 100 realizations from the posterior model conditioned on well observations, seismics and 3.33 years of production history. The production characteristics from the true reservoir are indicated by black circles overlayed by a white line.

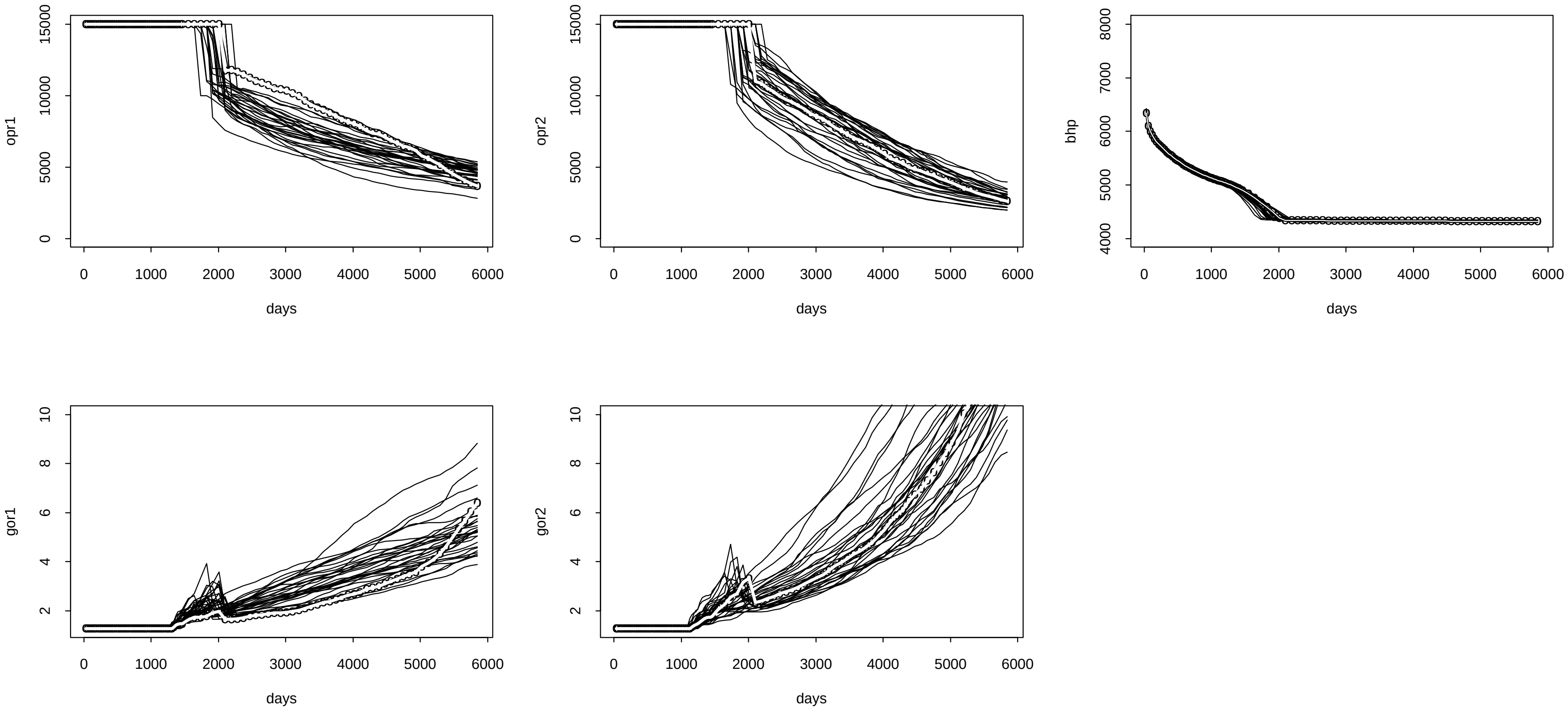

Figure 39: Production characteristics from 30 realizations from the posterior model conditioned on well observations, seismics and 4.5 years of production history. The production characteristics from the true reservoir are indicated by black circles overlayed by a white line.

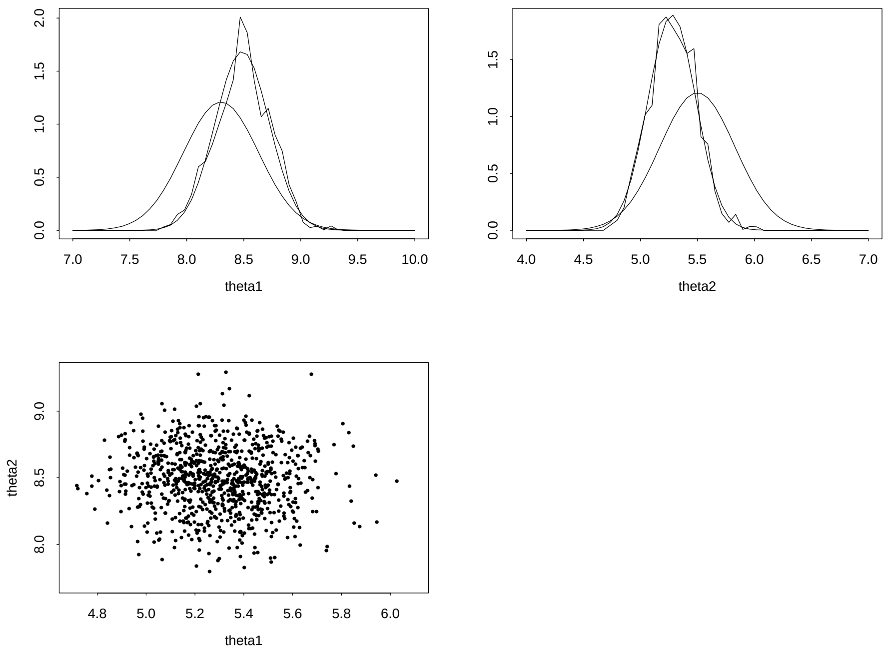

Figure 40: The first display shows plots of $f(\theta_1)$, $f(\theta_1|d_w)$, and $f(\theta_1|d)$ where d_p is 2.5 years of production history. The curve with the lowest mode is the prior pdf $f(\theta_1)$. The other smooth curve is the pdf for Θ_1 conditioned to well observations, $f(\theta_1|d_w)$. The irregular curve is a density estimate for $f(\theta_1|d)$, i.e when production history and seismics are included, too. The second display is similar, but with θ_2. The last display is a cross plot of samples of $\theta = (\theta_1, \theta_2)$ from $f(\theta|d)$.

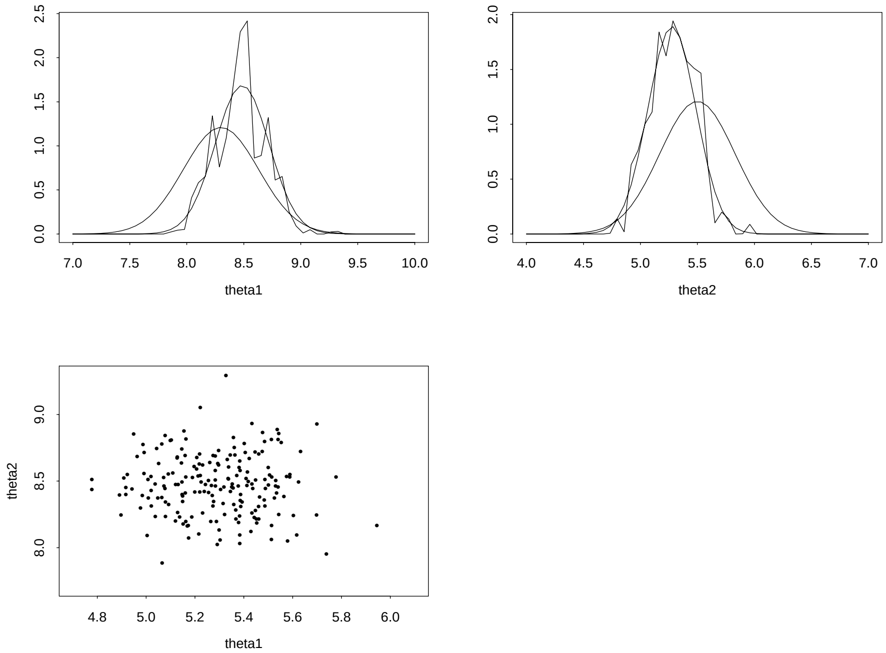

Figure 41: Plots of $f(\theta)$, $f(\theta|d_w)$, and $f(\theta|d)$ where d_p is 3.33 years of production history. See Figure 40 for details.

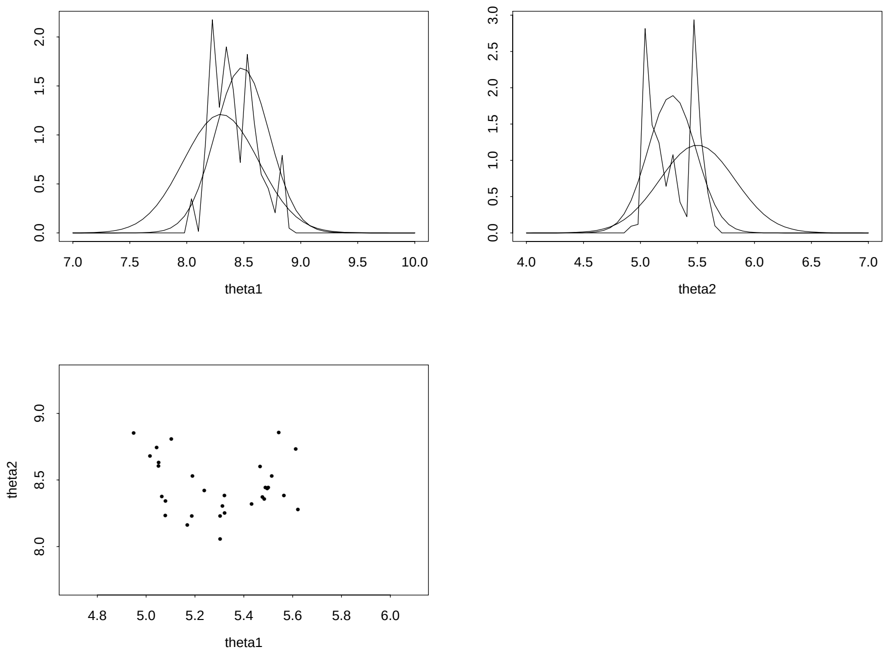

Figure 42: Plots of $f(\theta)$, $f(\theta|d_w)$, and $f(\theta|d)$ where d_p is 4.5 years of production history. See Figure 40 for details

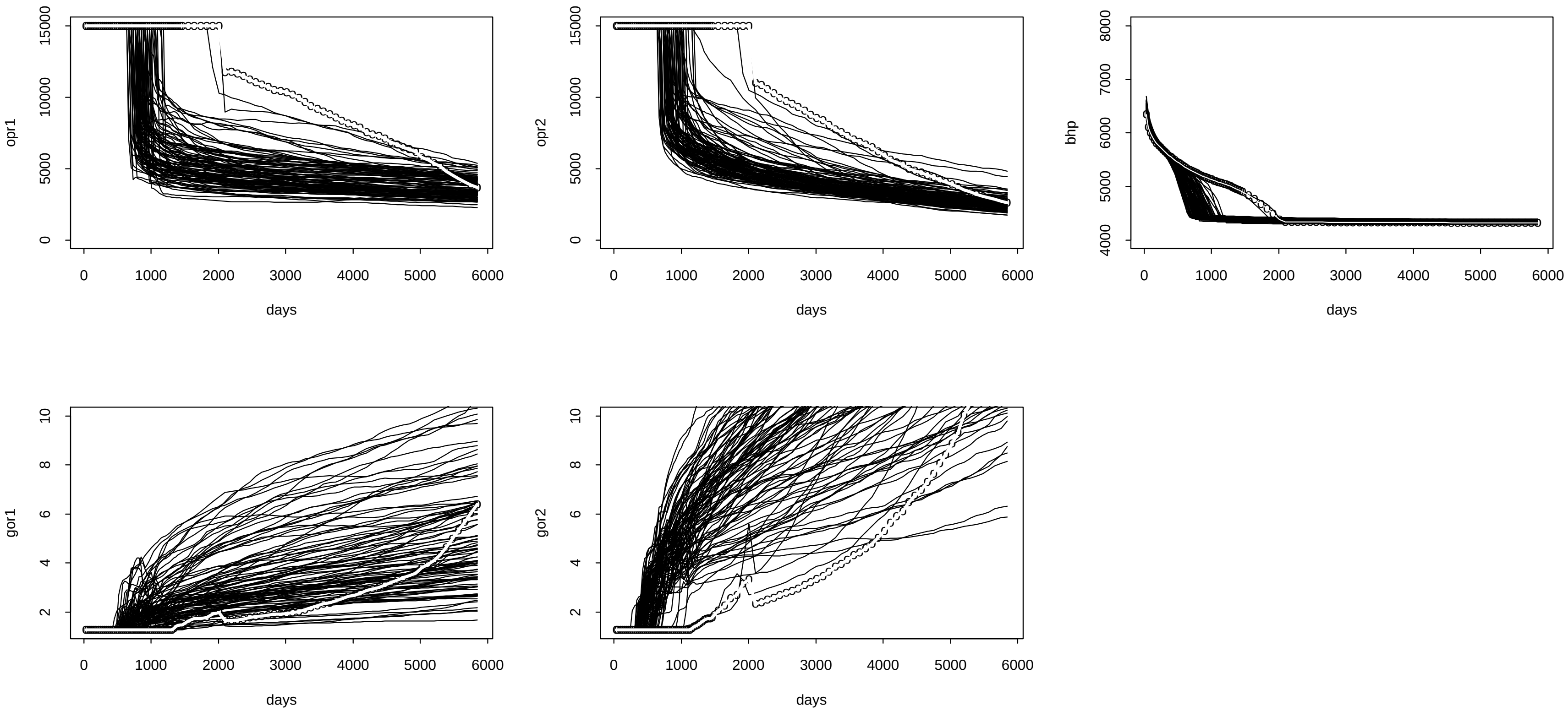

Figure 43: Production characteristics from one hundred realizations from the stochastic model having shorter correlations lengths, conditioned on well observations and θ. The production characteristics from the true reservoir are indicated by black circles overlayed by a white line.

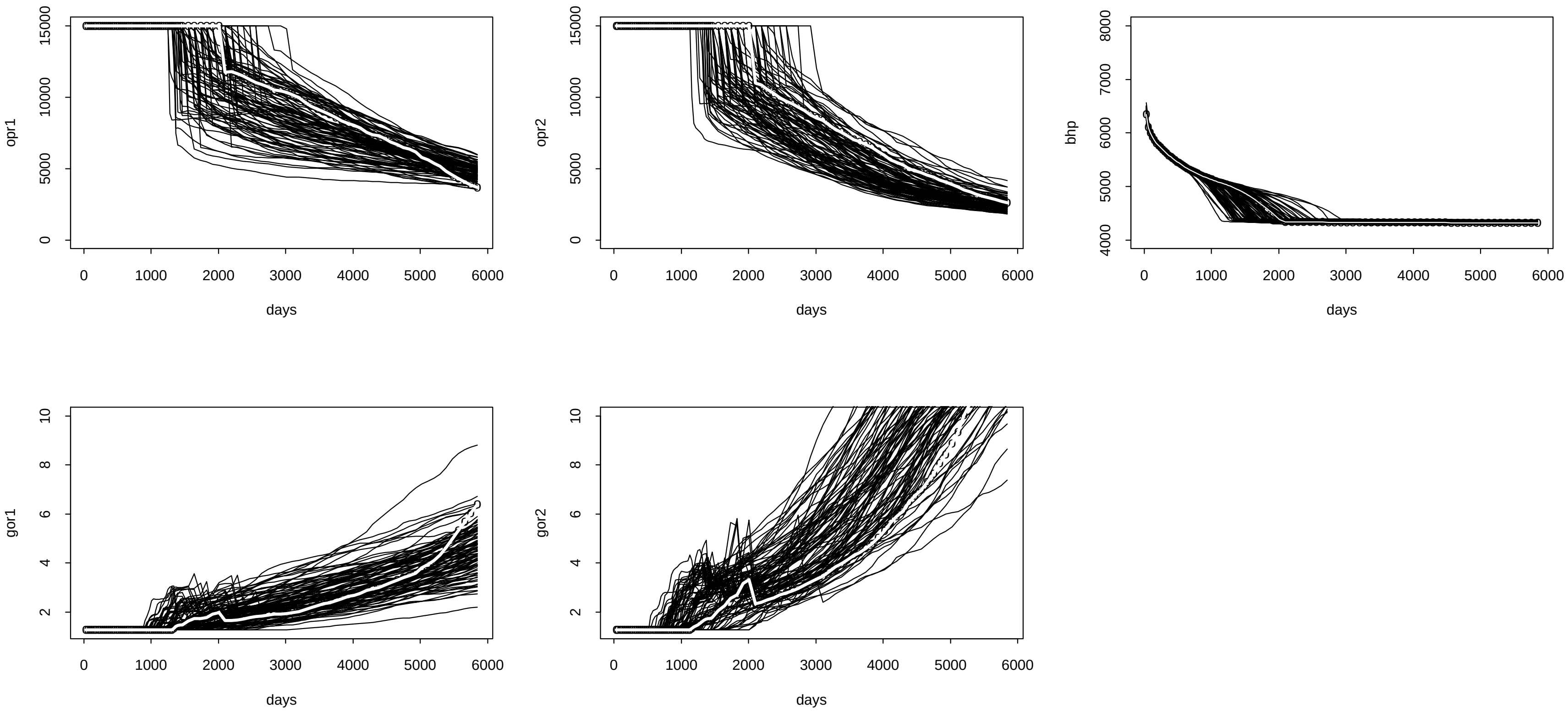

Figure 44: Production characteristics from one hundred realizations from the stochastic model having shorter correlation lengths, conditioned on well observations, seismic data and θ. The production characteristics from the true reservoir are indicated by black circles overlayed by a white line.

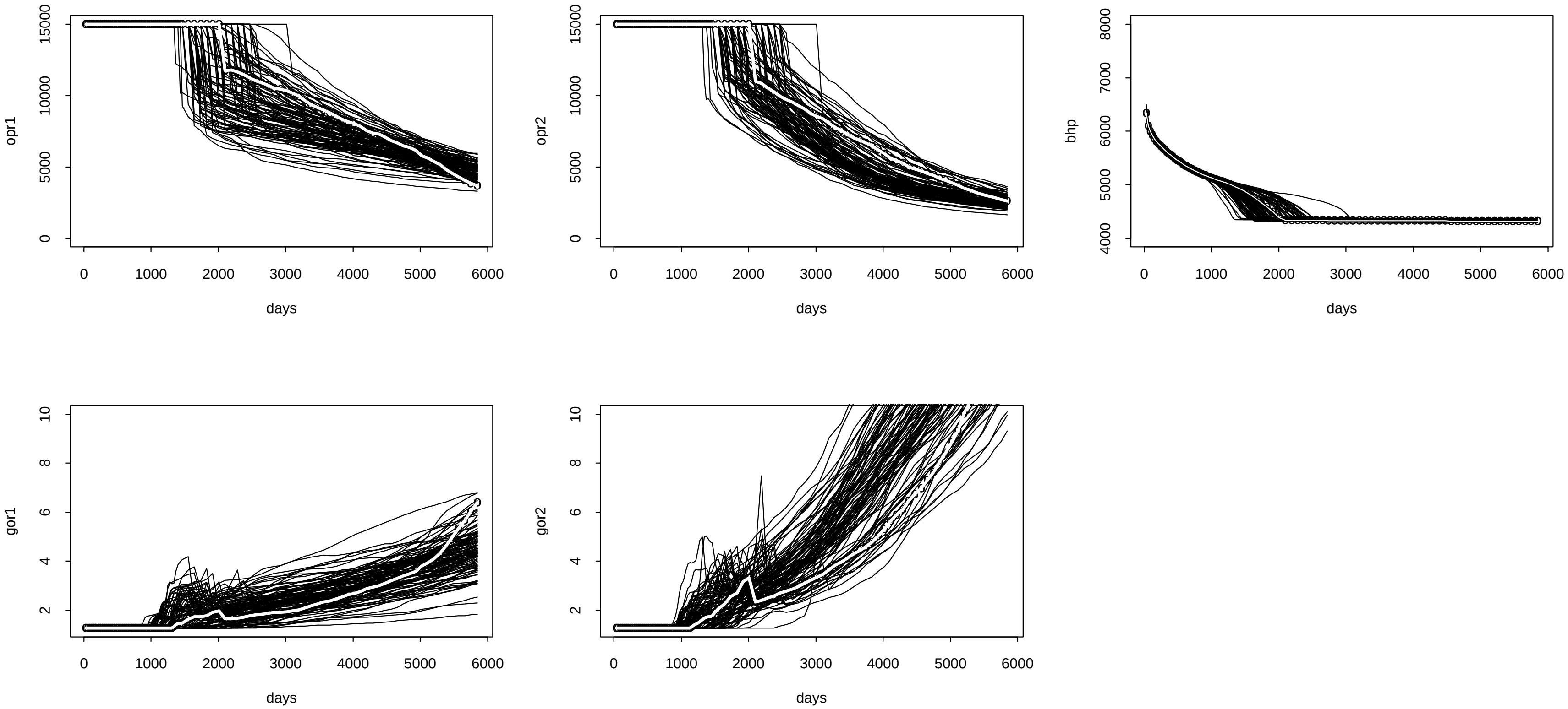

Figure 45: Production characteristics from 100 realizations from the posterior model conditioned on well observations, seismics and 2.5 years of production history. The production characteristics from the true reservoir are indicated by black circles overlayed by a white line.

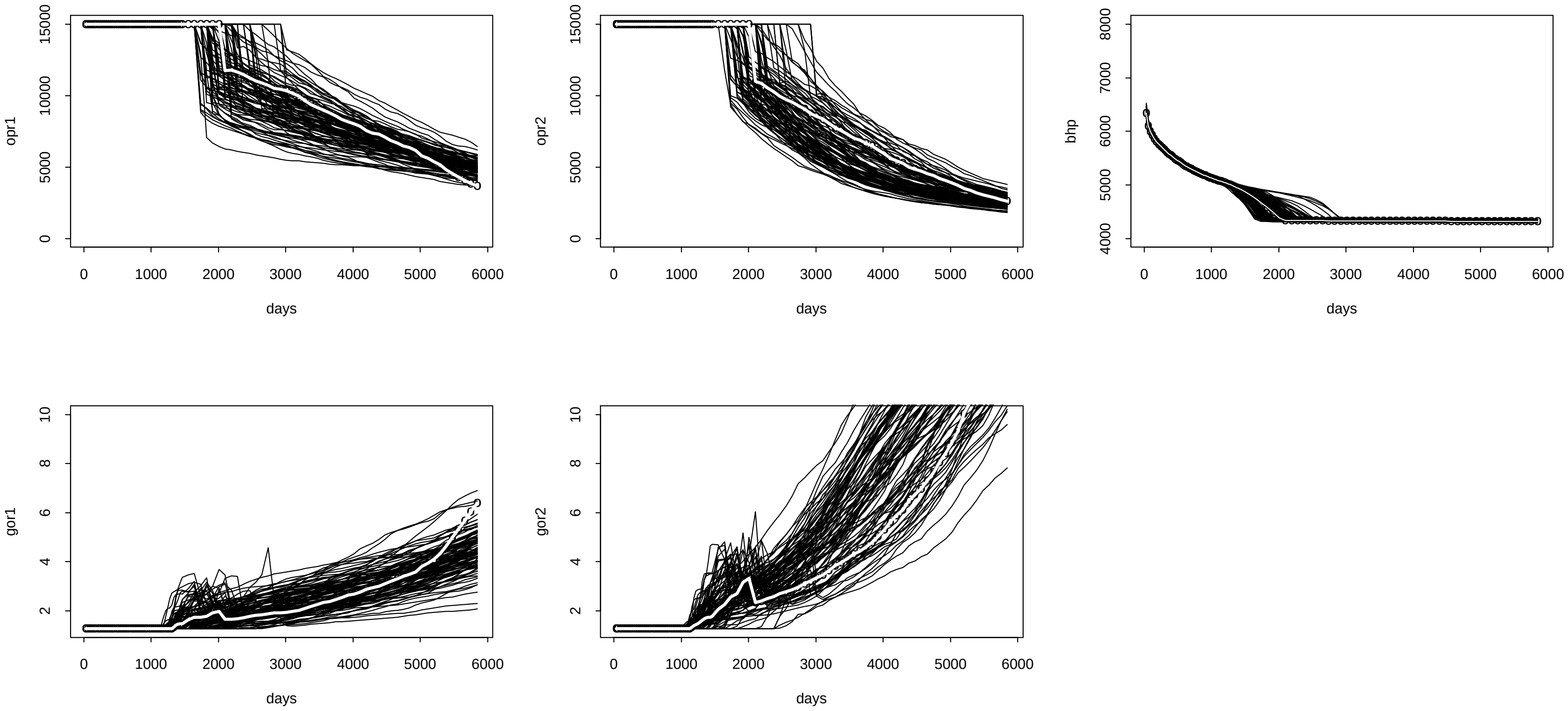

Figure 46: Production characteristics from 100 realizations from the posterior model conditioned on well observations, seismics and 3.33 years of production history. The production characteristics from the true reservoir are indicated by black circles overlayed by a white line.

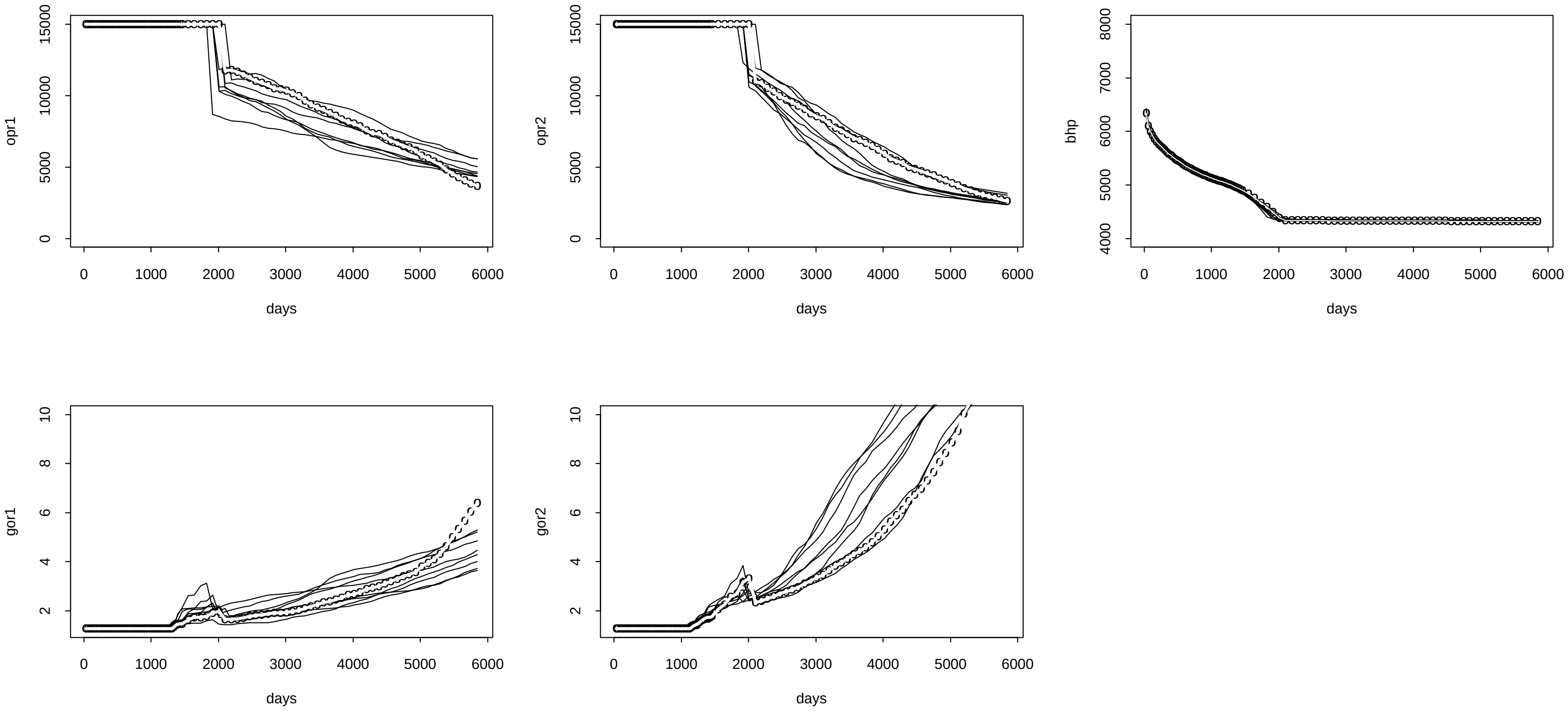

Figure 47: Production characteristics from 7 realizations from the posterior model conditioned on well observations, seismics and 4.5 years of production history. The production characteristics from the true reservoir are indicated by black circles overlayed by a white line.

A The ECLIPSE model file

```
RUNSPEC
 ODEH VARIENT PROBLEM - IMPLICIT OPTION
= NDIVIX NDIVIY NDIVIZ QRDIAL NUMRES QNNCON MXNAQN MXNAQC QDPORO QDPERM
  10     10     15      F      1      F      0      0      F      F /
= OIL WAT GAS DISGAS VAPOIL QAPITR QWATTR QGASTR NOTRAC NWTRAC NGTRAC
 T   T   T     T      F      F      F      F      0      0      0  /
= UNIT CONVENTION
   'FIELD '                                  /
=  NRPVT  NPPVT  NTPVT NTROCC QROCKC QRCREV
  12     12      1      1      F      T      /
= NSSFUN NTSFUN QDIRKR QREVKR QVEOP QHYST QSCAL QSDIR QSREV NSEND NTEND
  16      1      F      T     F      F     F     F     T     1     1 /
= NDRXVD NTEQUL NDPRVD QUIESC QTHPRS QREVTH QMOBIL NTTRVD NSTRVD
  10      1    100      F      F      T      F      1      1        /
=  NTFIP QGRAID  QPAIR
   1      F      F                           /
= NWMAXZ NCWMAX NGMAXZ NWGMAX
   3      10      1      3                    /
= QIMCOL NWFRIC NUPCOL
   F      0      4                           /
= MXMFLO MXMTHP MXMWFR MXMGFR MXMALQ NMMVFT
   0      0      0      0      0      0      /
= MXSFLO MXSTHP NMSVFT MXCFLO MXCWOC MXCGOC NCRTAB
   0      0      0      0      0      0      0      /
= NAQFET NCAMAX
   0      0                                  /
=   DAY   MONTH  YEAR
31    'DEC'    0 /
= QSOLVE NSTACK QFMTOU QFMTIN QUNOUT QUNINP
   T     25      T      F      F      F      /

GRID    ==============================================================
------ IN THIS SECTION , THE GEOMETRY OF THE  SIMULATION GRID AND THE
------ ROCK PERMEABILITIES AND POROSITIES ARE DEFINED.
------------------------------------------------------------------------
--  THE X AND Y DIRECTION CELL SIZES ( DX, DY ) AND THE POROSITIES ARE
--  CONSTANT THROUGHOUT THE GRID. THESE ARE SET IN THE FIRST 3 LINES
--  AFTER THE EQUALS KEYWORD. THE CELL THICKNESSES ( DZ ) AND
--  PERMEABILITES ARE THEN SET FOR EACH  LAYER. THE CELL TOP DEPTHS
--  ( TOPS ) ARE NEEDED ONLY IN THE TOP LAYER ( THOUGH THEY COULD BE.
--  SET THROUGHOUT THE GRID ). THE SPECIFIED MULTZ VALUES ACT AS
--  MULTIPLIERS ON THE TRANSMISSIBILITIES BETWEEN THE CURRENT LAYER
--  AND THE LAYER BELOW.
--     ARRAY  VALUE     ------- BOX ------
EQUALS
    'DX'   1000.      /
    'DY'   1000.      /
    'DZ'   6.66       1  10  1  10  1  5  /
    'TOPS'  8325.     1  10  1  10  1  1  /

    'DZ'    6.66      1  10  1  10  6 10  /

    'DZ'    6.66      1  10  1  10 11 15  /
/       EQUALS IS TERMINATED BY A NULL RECORD

BOX
        1 10 1 10 1 15 /

INCLUDE
'ECLIPSE/POROU.dat'
/

BOX
      1  10  1  10  1  15  /

INCLUDE
'ECLIPSE/PERMXU.dat'
/

EQUALS
        'MULTZ'  0.64    1  10  1  10  5  5  /
        'MULTZ'  0.26    1  10  1  10 10 10  /
/

ENDBOX

--   THE Y AND Z DIRECTION PERMEABILITIES ARE COPIED FROM PERMX
--    SOURCE  DESTINATION  ------- BOX ------
COPY
    'PERMX'    'PERMY'   1  10  1  10  1 15  /
    'PERMX'    'PERMZ'   /
/
--   OUTPUT OF DX, DY, DZ, PERMX, PERMY, PERMZ, MULTZ, PORO AND TOPS DATA
--   IS REQUESTED, AND OF THE CALCULATED PORE VOLUMES AND X, Y AND Z
--   TRANSMISSIBILITIES
RPTGRID
 0 0 0 1 0 0 0 1/
```

```
NOGGF

-- INIT

PROPS    ===============================================================
------ THE PROPS SECTION DEFINES THE REL. PERMEABILITIES, CAPILLARY
------ PRESSURES, AND THE PVT PROPERTIES OF THE RESERVOIR FLUIDS
--------------------------------------------------------------------
--   WATER RELATIVE PERMEABILITY AND CAPILLARY PRESSURE ARE TABULATED AS
--   A FUNCTION OF WATER SATURATION.
--
--  SWAT   KRW   PCOW
SWFN

  0.12  0       0
  1.0   0.00001 0  /

--   SIMILARLY FOR GAS
--
--  SGAS   KRG   PCOG
SGFN

  0     0       0
  0.02  0       0
  0.05  0.005   0
  0.12  0.025   0
  0.2   0.075   0
  0.25  0.125   0
  0.3   0.19    0
  0.4   0.41    0
  0.45  0.6     0
  0.5   0.72    0
  0.6   0.87    0
  0.7   0.94    0
  0.85  0.98    0
  0.88  0.984   0
/

--   OIL RELATIVE PERMEABILITY IS TABULATED AGAINST OIL SATURATION
--   FOR OIL-WATER AND OIL-GAS-CONNATE WATER CASES
--
--  SOIL     KROW     KROG
SOF3

  0        0        0
  0.18     0        0
  0.28     0.0001   0.0001
  0.38     0.001    0.001
  0.43     0.01     0.01
  0.48     0.021    0.021
  0.58     0.09     0.09
  0.63     0.2      0.2
  0.68     0.35     0.35
  0.76     0.7      0.7
  0.83     0.98     0.98
  0.86     0.997    0.997
  0.879    1        1
  0.88     1        1    /

--   PVT PROPERTIES OF WATER
--
--    REF. PRES. REF. FVF  COMPRESSIBILITY  REF VISCOSITY  VISCOSIBILITY
PVTW
     4014.7     1.029        3.13D-6           0.31            0 /

--   ROCK COMPRESSIBILITY
--
--    REF. PRES   COMPRESSIBILITY
ROCK
      14.7          3.0D-6          /

--   SURFACE DENSITIES OF RESERVOIR FLUIDS
--
--        OIL   WATER   GAS
DENSITY
       49.1   64.79  0.06054  /

--   PVT PROPERTIES OF DRY GAS (NO VAPOURISED OIL)
--   WE WOULD USE PVTG TO SPECIFY THE PROPERTIES OF WET GAS
--
--   PGAS   BGAS   VISGAS
PVDG
   14.7 166.666   0.008
  264.7  12.093   0.0096
  514.7   6.274   0.0112
 1014.7   3.197   0.014
 2014.7   1.614   0.0189
 2514.7   1.294   0.0208
 3014.7   1.080   0.0228
```

```
 4014.7   0.811   0.0268
 5014.7   0.649   0.0309
 9014.7   0.386   0.047   /

--   PVT PROPERTIES OF LIVE OIL (WITH DISSOLVED GAS)
--   WE WOULD USE PVDO TO SPECIFY THE PROPERTIES OF DEAD OIL
--
--   FOR EACH VALUE OF RS THE SATURATION PRESSURE, FVF AND VISCOSITY
--   ARE SPECIFIED. FOR RS=1.27 AND 1.618, THE FVF AND VISCOSITY OF
--   UNDERSATURATED OIL ARE DEFINED AS A FUNCTION OF PRESSURE. DATA
--   FOR UNDERSATURATED OIL MAY BE SUPPLIED FOR ANY RS, BUT MUST BE
--   SUPPLIED FOR THE HIGHEST RS (1.618).
--
--   RS      POIL  FVFO  VISO
PVTO
  0.001    14.7 1.062  1.04    /
  0.0905  264.7 1.15   0.975   /
  0.18    514.7 1.207  0.91    /
  0.371  1014.7 1.295  0.83    /
  0.636  2014.7 1.435  0.695   /
  0.775  2514.7 1.5    0.641   /
  0.93   3014.7 1.565  0.594   /
  1.270  4014.7 1.695  0.51
         5014.7 1.671  0.549
         9014.7 1.579  0.74    /
  1.618  5014.7 1.827  0.449
         9014.7 1.726  0.605   /
/

--   OUTPUT CONTROLS FOR PROPS DATA
--   ACTIVATED FOR SOF3, SWFN, SGFN, PVTW, PVDG, DENSITY AND ROCK KEYWORDS
RPTPROPS
1  1  1  0  1  1  1  1  /

SOLUTION ===============================================================
------ THE SOLUTION SECTION DEFINES THE INITIAL STATE OF THE SOLUTION
------ VARIABLES (PHASE PRESSURES, SATURATIONS AND GAS-OIL RATIOS)
-----------------------------------------------------------------------
--   DATA FOR INITIALISING FLUIDS TO POTENTIAL EQUILIBRIUM
--
--    DATUM  DATUM   OWC    OWC    GOC    GOC    RSVD   RVVD   SOLN
--    DEPTH  PRESS  DEPTH   PCOW  DEPTH   PCOG  TABLE  TABLE   METH
EQUIL
     8400   5800   8500    0     8200    0      1      0       0  /

--   VARIATION OF INITIAL RS WITH DEPTH
--
--    DEPTH    RS
RSVD
     8200  1.270
     8500  1.270  /

--   OUTPUT CONTROLS (SWITCH ON OUTPUT OF INITIAL GRID BLOCK PRESSURES)
RPTSOL
 1 11*0 /

SUMMARY  ===============================================================
------ THIS SECTION SPECIFIES DATA TO BE WRITTEN TO THE SUMMARY FILES
------ AND WHICH MAY LATER BE USED WITH THE ECLIPSE GRAPHICS PACKAGE
-----------------------------------------------------------------------
RUNSUM
RPTSMRY
0 /
RPTONLY
WOPR
 'PROD1'  'PROD2' /
WOPT
 'PROD1'  'PROD2' /
WGPR
 'PROD1'  'PROD2' /
WGPT
 'PROD1'  'PROD2' /
WGOR
 'PROD1'  'PROD2' /
WBHP
 'PROD1'  'PROD2' /
WBHP
 'INJECTOR' /
WGIR
 'INJECTOR' /
WGIT
 'INJECTOR' /


SCHEDULE ===============================================================
------ THE SCHEDULE SECTION DEFINES THE OPERATIONS TO BE SIMULATED
-----------------------------------------------------------------------
--   SET 'NO RESOLUTION' OPTION
DRSDT
    0  /
```

```
--   SET INITIAL TIME STEP TO 1 DAY AND MAXIMUM TO 6 MONTHS
TUNING
/
/
2* 50 /

--   WELL SPECIFICATION DATA
--
--     WELL   GROUP LOCATION  BHP   PI
--     NAME   NAME    I  J   DEPTH DEFN
WELSPECS
  'PROD1'    'G'      9 10    8400 'OIL'  /
  'PROD2'    'G'      2 10    8400 'OIL'  /
  'INJECTOR' 'G'      5  1    8335 'GAS'  /
/

--   COMPLETION SPECIFICATION DATA
--
--     WELL     -LOCATION- OPEN/ SAT CONN  WELL
--     NAME     I  J K1 K2 SHUT  TAB FACT  DIAM
COMPDAT
  'PROD1'       9 10 14 14 'OPEN' 0   -1   0.5   3* 'Y'/
  'PROD1'       9  9 14 14 'OPEN' 0   -1   0.5   3* 'Y'/
  'PROD1'       9  8 14 14 'OPEN' 0   -1   0.5   3* 'Y'/
  'PROD1'       9  7 14 14 'OPEN' 0   -1   0.5   3* 'Y'/
  'PROD1'       9  6 14 14 'OPEN' 0   -1   0.5   3* 'Y'/
  'PROD1'       9  5 14 14 'OPEN' 0   -1   0.5   3* 'Y'/
  'PROD1'       9  4 14 14 'OPEN' 0   -1   0.5   3* 'Y'/
  'PROD1'       9  3 14 14 'OPEN' 0   -1   0.5   3* 'Y'/
  'PROD1'       9  2 14 14 'OPEN' 0   -1   0.5   3* 'Y'/
  'PROD1'       9  1 14 14 'OPEN' 0   -1   0.5   3* 'Y'/
  'PROD2'       2 10 14 14 'OPEN' 0   -1   0.5   3* 'Y'/
  'PROD2'       2  9 14 14 'OPEN' 0   -1   0.5   3* 'Y'/
  'PROD2'       2  8 14 14 'OPEN' 0   -1   0.5   3* 'Y'/
  'PROD2'       2  7 14 14 'OPEN' 0   -1   0.5   3* 'Y'/
  'PROD2'       2  6 14 14 'OPEN' 0   -1   0.5   3* 'Y'/
  'PROD2'       2  5 14 14 'OPEN' 0   -1   0.5   3* 'Y'/
  'PROD2'       2  4 14 14 'OPEN' 0   -1   0.5   3* 'Y'/
  'PROD2'       2  3 14 14 'OPEN' 0   -1   0.5   3* 'Y'/
  'PROD2'       2  2 14 14 'OPEN' 0   -1   0.5   3* 'Y'/
  'PROD2'       2  1 14 14 'OPEN' 0   -1   0.5   3* 'Y'/
  'INJECTOR'    5  1  1  5 'OPEN' 1   -1   0.5  /
/

--   PRODUCTION WELL CONTROLS
--
--      WELL     OPEN/  CNTL   OIL  WATER   GAS  LIQU   RES   BHP
--      NAME     SHUT   MODE  RATE   RATE  RATE  RATE  RATE
WCONPROD
   'PROD1' 'OPEN' 'ORAT' 15000 4*                       4100 /
   'PROD2' 'OPEN' 'ORAT' 15000 4*                       4100 /
/

--   INJECTION WELL CONTROLS
--
--      WELL     INJ   OPEN/  CNTL    FLOW
--      NAME    TYPE   SHUT   MODE    RATE
WCONINJ
   'INJECTOR' 'GAS' 'OPEN' 'RATE'  65000  3*                8500 /
/

DATES
 31 'JAN'  1 /
 28 'FEB'  1 /
 31 'MAR'  1 /
 30 'APR'  1 /
 31 'MAY'  1 /
 30 'JUN'  1 /
 31 'JUL'  1 /
 31 'AUG'  1 /
 30 'SEP'  1 /
 31 'OCT'  1 /
 30 'NOV'  1 /
 31 'DEC'  1 /
      :
      :
      :
      :
 31 'MAR'  16 /
 30 'JUN'  16 /
 30 'SEP'  16 /
 31 'DEC'  16 /
/
```

B Derivation of z_{top} in the presence of horizontal wells

Recall that the reservoir characteristics observed in wells are permeability, porosity and acoustic impedance. Reflection coefficients are calculated from vertical changes in acoustic impedance. Hence it is not clear how reflection coefficients can be found in horizontal wells. Acoustic impedance is sampled as indicated in Sections 2.1.3 and 2.3.2. A simple sampling scheme is: let z_{top} be a constant field, simulate reflection coefficients conditioned on seismics and well observations of reflection coefficients; $f(c|c^o, d_s)$, and calculate the acoustic impedance field by the relation (8) in all vertical traces. This procedure does however not reproduce acoustic impedance observations in horizontal wells. Hence z_{top} has to be chosen such that observed acoustic impedance is reproduced also in horizontal wells. An ad hoc procedure where z_{top} is found by kriging is defined as follows:

1. Generate a field of reflection coefficients from $f(c|c^o, d_s)$.
2. Calculate impedance upwards from vertical wells and all observations in horizontal wells by manipulation relation (8) as

   $$Z_i = \frac{1 - C_i}{1 + C_i} Z_{i+1}$$

   and determine all z_o's above vertical wells and all observations in horizontal wells.
3. Let z_{top} be the kriged surface conditioned on the calculated z_o's.

See Figure 48 for a realization of $f(z_{\text{top}}|z^o, c)$ which is deterministic, i.e. represented by a Dirac delta function putting all mass in the z_{top} calculated by this procedure. The horizontal wells are running in the horizontal direction on the contour plot and from left to right on the 3D-plot. The irregularities originating from the well observations are clearly visible on the plots. The "hill" is due to large values of acoustic impedance observed in the first half of one of the horizontal wells. Simple kriging is used with expectation equal z_{top} defined in Table 1.

A generalization is to let z_{top} be a realization of a Gaussian field conditioned on the kriged surface, i.e. the pdf $f(z_{\text{top}}|z^o, c)$ is Gaussian. Note that also by using kriging, Gaussianity is implicitly assumed. Gaussian assumptions are however not in accordance with the resulting field of acoustic impedance Z, defined in the stochastic model. See the discussion in Section 2.1.3.

C Generation of Gaussian fields conditioned on seismic data

According to the prior model both $[S^o|C = c]$ and $[C]$ are Gaussian fields, hence also the variables $[C|S^o = d_s]$ and $[C|C^o = c^o, S^o = d_s]$ with corresponding pdfs $f(c|d_s)$ and $f(c|c^o, d_s)$. Since seismics data are covering the entire reservoir, the dimension of d_s is of the same order as the dimension of c. Hence using numbers from the base case, evaluating or sampling from $f(c|d_s)$ would require inverting or Choleski-decomposition of at 37000×37000 matrix, that is more than $1.4 \cdot 10^9$ entries. Hence this is extremely time consuming. An approximate method based on sequential sampling is developed and implemented by Tjelmeland and Eide, see Eide (1999). This method uses one dimensional pdfs conditioned on a neighborhood determined

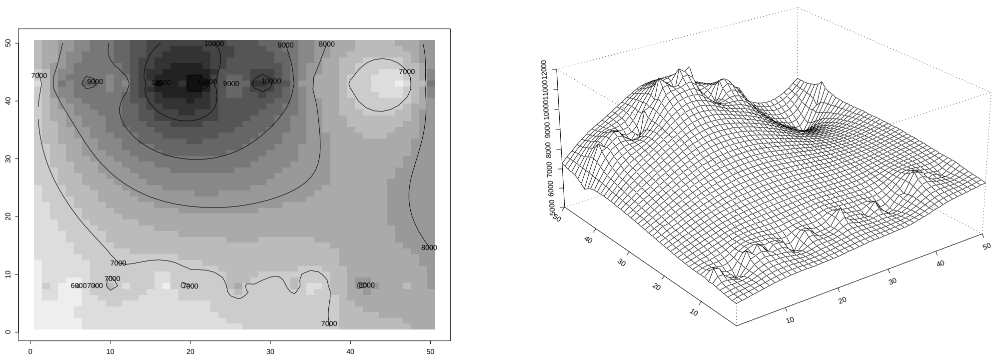

Figure 48: The kriged impedance surface on top of the reservoir. Based on the impedance observations in the horizontal wells, the vertical well and a realization of reflection coefficients, two horizontal stripes and a single node respectively, are calculated. The rest is interpolated by simple kriging.

by an adaptive method. These one-dimensional conditional pdfs are used in the sequential sampling. Establishing the neighborhoods and performing simulations may however take 70-80 cpu-hours on a fast computer in the case studies reported here. Within the current project the software is further developed to gain speed and flexibility. After one long time consuming run establishing the neighborhood structure, simulation runs can be performed within minutes, and all kind of parameters, except those defining correlation structure and grid dimensions may be altered. If correlation structure is subject to changes, the time consuming part has to be executed again.

D Extending the stochastic model

The stochastic model illustrated in Figure 1 can be extended to allow additional stochastic elements, both on the prior models and in the likelihood models. An example of extension of the stochastic model is illustrated in Figure 49.

The bottom rectangle consists of stochastic parameters Θ, in the prior model. The pdfs for the reservoir characteristics and the production characteristics are specified conditioned on these parameters. The parameters could define variance and correlation structure in model-error terms and be elements in the definition of expectations. Some examples of parameters that could be treated as stochastic are listed under.

Θ_p: This is parameters related to the fluid flow model. Examples are variance, range, correlation structure in the error term U_p, parameters in the fluid flow simulator as upscaling procedures, boundary conditions, viscosity, initial saturation, initial pressure etc. .

Θ_Φ: This could be the parameters a and b described in relation (3), i.e. $\theta_\Phi = (a, b)$. Then $f(\phi|a, b, z)$ is defined a priori to be Gaussian with expectation $a - bz$. The prior pdf for these model parameters, $f(a, b)$ must then also be defined.

Θ_K: An example is already given in the description of the prior model in Section 2.1.1. Another example is z_{th} used in facies classification.

Θ_Z: This could for example be expectation and variance in the top layer impedance defined by the field z_{top} and discussed in Section 2.1.3.

The top rectangle consists of stochastic parameters Ψ, in the likelihood model. The likelihoods are specified conditioned on these parameters. These parameters could in general be related to the data observation process. This could be parameters describing variance and correlation structure in observation-error terms and parameters in the definition of the transfer functions $g.()$. Some examples of parameters that could be treated as stochastic are listed under.

Ψ_P: This is parameters related to observations of production characteristics. Examples are variance and correlation structure in the error term U_{P^o} and observation bias.

Ψ_K: This could be σ_{K^o} being the variance in observing permeability in wells, and parameters in the transfer function $g_K(k)$ as e.g. the observations being an average over some area defined by these parameters.

Ψ_S: This could be variance σ_S in the noise corruption the seismic data, the frequency of the Ricker-wavelet, the thickness of grid blocks in time and other parameters connected to the depth-conversion process.

Based on this figure the derivations and considerations in Section 2.3 can be repeated but with the additional parameters and corresponding prior pdfs in the expressions.

To further extend the model also time dependent reservoir characteristics as saturation can be included in the rectangle marked with an R. Then seismics will dependent on both impedances and saturations and will hence be time dependent, or so called 4D-seismics. By using this graphical model extensions of the stochastic model can easily be conceptually illustrated and simplifications, derivations and necessary assumptions in the posterior pdf can be viewed.

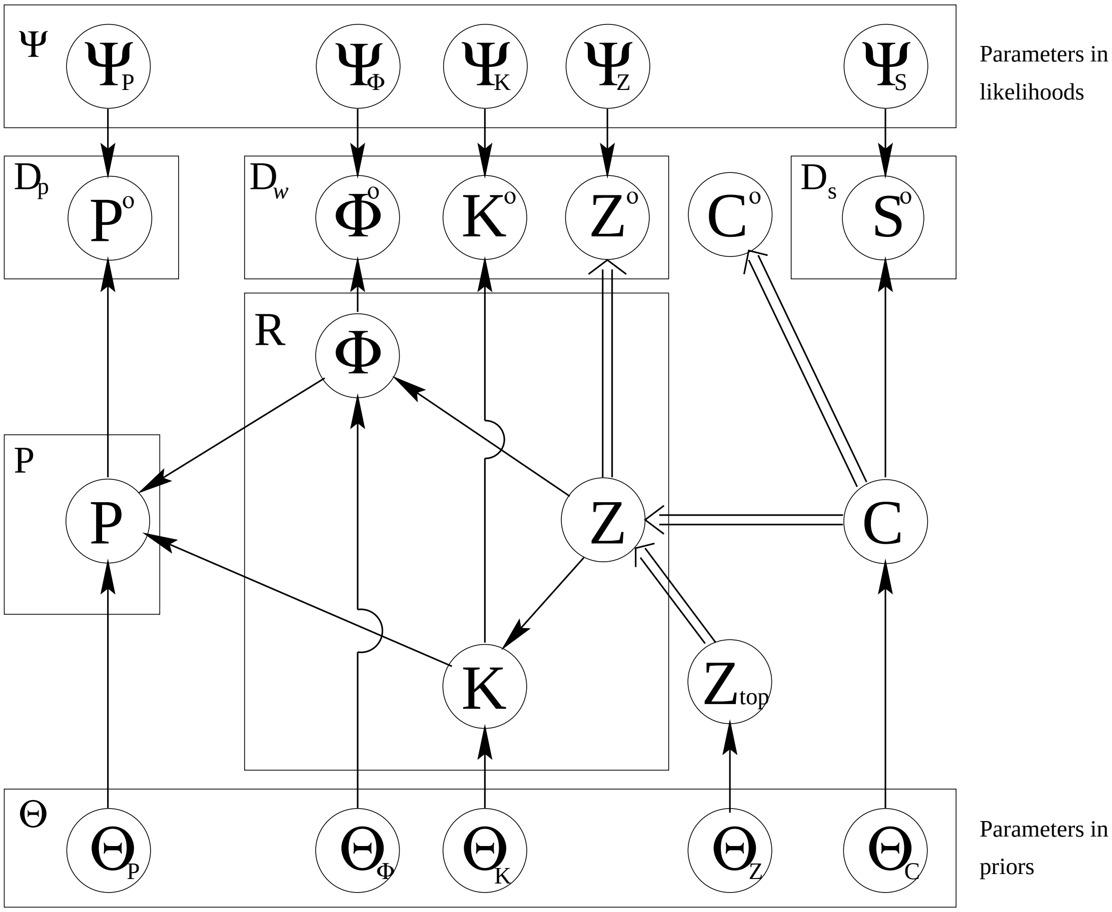

Figure 49: Graphical representation of the extended stochastic model, see also Figure 1. Recall that a circle indicates a stochastic variable. All likelihood functions are defined conditional of the Ψ parameters. This is illustrated by the arrows from the Ψ's to the reservoir specific observations. The prior distributions of the Ψ-parameters must be specified. Similarly all prior distributions for reservoir characteristics and production characteristics are defined conditionally on the Θ-parameters. This is illustrated by the arrows from the Θ-parameters to the reservoir characteristics and the production characteristics.